Thermal Insulation of High Performance Fibrous Materials

Disertační práce

TECHNICAL UNIVERSITY OF LIBEREC
Faculty of Textile Engineering

Thermal Insulation of High Performance Fibrous Materials

Dissertation

Study programme: P3106 – Textile Engineering
Study branch: 3106V015 – Textile Technics and Materials Engineering

Author: **Mohanapriya Venkataraman, M.Tech.**
Supervisor: doc. Rajesh Mishra, Ph.D.

Liberec 2015

Prohlášení

Byla jsem seznámena s tím, že na mou disertační práci se plně vztahuje zákon č. 121/2000 Sb., o právu autorském, zejména § 60 – školní dílo.

Beru na vědomí, že Technická univerzita v Liberci (TUL) nezasahuje do mých autorských práv užitím mé disertační práce pro vnitřní potřebu TUL.

Užiji-li disertační práci nebo poskytnu-li licenci k jejímu využití, jsem si vědoma povinnosti informovat o této skutečnosti TUL; v tomto případě má TUL právo ode mne požadovat úhradu nákladů, které vynaložila na vytvoření díla, až do jejich skutečné výše.

Disertační práci jsem vypracovala samostatně s použitím uvedené literatury a na základě konzultací s vedoucím mé disertační práce a konzultantem.

Současně čestně prohlašuji, že tištěná verze práce se shoduje s elektronickou verzí, vloženou do IS STAG.

Datum:

Podpis:

"This doctoral thesis is dedicated to all the wonderful people who helped me over the course of my research - some named here but many left unnamed because there are so many and there is so little space here. They all have plentiful space reserved in my heart!!!"

Acknowledgement

"You have to dream before your dreams can come true."

- Dr. APJ Abdul Kalam (*Scientist, Poet & President*)

These words from a great person inspired me to dream. I thank Technical University of Liberec for providing the platform and doc. Rajesh Mishra for providing the direction. I have achieved this due to his monumental guidance, support and patience. My heartfelt gratitude and thanks to him. prof. Jiri Militky who was kind enough to share his ocean of knowledge and inspired me with his infectious fervor to share his genius. I would also like to thank my co-supervisor Dr. Jaromír Marek and prof. Jakub Wiener for sharing their immense expertise.

My hearty thanks to management for the sustained support to pursue Ph.D degree in this esteemed institution. My special thanks to the Dean of Faculty of Textile Engineering, Ing. Jana Drašarová for her continuous support and Vice Dean Dr. Gabriela Krupincová for kindly providing SGS grants (2013 - 48019 & 2014 - 21038). I thank and congratulate Secretary. Kateřina Štruplová and Kateřina Nohýnková for their seamless coordination and efficiency. doc. Dr. Ing. Dana Křemenáková inspired me with her commitment and constant pursuit of knowledge. My grateful appreciation to the lab-incharges who were kind enough to provide access to laboratory facilities at any hour of the day. This thesis may not have been possible without the contribution, support, help and coordination of the faculty and staff of Department of Material Engineering, Faculty of Textile Engineering. I thank all my friends and colleagues who were supportive throughout the research period.

I am extremely lucky to have a loving husband, Prasad, and children Shashwath and Kirandeep, who have supported me through this journey. We've lived apart for years but our love has filled the distances. Special thanks to my parents Venkataraman and Usha Punithavathi and in-laws Ramachandran and Syamala for taking care of my children during my prolonged absence. My sister's family Jamuna, Ramprakash and Mayank were my pillars of strength. I can proudly claim that I have the best family in the world. My prayers to almighty god who moral and physical strength to persevere and achieve the dream.

My path to Ph.D has been a fulfilling experience. I never knew learning can be so exciting and fulfilling when surrounded by an inspiring and supportive group of people.

In the past few years, I have lived my dream which has come true now.

Synopsis

Clothing protects mankind from the extremes of nature. In addition, it is also imperative that they provide physiological comfort too. The mixture of fibers, air and moisture define the thermal properties of textiles. The construction parameters of multilayer clothing are its thickness, weight per unit area and fiber density. The efficacy of the fabric is important for performance under extreme conditions. Different fabrics and coating materials need to be studied in order to improve the thermal properties of high performance textiles. Silica aerogel, invented by Kistler in 1930s, is characterized as a low density solid, low optical index of refraction, low thermal conductivity, and low speed of sound through materials, high surface area, and low dielectric constant. Due to its super-insulating characteristics and the heat transfer phenomenon associated with its complex nanoporous structure, it holds great promise as an insulation medium. Measurement of thermal properties of textile materials is important to evaluate usefulness of textiles in extreme weather condition. Devices that work according to principles of thermodynamic systems are largely used for measuring thermal properties of textile fabrics.

The purpose of this research to study thermal insulation of high performance fibrous materials. Various measurement techniques for different combinations of insulation materials and coatings were studied. New methods were explored to measure thermal characteristics at extreme temperatures. Clear understanding of conductive and convective heat transfer was sought. Different types of insulation materials were chosen for thermal measurement, both laboratory preparations and some open market materials. Thermal properties of insulating materials were compared to identify the one best suited for thermal insulation applications at extreme temperature. Further, a few instruments were to be fabricated to measure and correlate thermal properties at sub-zero temperatures. The study also included the mechanisms of heat transfer through fibrous insulation where the fiber diameter is less than 1 micrometer. The research could help in identifying the optimal thermal measurement technique and the insulation material most suitable for use.

Prior to initiation of research, a detailed literature review was conducted to understand and identify their gaps to address in this work. The influence of insulating materials on the thermal conductivity and thermal resistance of nonwoven fibrous materials at extreme temperatures was studied. This comparison was expected to provide insights into optimal measurement technique and the choice of best insulation material and study its application for extreme temperature conditions. In addition to standard equipments, custom-built equipments

were developed to study the thermal properties of textile fabrics. The research considered various unconventional measurement techniques for thermal measurement of insulation materials, and the results were correlated with existing methods. The results from the new measurement techniques like PIV and laboratory set-up instrument will be relevant for classification of materials and eventually for quality assessment of all type of insulation materials. Convective heat transfer through insulation material was studied and analyzed in detail. Modeling and simulation were used to study the heat transfer through porous aerogel materials in fabrics. Polyester and polyethylene nonwoven fabrics embedded with silica aerogel of varying thicknesses, struto nonwoven fabrics and a few commercially available thermal insulation clothing materials were selected. Hydrophobic amorphous silica aerogel was chosen due to its super insulating properties. Nanofibers embedded with silica aerogel could possibly decrease the weight and bulk of current thermal protective clothing, and increase mobility for the users. Thermal properties of electrospun polyurethante (PUR) and Polyvinylidene fluoride (PVDF) nanofibers embedded with silica aerogel was studied. Flexible electrospun nanofiber with silica aerogel was produced via electrospinning process. The aerogel particles were also added during thermal bonding of the standard non-woven web. These studies were carried out under different temperature conditions and differ widely from commonly used conditions.

Samples were characterized by scanning electron microscope (SEM), confocal microscope and fourier transform infrared spectroscopy (FTIR). Surface area and porosity analysis was conducted using BET method. Thermal properties like thermal conductivity and thermal resistance were measured using kawabata (thermolabo) - small hot plate, C-Therm Thermal conductivity analyzer (TCi) and alambeta instrument. The air permeability was measured with air permeability tester. Heat transfer by convection through the samples was measured by particle image velocimetry technique and custom built instruments. Compression test and thickness measurement were carried out using the KES-FB3. The Kawabata Thermolabo-II unit was used to quantitatively measure the thermal properties and heat retention properties. P.T.Teknik thermal manikin was used to measure thermal insulation properties under dynamic conditions.

On scientific evaluation of results, thermal conductivity was found to be differing with respect to different temperatures and fabric density. Thermal conductivity is attributed to the fiber volume fraction of the fabric structure and mainly aerogel particles present in the fabric. The thermal resistances of samples were found to be directly proportional to its thickness. This may be attributed to decrease in heat losses due to space insulated by fibrous structure and

nanoporous aerogel structure. The air permeability was found to be directly proportional to percentage of nanoporosity of the aerogel based fibrous structure. It was also noticed that, when the pressure level increases the flow rate also increases simultaneously. The fabric density and the aerogel present in the fabric have a significant effect on thermal properties of the overall structures. Compared to other fabrics, the aerogel-based fabric samples were found to have considerably high thermal resistance even at extreme temperatures. The results also showed enhancement of thermal insulation by increasing the number and the weight per unit area of nanofiber layers. The newly fabricated equipment was found to be suitable for thermal measurements at sub-zero temperatures. Modeling and simulation was used to extend the findings on heat transfer of aerogel embedded insulation materials. The experimental data was correlated with theoretical calculations and were found to be in good correlation.

The study concludes that the selected aerogel treated fabrics have high thermal performance and thermal response as insulators as compared with other fabrics. Based on the results, it could be concluded that nanofibers are useful for thermal insulation. The newly fabricated instruments and PIV are suitable to measure conductivity and convection at sub-zero temperatures and convenient for the measurement and evaluation of various temperature variations at different positions of the fabric. This method of measurement still needs optimization and will be the subject of further research.

The findings in this study are significant and can be used for further research in the areas of aerogel-treated nonwoven fabrics, heat transfer through porous media, fabrication of custom equipments, alternative techniques for thermal measurements and different mathematical and computational models for heat transfer.

Keywords: Thermal measurement, Insulation materials, Heat transfer, Aerogel, Electrospinning.

Abstrakt

Oblečení chrání lidstvo před extrémními projevy přírody. Kromě poskytování ochrany, je také nutné, aby textilie zajištovaly fyziologické komfort. Typ a uspořádání vláken v textiliích, vlastnosti okolního vzduchu a fyziologické projevy nositele jsou hlavní složky tepelné pohody. Základní konstrukční parametry vícevrstvého oblečení jsou tloušťky, plošné hmotnosti a hustoty vláken jednotlivých vrstev. Různé tkaniny a povrchové úpravy by měly být studovány za účelem optimalizace tepelných vlastností vysoce výkonných textilií. Aerogel na bázi oxidu křemičitého, objevený Kistlerem v 1930, je pevná látka s nízkou hustotou, nízkou optickou indexem lomu, nízkou tepelnou vodivostí, nízkou rychlosti šíření zvuku, vysokou měrnou povrchovou plochou a nízkou dielektrickou konstantou. Vzhledem ke svým super-izolačním vlastnostem a speciálním přenosem tepla v komplexní nanoporézní struktuře, jde o velmi slibný material pro vysoce funkční textilie. Měření tepelných vlastností textilních materiálů je důležité pro vyhodnocení použitelnosti textilií v extrémních povětrnostních podmínkách. Zařízení používaná pro měření tepelných vlastnosti textilií však pracují na základě různých fyzikálních principů a různých podmínek, což limituje možnosti jjich přímého porovnání. Cílem tohoto výzkumu bylo porovnání různých metod měření tepelných vlastnosti textilií pro různé kombinace textilních materiálů a povrchových úprav; prozkoumání možností nové metody pro měření tepelných vlastností textilií při různých teplotách a popis výsledků s ohledem na jednotlivé typy (zejména vedení a proudění) přenosu tepla. Pro tepelná měření byly vybrány různé typy tepelně izolačních textilií, připravených v laboratorním měřítku nebo volně přístupných na trhu. Byly porovnány tepelné vlastnosti těchto materiálů s ohledem na tepelně izolační vlastnosti při extrémních klimatických podmínkách (teploty pod bodem mrazu). Byly připraveny speciální měřicí sytémy pro měření za těchto nestandardních podmínek. Do studie bylo zahrnuto zkoumání mechanismů přestupu tepla přes vláknité izolační vrstvy, kde je průměr vláken je menší než 1 mikrometr. Tento výzkum je příspěvkem k selekci měřicích technik a nalezení vhodných izolačních struktur vhodných pro tyto extrémní podmínky. Zjištění uvedená v této studii jsou zajímavá jak pro další výzkum, tak i pro parktické aplikace. Mohou být použita pro další výzkum v oblasti aerogelem ošetřených netkaných textilií, přenosu tepla přes porézní média, výrobu nestandardních měřicích zařízení využívající alternativních technik pro tepelná měření a v neposlední řadě pro realizaci simulačních výpočtů pomocí různých matematických a výpočetních modelů.

Klíčová slova: Měření tepelných projevů, Izolační materiály, Přenos tepla, Aerogel, Elektrostatického zvlákňování.

Table of Contents

List of Figures

List of Tables

List of Symbols and Abbreviations

Symbols		Description
ΔU	[J]	Internal energy
Q	[W]	Heat flow
λ	[W/(mK)]	Thermal conductivity
A	[m]	Surface area
T	[K]	Temperature
h	[m]	Thickness
γ		Temperature coefficient of thermal conductivity
h_c	[W/(m^{2}K)]	Heat transfer coefficient
L	[m]	Charactersitic length of the fabric
q	[W/m^2]	Heat flux per unit area
C_p	[J/(kg K)]	Specific heat capacity of the fluid particle
ρ	[kg/m^3]	Density
v, u_∞	[m/s]	Velocity of the object relative to the fluid
μ	[kg/(m s)]	Dynamic viscosity of the fluid
Kn		Knudsen number
β		Coefficient characterizing the molecule-wall collision energy transfer efficiency
k_B	[J/K^4 m^2 s)]	Stefan-Boltzmann constant
d	[m]	Gas molecule collision diameter
p	[Pa]	Pressure
δ	[m]	Characteristic pore diameter
σ_{mean}	[m]	Mean free path of the molecules
I_T	[clo]	Total thermal insulation of clothing
K		Units constant
H		Power input
b	[W s$^{1/2}$/(m^2 K)]	Thermal absorptivity
R	[(m^2 K)/W]	Thermal resistance
q_{max}	[W/m^2]	Maximum heat transfer rate
α	[%]	Relative insulation
G	[g/m^2]	Mass per unit area
T_g	[^{o}C]	Glass transition temperature
V_v		Pore volume
P		Porostiy
χ^2		Chi-squared distribution
M	[kg/(k mol)]	Molecular mass
P_i		Cumulative probability
$x_{(i)}$		Order statistic
δt		Thermal boundary layer

Abbreviations	Description
ASME	American Society of Mechanical Engineers
ASTM	American Society for Testing and Materials
BET	Brunauer–Emmett–Teller
BJH	Barrett-Joyner-Halenda
BS	British Standards
CCD	Charge-Coupled Device
Clo	Clothing Insulation
DSC	Differential scanning calorimetry
DX	Particle Displacement
EMC	Compressibility
EN	European Standards
FEM	Finite Element Method
FRMT	Fabric IR Radiation Management Tester
FTIR	Fourier transform infrared spectroscopy
GSM	Grams per Square Meter
IA	Interrogation Areas
IUPAC	International Union of Pure and Applied Chemistry
KES	Kawabata Evaluation System
L-R	Leverage-Residual
MEP	Mean Quadratic Error of Prediction
MTPS	Modified Transient Plane Source
NFA	Nanofibrous layer with Aerogel
NT-H1	N - Nishimatsu; T - Toyonori
PIV	Particle image velocimetry
PP	PolyPropylene
P-P	Probability-Probability
PUR	PolyUrethane
PVDF	PolyVinylidene DiFluoride
QF	Quantile Function
Q-Q	Quantile-Quantile
RTDs	Resistance Temperature Detectors
SEM	Scanning Electron Microscope
STP	Standard Temperature and Pressure
TCi	Thermal Conductivity Instruments
TPS	Transient Plane Source
UHF	Uniform Heat flux
UST	Uniform Skin Temperature
YAG	Yttrium Aluminium Garnet

Chapter 1. Introduction

1.1   General Introduction

Textile materials have found a range of applications in the field of thermal insulation. Thermal insulation is an important factor for estimating physiological comfort for the application area. Combination of different types of fabrics, with various coatings and treatments, are being studied to understand and improve the effectiveness of textile materials as thermal insulators. In extreme cold applications, the role of the middle layer in multilayer clothing is to protect the human body against chilling. Different kinds of fibrous materials such as traditional nonwovens are used as the middle thermal insulating layer. Nonwoven fabrics are important components for good thermal insulation of the body from the surroundings, and they offer both space and weight savings [1]. The important constructive parameters are thickness, weight per unit area and packing fraction p.f., which is the ratio between the bulk density of fibrous structure samples and of the same sample if it was made up wholly from the same polymer [2]. Thermal insulation properties are determined by the physical parameters of fibrous structures as well as the structural parameters [3].

For humans living in extreme conditions, it is important to provide comfort as well as protection. They should be relieved of the burden of struggling with environmental hazards. Humans must have specially designed clothing to protect against cold and wind. This clothing must have very good thermal insulating properties, and also wind-proofness to a great degree. However, warm and windproof clothing brings further difficulties due to the fact that presently designed ones are not easily adjustable to the activities of the human beings. The result can often be that person gets overheated, and sweats, thus causing excessive amounts of moisture to accumulate inside the clothing. Under cold external conditions, some of this moisture will condense to water or even to ice in the outer layers of clothing. The change from water vapor to liquid water is one in which a large latent heat is given up, and the further change to ice also releases significant amounts of thermal energy. Hence a very complex situation arises in thick, arctic clothing. Heat transfer from the man's body to the environment is not just a simple conduction through a thick layer of material of constant insulation value. Moisture plays a very prominent role in the transfer of the energy, and a role that changes with activity. In addition to transfer of latent heat by diffusion through the spaces of various materials, water vapor may be absorbed by the fibers giving rise to a further exothermic change, and the thermal conductivity of the wet fibers then becomes very different from that of the dry fibers. When the human ceases the activity

which caused sweating, they lose heat more rapidly through the wet insulation, than through the same insulation when dry, and this may cause chilling. These problems with moisture are difficult to deal with while designing efficient cold weather clothing. Inspite of improvements made in cold weather clothing over the past two decades, users at extreme environments still suffer from lack of comfortable and effective clothing at affordable cost. Therefore, an alternative solution must be found. To achieve this, a close examination of heat and moisture transfer mechanism is required. A thorough understanding of these mechanisms is essential before advances can be made in materials and clothing design. The materials of good thermal insulating properties as used for cold weather clothing, review the methods of measuring the equations for the effect of variables on the heat and moisture transfer mechanisms [4].

Heat is a form of energy that can cross the boundary of a system. Heat can, therefore, be defined as "the form of energy that is transferred between a system and its surroundings as a result of a temperature difference". There can only be a transfer of energy across the boundary in the form of heat if there is a temperature difference between the system and its surroundings. Conversely, if the system and surroundings are at the same temperature there is no heat transfer across the boundary. The term *"heat"* is a name given to the particular form of energy crossing the boundary. However, heat is more usually referred to in thermodynamics through the term "heat transfer", which is consistent with the ability of heat to raise or lower the energy within a system. There are three different modes of heat flow in porous media are conduction, convection and radiation. Convection relies on movement of a fluid in porous material. Conduction relies on transfer of energy between molecules within a porous solid or fluid. Conduction occurs through air and through material itself but heat transfer by conduction is too small to measure [5]. Conduction is due to fiber-to-fiber attachment [6]. Since textile fabric is a heterogeneous system of air and fabric, conduction through air and fibers contributes to total thermal conduction of the fabric [7]. Radiation is a form of electromagnetic energy transmission and is independent of any substance between the emitter and receiver of such energy. However, all three modes of heat flow rely on a temperature difference for the transfer of energy to take place. The greater the temperature difference the more rapidly will the heat be transferred. Conversely, the lower the temperature difference, the slower will be the rate at which heat is transferred. When discussing the modes of heat transfer it is the rate of heat transfer Q that defines the characteristics rather than the quantity of heat. Although two, or even all three, modes of

heat flow may be combined in any particular thermodynamic situation, the three are quite different and will be introduced separately [8].

Silica aerogel is a low-density, highly porous material, known for its super-insulating characteristics. Heat transfer phenomenon in silica aerogel is associated with its complex nanoporous structure [9, 10]. Heat flow in porous media is the study of energy movement in the form of heat which occurs in many types of processes. The transfer of heat in porous media occurs from the high to the low temperature regions. Therefore a temperature gradient has to exist between the two regions for heat transfer to happen. It can be done by conduction (within one porous solid or between two porous solids in contact), by convection (between two fluids or a fluid and a porous solid in direct contact with the fluid), by radiation (transmission by electromagnetic waves through space) or by combination of the above three methods. The general equation for heat transfer in porous media is:

$$\begin{pmatrix} \text{rate of} \\ \text{heat in} \end{pmatrix} + \begin{pmatrix} \text{rate of generation} \\ \text{of heat} \end{pmatrix} = \begin{pmatrix} \text{rate of} \\ \text{heat out} \end{pmatrix} + \begin{pmatrix} \text{rate of accumulation} \\ \text{of heat} \end{pmatrix} \qquad (1.1)$$

Measurement of thermal properties of textile materials plays an important role. A number of instruments have been developed for this purpose. These instruments can broadly be categorized as steady state measurement and transient measurement devices. Thermal resistance is commonly measured using steady state method and thermal diffusivity in the transient state method. Study of recent developments show that further studies have been conducted to understand the transient properties of fabrics than the steady state aspects. Hence, sweating plates and copper manikins are being increasingly used instead of simple hot plate or cylindrical devices. However, a measurement based on the standardized steady-state dry heat transfer method has its own advantages in experimental simplicity and low equipment cost. Research is ongoing to achieve understanding of heat transfer principles through fabrics and a number of theories have been put forth to understand and predict the steady state thermal properties of textile materials [11]. As part of review of existing literature [13-16] many papers devoted to thermal insulation, comfort properties of clothing and to the related experimental techniques and measurement methods were reviewed. In addition, several existing standard procedures and testing methods have been developed in order to specify fabric IR properties [12, 13] . Some of the proposed approaches are based on the establishment of a steady-state thermal conductivity regime where an electric heater provides a temperature field in a given sample [14] . In addition, other experimental devices like the "hot disk" [15] and the FRMT [16] have also been proposed in recent years to test

the thermal comfort of textile fabrics . These have been successfully applied [4, 17] to the characterization of several kinds of textile fabrics, including the effect of different fabric covering factors and finishing agents. Two such commercially available devices are (1) Thermolabo KES-FB7 system developed by Kawabata [18] and (2) Alambeta apparatus built by Hes and Dolezal [19, 20]. The former allows the measurement of the textile thermal contact properties which enter into the definition of the so-called "warm/cool feeling". The measurement protocol of thermal and transpiration properties is coded in the European Standard UNI EN 31092 [21]. This code is based on the use of a steady-state device – the so-called "Skin Model" – simulating the amounts of heat and humidity exchanged between the human body and the external environment through the clothes worn. However, the methods employed have the disadvantage of measuring the fabric surface temperature in a single point, and then assuming a uniform temperature distribution over the textile surface. This is not the case for fabrics characterized by low covering factors showing highly variable temperature values over their structure [22]. It is important that the standard measurement techniques are studied to understand their strengths and weaknesses and also fabricate new equipments to compliment or replace existing measurement techniques and equipments.

Electrospinning is a simple and low-cost method for making polymer and ceramic fibers with superfine diameters [23-25]. In recent years, it has attracted an increasing interest in the electrospinning technique owing to the promising properties of the electrospun nanofibers. Various structured and assembled nanofibers have been developed via electrospinning. Recent advances in the technology of producing nanofibers have revealed a gap in our knowledge about the heat transfer behavior of low-density nanofibrous layers. Understanding heat transfer through nanofiber structures will allow us to exploit the unique properties of polymer nanofibers for applications such as cold weather clothing and hand wear, sleeping bags, and tent liners, food service refrigeration and storage equipment [4]. Literature searches on the subject of submicron fibers in thermal insulation reveal no fundamental or applied work using polymer nanofibers for thermal insulation applications.

1.2   Research Objectives

The purpose of this research is to study the thermal behavior of high performance textiles. This was expected to be done by studying various combinations of insulation materials, battings and coatings, explore new methods to measure thermal measurements at various temperatures and seek further understanding of conductive heat transfer. Compare the thermal properties of insulating materials to identify the one best suited for thermal insulation applications at subzero temperature. The research could help in identifying the best insulation material and the best means to measure its efficacy. The major objectives of this research are as follows:

1.2.1   Comparative Analysis of Thermal Measurement Techniques

To analyze the thermal measurement techniques used for insulation materials. Usage of such techniques to measure different thermal insulation materials at different temperatures will provide insights necessary for choice of an optimal technique for different scenarios. To analyze and compare the thermal properties of the insulation materials produced in our laboratories and selected from the market. This comparison will enable us to choose the best insulation material and study its application for extreme temperature conditions.

1.2.2   New Method and Fabrication of Instruments for Thermal Measurements

To explore new experimental methods and to fabricate new instruments to study the thermal properties of textile fabrics under extreme temperatures (subzero). As thermal measurement techniques like alambeta and TCi are the methods in which the experiments are carried out at room temperatures, the major objective was to develop new methods and new equipments to test the samples by conductive and convective heat transfer at extreme temperatures.

1.2.3   Correlation of Theoretical Model and Experimental Measurements

To correlate conventional and unconventional thermal measurement techniques which are different in conception. The results from the conventional and unconventional method of measurements will throw light on possibility of using the new equipment for selected thermal measurement experiments. Correlation of theoretically calculated data and measured data will provide further insights into efficacy of various techniques for thermal measurements.

1.2.4   Study and Analyze Convective Heat Transfer through Insulation Material

To understand the convective heat transfer phenomena through insulation materials. In this regard, different techniques like particle image velocimetry (PIV) and laboratory set-up equipments were used. This method involves particle image velocimetry (PIV), which is a reliable nonintrusive laser optical measurement technique based on seeding a flow field with micron-sized tracer particles and illuminating a two-dimensional (2D) slice or target area with a laser light sheet. Vector and scalar maps of the fluid flow caused by thermal convection above the textile sample were studied and characterized using PIV for different temperature gradients. New laboratory set-up equipment was also fabricated to perform the experiments to study heat transfer by convection.

1.2.5   Electrospinning of PUR and PVDF Nanofibrous Layer with Silica Aerogel

To understand the heat transfer behavior of low-density nanofibrous layers. Understanding heat transfer through nanofibrous layers embedded with silica aerogel structures will allow us to exploit the unique properties of polymer nanofibers for high performance textile applications. It was intended to study the mechanisms of heat transfer through fibrous insulation where the fiber diameter is less than 1 micrometer (μm). Production of flexible electrospun PUR and PVDF nanofibrous layers embedded with silica aerogel using electrospinning process. Further, to analyze the thermal properties of the electrospun nanofibrous layers embedded with SiO_2 aerogel and find their application in enhanced thermal insulation.

1.2.6   Modeling and Simulation of Heat Transfer

To develop suitable computational models to simulate and predict the insulation behavior of nonwoven fabrics without and with aerogel. The results of simulation to be correlated to experimental measurements for validation.

1.3   Dissertation Outline

The dissertation is divided into five chapters.

Chapter	Description
Chapter 1. -	*Introduction:* General introduction about the topic of research. It contains details of the purpose and objectives of this research.
Chapter 2. -	*State of the Art in Literature:* A detailed study of previous literature and understanding of studies conducted and identify the limitations in past research.
Chapter 3. -	*Experimental Materials and Methods:* An overview about sample materials, formulae, scientific concepts, experimental and production methods used in this research. Elaborate explanation about methods and techniques used for characterization, thermal measurements and other experiments conducted.
Chapter 4. -	*Results and Discussion:* A detailed analysis of the results derived from various experiments. The results were tabulated and detailed statistical analysis was performed. Various interpretations were drawn from the analysis.
Chapter 5. -	*Conclusion:* This chapter contains the broad conclusions drawn from the result and analysis of the research. It also describes the future direction of this research. The outputs are in the form of scientific papers, book chapters and conference proceedings.

Chapter 2. State of the Art in Literature

2.1 Introduction

The thermal insulating power is defined as the property of a material which resists heat flow and thus reduces heat loss from the heat source, e.g. the human body. Heat loss from the body through layers of damp or wet clothing involves a three phase system, composed of the solid (fiber and/or ice), the liquid (water) and the gas (air and water vapor). The boundaries of the system are defined by the surfaces of the inner and outer layers. In such a system [26], there are seven heat transfer mechanisms which operate simultaneously:

1. Conduction in the solid phase
2. Conduction in the liquid phase
3. Conduction in the gas phase
4. Radiation through the gas phase
5. Convection through the liquid phase
6. Convection through the gas phase
7. Evaporation-diffusion-condensation-solidification.

In most textile engineering problems, the primary interest lies not in the molecular behavior of textiles, but rather in how the textile behaves as a continuous medium. In the study of heat conduction, the molecular structure of the textile can therefore be neglected and considered to be a continuous medium-continuum, which is a valid approach to many practical problems were only macroscopic information is of interest. Such a model may be used if the size and the free path of molecules are small compared with other dimensions existing in the medium, so that a statistical average is meaningful. This approach, which is also known as the phenomenological approach to heat conduction, is simpler than microscopic approaches and usually gives the answers required in textile engineering.The first and second laws of thermodynamics can be used for heat conduction problems. Other laws employed in the analysis of conduction heat transfer are (a) Fourier's law of heat conduction (b) Newton's law of cooling and (c) Stefan-Boltzmann's law of radiation.

2.2 Heat Conduction and Thermal Conductivity

The rate of heat conduction through a material may be proportional to the temperature difference across the material and to the area perpendicular to the heat flow and inversely proportional to the length of the path of heat flow between the two temperature levels. This dependence was established by well known French scientist J.B.J. Fourier, who used it in his

work, *Theorie Analytique de la Chaleur*, published in Paris in 1822. In this book he gave a very complete exposition of the theory of heat conduction. The constant of proportionality in Fourier's law, denoted by λ, is called the thermal conductivity. It is a property of the conducting material and of its state. with the notation indicated in figure 1, Fourier's law is,

$$q = \frac{\lambda A}{h} \; (T_1 - T_2) \quad [\text{W/m}^2] \tag{2.1}$$

where $\lambda A/h$ is called the conductance of the geometry in figure 1, since there is a temperature difference of $(T_1 - T_2)$ between the surfaces, q is the heat flow through the material. From the second law of thermodynamics, it is known that the direction of this flow is from the higher temperature surface to the lower one. According to the first law of thermodynamics, under steady conditions, this flow of heat will be at a constant rate [8].
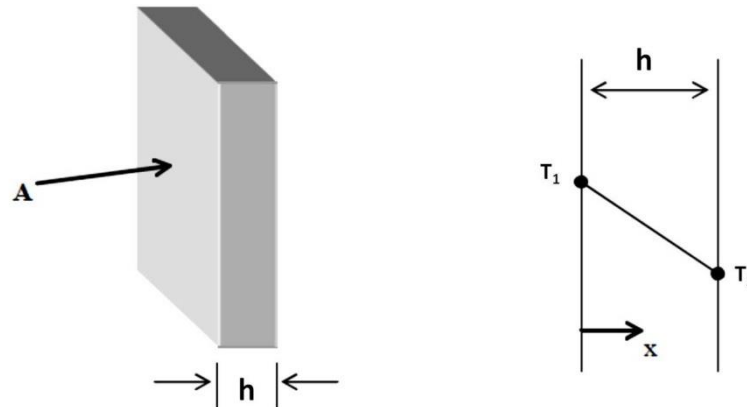
Figure 1. One-dimensional steady-state heat conduction [8].

The thermal conductivity λ, which is analogous to electrical conductivity, is a property of the thermal material. It is equivalent to the rate of heat transfer between opposite faces of a unit cube of the material which are maintained at temperatures differing by 1˚. In SI unit, λ is expressed as [W/(m K)]. The thermal conductivity of a material depends on its chemical composition, physical structure, and state. It is also varies with the temperature and pressure to which the material is subjected. In most cases, however, thermal conductivity is much less dependent on pressure than on temperature. So, the dependence on pressure may be neglected and thermal conductivity can be tabulated as a function of temperature. In some cases, thermal conductivity may also vary with direction of heat flow as in anisotropic materials. The variation of thermal conductivity with temperature may be neglected when the temperature range under consideration is not too severe. For numerous materials,

especially within a small temperature range, the variation of thermal conductivity with temperature can be presented by the linear function,

$$\lambda(T) = \lambda_0 \left[1 + \gamma(T - T_0) \right] \tag{2.2}$$

where $\lambda = \lambda(T_0)$; T_0 is a reference temperature, and γ is a constant called the temperature coefficient of thermal conductivity. Heat conduction in gases and vapors depends mainly on the molecular transfer of kinetic energy through the molecular movement. That is, heat conduction is transmission of kinetic energy by the more active molecules in high temperature regions to the molecules in low molecular kinetic energy regions by successive collisions. According to kinetic theory of gases, the temperature of an element of gas is proportional to the mean kinetic energy of its constituent molecules. Clearly, the faster the molecules move, the faster they will transfer energy. This implies, therefore, that thermal conductivity of a gas should be dependent on its temperature.

2.2.1 *Thermal Conduction Mechanisms*

For many types of substances, theoretical predictions and measurements have been made for the value of thermal conductivity, λ. In gases, heat is conducted (*i.e.*, thermal energy is diffused) by random motion of molecules. Higher-velocity molecules from higher-temperature regions move about randomly, and some reach regions of lower temperature. By a similar random process, lower-velocity molecules from lower temperature regions reach higher temperature regions. Thereby, net energy is exchanged between the two regions. The thermal conductivity depends upon the space density of molecules, upon their mean free path, and upon the magnitude of the molecular velocities. The net result of these effects, for gases having very simple molecules, is dependence of λ upon T, where T is the absolute temperature. This results from kinetics of gases [8, 27, 28].

2.2.2 *Conductive Heat Flow in Porous Materials*

Conduction is the process of heat transfer by molecular motion, supplemented by the flow of heat through textile material from a region of high temperature. Heat transfer by conduction takes place across the interface between two bodies in contact when they are at different temperatures [8]. If a fluid could be kept stationary, heat transfer may occur by conduction and not convection. Conduction depends on the transfer of energy from one molecule to another within the heat transfer medium and, in this sense, thermal conduction is analogous to electrical conduction. Conduction can occur within both porous solids and fluids. The rate of heat transfer depends on a physical property of the particular porous solid of fluid, termed

its thermal conductivity λ, and the temperature gradient across the porous medium. The thermal conductivity is defined as the measure of the rate of heat transfer across a unit width of porous material, for a unit cross-sectional area and for a unit difference in temperature. From the definition of thermal conductivity λ, it can be shown that the rate of heat transfer is as given in equation 2.1. Fourier's Law can be integrated through a flat wall of constant cross section A for the case of steady-state heat transfer when the thermal conductivity of the wall λ is constant.

2.3 Heat Transport Mechanisms in Porous Media

The study of flow systems which compose of a porous medium and a homogenous fluid has attracted much attention since they occur in a wide range of the industrial and environmental applications. In the single-domain approach, the composite region is considered as a continuum and one set of general governing equations is applied for the whole domain. The explicit formulation of boundary conditions is avoided at the interface and the transitions of the properties between the fluid and porous medium are achieved by certain artifacts. Although this method is relatively easier to implement, the flow behavior at the interface may not be simulated properly, depending on how the code is structured. In the two-domain approach, two sets of governing equations are applied to describe the flow in the two regions and additional boundary conditions are applied at the interface to close the two set of equations. This method is more reliable since it tries to simulate the flow behavior at the interface. Hence, in the present study, the two-domain approach, and the implementation of the interface boundary conditions, will be considered. The average convection coefficients depend on the surface geometry of the material and the flow conditions. The heat transfer coefficient, h_c can be determined by the average Nusselt number, *Nu:*

$$Nu = \frac{h_c L}{\lambda_A} = f[\text{Re}, \text{Pr}] \tag{2.3}$$

where λ_A is the heat conductivity for air and L is the characteristic length of the material. *Nu* shows the ratio of the heat transfer that depends on convection to the heat transfer that depends on conduction in the boundary layer. The Nusselt number is a function of the Reynold number, *Re*, and the Prandtl number, *Pr. Pr* is the relation between the thickness of thermal and the velocity boundary layers. If *Pr* is equal to 1, the thickness of the thermal and velocity boundary layers are equal. For air, *Pr* is equal to 0.7 [29].

2.3.1   *Convective Heat Flow in Porous Media*

Convection is a mode of heat transfer that takes place as a result of motion within a fluid. If the fluid, starts at a constant temperature and boundary surface temperature is suddenly increased in temperature to above that of the fluid, there will be convective heat transfer from the surface of the fabric to the fluid as a result of the temperature difference. Under these conditions the temperature difference causing the heat transfer can be defined as:

$$\Delta T = boundary\ surface\ temperature - mean\ fluid\ temperature \qquad (2.4)$$

Using this definition of the temperature difference, the rate of heat transfer due to convection can be evaluated using Newton's law of cooling:

$$q = h_c A\ \Delta T \quad [\text{W/m}^2\text{K}] \qquad (2.5)$$

Where A is the surface area through which the heat transfer occurs and h_c is the coefficient of heat transfer from the surface to the fluid, referred to as the "convective heat transfer coefficient". The relationship given in equation 2.4 is also true for the situation where a surface is being heated due to the fluid having higher temperature than the boundary surface. However, in this case the direction of heat transfer is from the fluid to the boundary surface and the temperature difference will now be,

$$\Delta T = mean\ fluid\ temperature - boundary\ surface\ temperature \qquad (2.6)$$

The relative temperatures of the boundary surface and fluid determine the direction of heat transfer and the rate at which heat transfer takes place. As given in previous equations, the rate of heat transfer is not only determined by the temperature difference but also by the convective heat transfer coefficient h_c. This is not a constant but varies quite widely depending on the properties of the fluid and the behavior of the flow. The value of h_c must depend on the thermal capacity of the fluid particle considered, i.e. mC_p for the particle. So the higher the density and C_p of the fluid the better the convective heat transfer [8]. Typical values of convective heat transfer coefficients are as given in table 1 below:

Table 1. Typical values of convective heat transfer coefficient [8].

Fluid	h_c [W/(m^2 K)]
Water	500-10000
Air	5-100

The variation in the values reflects the variation in the behavior of the flow, particularly the flow velocity, with the higher values of h_c resulting from higher flow velocities over the surface. When a fluid is in forced or natural convective motion along a surface, the rate of heat transfer between the solid and the fluid is expressed by the equation (2.6). The coefficient h_c is dependent on the system geometry, the fluid properties and velocity and the temperature gradient. Most of the resistance to heat transfer happens in the stationary layer of fluid present at the surface of the solid, therefore the coefficient h_c is often called film coefficient. Correlations for predicting film coefficient h_c are semi empirical and use dimensionless numbers which describe the physical properties of the fluid, the type of flow, the temperature difference and the geometry of the system. The Reynolds Number characterizes the flow properties (laminar or turbulent).

$$N_{Re} = \frac{\rho L v}{\mu} \tag{2.7}$$

Where ρ is the density of the fluid [kg/m^3], L is the characteristic length of fabric [m], v is the maximum velocity of the object relative to the fluid [m/s], μ is the dynamic viscosity of the fluid [kg/(m s)]. The Prandtl Number characterizes the physical properties of the fluid for the viscous layer near the fabric surface.

$$N_{Pr} = \frac{\mu C_p}{\lambda} \tag{2.8}$$

where μ is the dynamic viscosity [kg/(m s)], C_p is the specific heat [J/(kg K)], λ is the thermal conductivity [W/(m K)]. The Nusselt number relates the heat transfer coefficient to the thermal conductivity of the fluid (air).

$$N_{Nu} = \frac{h_c L}{\lambda} \tag{2.9}$$

where h_c is the convective heat transfer coefficient of the flow, L is the characteristic length of the fabric, λ is the thermal conductivity of the fluid.

Convection in porous materials can be separated into two cases, the convection inside the pore cells and the convection through the material on a macro scale. For closed pore systems, there is no macro scale convection and for small pores, the pore cell convection can be neglected, partly because of small temperature differences on the cell walls. That means, the heat transfer through convection often can be neglected for materials with a closed pore system. For materials with open cells, the macro scale convection might have a considerable

effect and thus cannot be neglected [30]. The macro scale convection is either caused by natural or forced convection. For natural convection the air movement is created by density differences as a consequence of temperature differences, while forced convection is created by a pressure difference due to e.g. wind or fan induced. Natural convection is described by the dimensionless quantity Nusselt number, shown in equation (2.9).

2.4 Porosity and Pore Size Distribution in a Material

Porosity refers to volume fraction of void spaces. This void space can be actual space filled with air or space filled with both water and air. The distinction between porous and capillary-porous is based on the presence and size of the pores. Porous materials are sometimes defined as those having pore diameter greater than or equal to 10^{-7} [m] and capillary-porous as one having diameter less than 10^{-7} [m]. Porous and capillary porous materials were defined as those having a clearly recognizable pore space. Soil, porous or fissured rocks, ceramics, fibrous aggregates, sand filters, snow layers and a piece of sugar or bread are few examples of porous materials. All these have properties in common that intuitively lead us to classify them into a single denomination: *porous media*. Indeed, one recognizes a common feature to all these examples. All are described as "solids" with "holes", i.e. presenting *connected void spaces*, distributed - randomly or quite homogeneously - within a *solid matrix*. Fluid flows can occur within the porous medium, and so one essential feature was added: this *void space* consists of a complex tridimensional network of *interconnected* small empty volumes called "*pores*", with several continuous paths linking up the porous matrix spatial extension, to enable flow across the sample. If a porous medium that is not consolidated is considered, it is possible to derive the *particle-size distribution* of the constitutive solid grains. The problem is obvious when dealing with spherical shaped particles, but raises the question of what is meant by particle size in the case of an irregular shaped particle. The definition of a porous medium can be based on the objective of describing flow in porous media. A porous medium is a heterogeneous system consisting of a rigid and stationary solid matrix and fluid filled voids. The solid matrix or phase is always continuous and fully connected. A phase is considered a homogeneous portion of a system, which is separated from other such portions by a definitive boundary, called an interface. A porous medium is homogeneous if its average properties are independent of location, and heterogeneous if they depend on location [8].

2.4.1   Pore-Size Distribution in Porous Structure

A detailed description of the complex tri-dimensional network of pores is obviously impossible to derive. For consolidated porous media, the determination of a *pore-size distribution* is nevertheless useful. For those particular media, it is indeed impossible to handle any particle-size distribution analysis. One approach to define a *pore size* is in the following way: the *pore diameter* δ *at* a given point within the pore space is the diameter of the largest sphere that contains this point, while still remaining entirely within the pore space. To each point of the *pore space* such a "diameter" can be attached rigorously, and the *pore-size distribution* can be derived by introducing the *probability density function θ (δ)* defined as the fraction of the total relative void space that has a pore diameter comprised between *δ* and *δ+dδ*. This probability density function is normalized by the relation:

$$\int_0^\infty \theta(\delta)d\delta = 1 \qquad (2.10)$$

A porous structure should be a material medium made of heterogeneous or multiphase matter. At least one of the considered phases is not solid. The solid phase is usually called the *solid matrix*. The space within the porous medium domain that is not part of the *solid matrix* is named *void space* or *pore space*. It is filled by gaseous and/or liquid phases. The solid phase should be distributed throughout the porous medium to draw a network of pores, whose characteristic size can vary greatly.
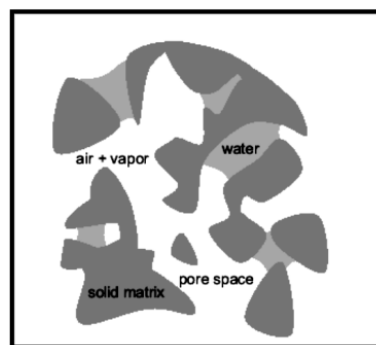
Figure 2. Sketch of a porous material [8].

Some of the pores comprising the void space must enable the flow across the solid matrix, so that they should then be interconnected. The interconnected pore space is often denoted as the *effective pore space*, while unconnected pores may be considered from the hydrodynamic point of view as part of the solid matrix, since those pores are ineffective as far as flow through the porous medium is concerned. They are *dead-end pores* or *blind pores*, that contain stagnant fluid and no flow occurs through them. A porous material is a

set of pores embedded in a matrix of mostly solid material. The pores are the voids in the material itself. Pores can be isolated or interconnected. Furthermore, a pore can contain a fluid or a vapor, but it can also be empty. If the pore is completely filled with the fluid, it will be called saturated and if it is partially filled, it will be called non-saturated. So the porous material is primarily characterized by the content of its voids and not by the properties of the material itself. Figure 2 gives a sketch of a porous material [8].

2.5 Heat Transfer in Insulation Materials

The function of insulation materials is to minimize the transport of heat through the construction. The insulation materials are highly porous with small amount of solid structure. In a material with a small amount of solid, the importance of the radiation will increase, as shown in figure 3.
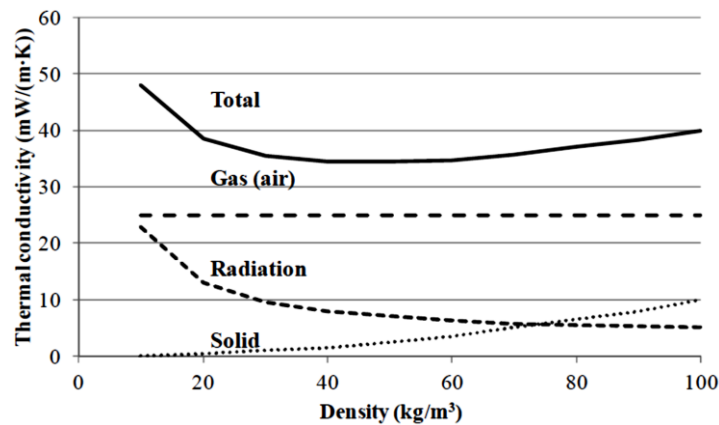
Figure 3. Thermal conductivity in porous materials divided in conduction through the solid, conduction through gas phase and radiation through pores [31].

This creates an optimal point from insulation perspective, for a certain material, where the sum of the contributions from radiation and solid conduction is at a minimum. This sum will add to the gas conduction which for conventional insulation materials can be considered as constant. This gives a total thermal conduction down to a minimum around 0.03 W/(m K), which can be compared to the air conductivity of 0.025 W/(m K). Figure 3 also shows the strong correlation between density and conductivity [30]. The thermal conductivities of typical materials of this category are presented in table 2.

Table 2. Thermal conductivity of a number of common porous insulation materials [32].

Insulation material	Thermal conductivity, λ [W/(m K)]
Mineral wool	0.033 - 0.040
Expanded/extruded polystyrene	0.030 - 0.040
Loose-fill cellulose fiber	0.039 - 0.042
Foam glass	0.039 - 0.045

2.5.1 Solid Conduction

There is also some difference in the solid conduction for various materials, due to its physical properties. The solid conduction will be decreased if the density is decreased. The actual conductivity in the solid will not change but the area of the solid in a cross section of the material will decrease, and thereby lower the solid conduction per square meter of the porous material. As mentioned earlier, a decreased density will increase the heat flow due to radiation which will counter the gain in the solid conduction [30].

2.5.2 Radiation

Heat transfer by radiation is caused by the electromagnetic radiation which is emitted by all surfaces. The net radiation is the difference between the radiation from the warm surface and the radiation from the cold surface. The rate of heat transfer by radiation is dependent on the temperature of a surface.

2.5.3 Gas Conduction

The gas conduction is based on the type of gas and the possibility for the gas to transfer heat. To get a lower value, the gas could either be exchanged to a gas with lower conductivity or by preventing the gas to transfer the heat.

Table 3. Thermal conductivity and molecular mass of gases [33].

Gas	Thermal conductivity, λ [W/(m K)]	Molecular mass, M [kg/(k mol)]
Air	0.0255	29
Nitrogen, N_2	0.0241 (0°C)	28
Argon, Ar	0.0162 (0°C)	40
Carbon dioxide, CO_2	0.0162 (25°C)	44
R-11, $CFCl_3$	0.0083 (30°C)	137

Examples of different gases and their thermal conductivity is shown in table 3 together with their molecular mass [30]. The gas conductivity can be decreased by decreasing the pore size of the material. The collisions between the gas molecules and the solid are elastic which transfer small amounts of energy compared to the collisions between gas molecules. Smaller pores lead to a higher probability of collisions with pore walls instead of other gas molecules. This is called the Knudsen effect where the gas thermal conductivity in the pores, λ_{gas}, is governed by equation (2.11) based on the Knudsen number, Kn, calculated by equation (2.12) [34].

$$\lambda_{gas} = \frac{\lambda_{gas,0}}{1+2\ \beta\ Kn} = \frac{\lambda_{gas,0}}{1+\dfrac{\sqrt{2}\ \beta\ k_B\ T}{\pi\ d^2\ p\ \delta}} \quad [\text{W/(m K)}] \tag{2.11}$$

$$Kn = \frac{\sigma_{mean}}{\delta} = \frac{k_B\ T}{\sqrt{2}\ \pi\ d^2\ p\ \delta} \tag{2.12}$$

where $\lambda_{gas,0}$ [W/(m K)] is the gas thermal conductivity in the pores at STP (standard temperature and pressure), β coefficient characterizing the molecule wall collision energy transfer efficiency (between 1.5 - 2.0), $Kn = \sigma_{mean}/\delta = k_B T/(2^{1/2}\ \pi d^2\ p\delta) = $ the Knudsen number, k_B [1.38 x 10^{-23} J/K] is the Boltzmann constant, T [K] is the temperature, d is the gas molecule collision diameter [m], p is the gas pressure in pores [Pa], δ [m] is the characteristic pore diameter, σ_{mean} [m] is the mean free path of the molecules [34].
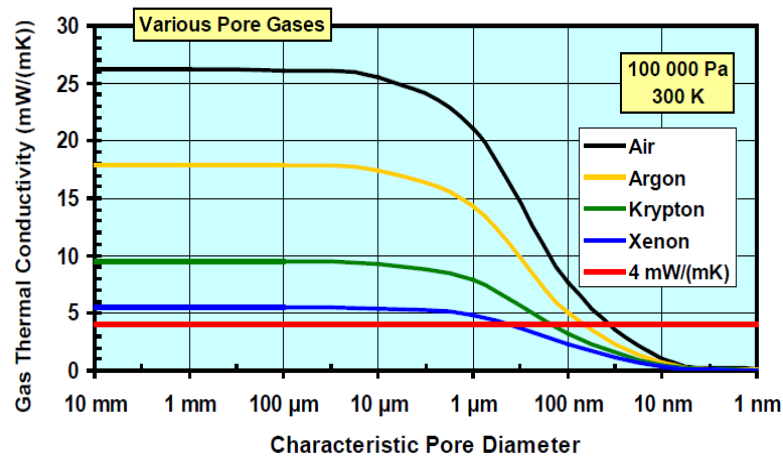
Figure 4. Calculated gas thermal conductivity versus pore diameter [31].

The gas conductivity is strongly dependent on the ratio between the pore size and the mean free path of the gas inside of the pores. The mean free path, σ_{mean}, is the average distance a molecule travels before colliding with another molecule. The distance can be calculated by

equation (2.12). For nitrogen and oxygen, the main components of air, the molecular cross-sectional area is around 0.4 nm [35]. The mean free path becomes approximately 70 nm at normal temperature and pressure (300 K and 100 kPa). The effect on the thermal conductivity is shown in figure 4. It shows the calculated gas conductivity for various pore size as a function of characteristic system size based on equation (2.11) and equation (2.12). The input temperature is 300 K and the pressure is 100 kPa. The characteristic system size can be related to the pore diameter of a material [31]. The characteristic system size can be difficult to determine but it is correlated to the pore size. However, when the pores grow larger, the conductivity gets close to the normal conductivity of the gas. It seem as the Knudsen effect is negligible for pores larger than 10000 nm or 0.01 mm. The effect on thermal conductivity, from a lowered pressure is strongly dependent of pore size. In equation (2.12), pressure is seen in the denominator for the calculation of the mean free path. A lower pressure gives a longer mean free path which gives a larger Knudsen effect. From equation (2.11) and equation (2.12) it is seen that an increase in the mean free path will increase the Knudsen number and thereby decrease the gas conductivity.
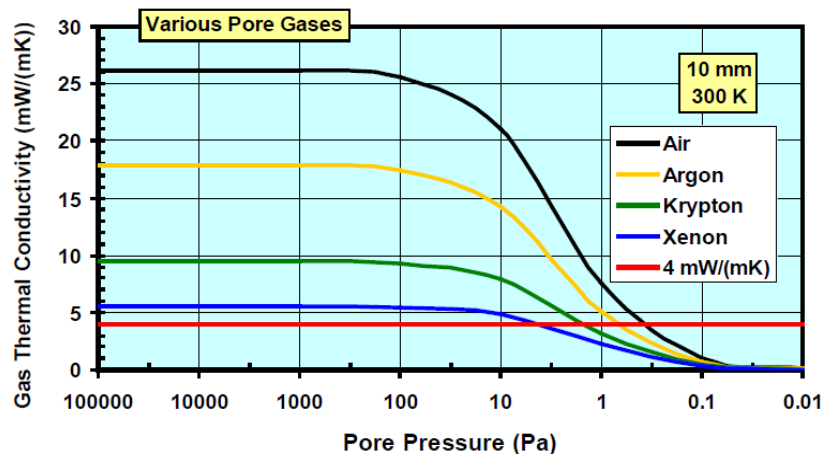
Figure 5. Calculated gas thermal conductivity versus pore pressure [31].

Figure 5 shows calculated gas conductivity of various pore gases as a function of pore pressure for different characteristic system size based on equations (2.11 and 2.12) [31].

2.6 State of the Art on Thermal Measurement Techniques

Most of the studies carried out until now have focused on measurements of static thermal properties such as thermal conductivity and thermal resistance. There are a number of techniques to measure thermal conductivity with each of them suitable for limited range of materials, depending on the thermal properties and the temperature of the medium. In general, various methods [23, 36] are used for measuring the thermal insulation values of

textile materials. Generally, three different methods have been used in the determination of the thermal insulation of fabrics. The first is cooling method in which a hot body is surrounded by a fabric whose outer surface is exposed to the air, and the rate of cooling of the body is determined. Second is disc method, where the fabric is held between two metal plates at different temperatures, and the rate of flow of heat is measured and third is constant temperature method, where the fabric is wrapped around a hot body and the energy required to maintain the body at a constant temperature is found. The thermal properties of a fabric will determine not only its warmth in wear but also how warm or cool the fabric feels when first handled. The heat transport properties can be divided into two groups [37]: steady-state thermal properties such as thermal conductivity and resistance which provide the information on the warmth of a fabric; and transient-state thermal properties such as thermal absorptivity which provides the information of warm–cool feeling when fabric is first handled. In practice, the measurement of the rate of heat flow in a particular direction is difficult as the heater, even when supplied with a known amount of power, dissipates its heat in all directions. Most successful heat transport measuring instruments are Togmeter (BS 4745, 1971) [38], Guarded hot plate (ASTM D 1518-85, 1990) [39], Alambeta instrument (SENSORA, 1990) [40] and Thermal conductivity analyzer (TCi). Some of the methods used to measure heat and moisture transfer are the constant temperature method [41, 42], the cooling method [43], and the temperature drop across materials of known and unknown resistances method [44]. The exception is the dynamic Angstrom method, in which the propagation velocity of a heat wave through a porous material is measured [26, 45]. The thermal diffusivity and subsequently the thermal conductivity of the material are obtained.

Zeng et al. developed a thin-film heater apparatus using a 10 mm thick gold film for uniform spatial distribution of heat [46]. Tests were conducted on opacified silica aerogel and thermal conductivity values of 10 to 15 [mW/(mK)] were reported. Harnath et al. used the transient, hot-wire probe method to determine thermal conductivity of silica aerogel prepared by varying molar ratios of water, methanol and catalyst [47]. This method yielded a maximum thermal conductivity of 0.1 [W/(mK)] and a minimum of less than 0.02 [W/(mK)] for the various compositions considered. Other measurements of thermal conductivity have been made using heat flux meters [48], hot disk thermal constant analyzers [49] and a laser flash apparatus [50]. As recommended by the ASME Standard, the effectiveness of thermal conductivity of fibrous sheets (fabrics) is tested by the guarded hot plate method [51, 52]. However, the guarded hot plate is based on the principle of thermal equilibrium, and it works best when the tested specimen can reach the steady-state

quickly. In porous materials such as fabrics, the multiphase phenomenon makes the heat equalizing process slow and unstable and thus making the conventional steady state techniques become ineffective or even inaccurate. Since 1987, the application of unsteady transient methods to fibrous materials were explored [6, 53]. However, researchers hold varied and even controversial opinions about usage of unsteady method to test fibrous material. Traditional steady-state methods are inconvenient due to the time (usually several hours) required to obtain a measurement and their restricted size of testing samples. Jirsak et al. [54] pointed out in their paper that the test result of effective thermal conductivity obtained using unsteady method was unreliable due to the heat convection inside the material invoked by the temperature gradient applied during testing. Morris [55], in a review of the literature on the thermal properties of textile materials, covering the years 1930 to 1950, classified the methods, then available, for measuring the thermal insulation of fabrics as the cooling method, the constant temperature method and the disc Method. Both the cooling method and the constant temperature method take into account heat loss from the outer surface by radiation and convection as well as conduction through the clothing system. For the cooling method [60-63], a hot body whose outer surface is exposed to the air is covered with fabric and the rate at which the body cools is determined. For the constant temperature method, the fabric is wrapped around a hot body and the energy required to maintain the body at this constant temperature is measured. Baxter and Cassie [56] defined the percent reduction of heat loss when the hot body is covered with fabric as the Thermal Insulating Value, T.I.V. In an alternative method [57], the equilibrium temperature at a constant power input is measured with and without the heat source covered with a test fabric. Again, the percentage decrease in heat loss with the fabric in place is a measure of the fabric's insulating power. The constant temperature method has been used extensively [66-72] by researchers because the conditions are similar to those which occur in actual wear. The disc method measures the heat flow across a test fabric to imitate the heat flow from the body to the outer surfaces of the clothing. In this method, the fabric is held in place between two plates which are maintained at different temperatures. The rate of heat flow (which has been measured in terms of power, current or the actual at flow) across the temperature gradient is measured and the thermal conductivity constant, λ, is determined by equation 2.1, Whenever this constant, λ, is used to describe the thermal conductivity of textile materials, it is re-defined as the rate of heat transfer per unit temperature gradient to include all possible modes of heat transfer down the temperature gradient, not just heat transfer by conduction. To emphasize this point, the term 'thermal conductivity' often is

replaced by 'thermal transmissivity', 'heat transmission' or instead, the reciprocal, 'resistivity' is used. The latter is expressed in units of Clo, Tog or T-ohm [58]. One *clo* corresponds to intrinsic insulation of business suit worn by sedentary resting male in a normally ventilated room at 21°Cand 50 % R.H and air ventilation of 0.1 m/s. In these conditions men feel quite comfortable. For winter clothes *clo* around 0.8 and for summer conditions *clo* around 0.5 is suitable (generally, lower R leads to state to be more cool) [59]. The total insulation (I_T) of a garment or ensemble including the air layer around the clothed body is given by the equation (2.13):

$$I_T = \frac{K(T_s - T_a) A_s}{H} \qquad (2.13)$$

where I_T is the total thermal insulation of clothing plus air layer, [clo], H is the power input, [W], K is the units constant = 6.45 clo [W/(m^2 °C)], A_s is the manikin surface area, [m^2], T_s is the mean skin temperature, °C, T_a is the ambient air temperature, °C [60].

One Clo is equal to 1.55 Togs and 15.5 T-ohms. A recent method for measuring thermal insulation [61] is somewhat similar to the disc method, but simpler. It is based on the principle that the ratio of the temperature drop across conductors in series, with respect to the direction of heat flow, equals the ratio of their thermal resistances. The thermal resistance of an unknown material is found by measuring the temperature drop across it and across a material of known resistance.

2.6.1   *Principle of alambeta Instrument*

Alambeta is an objective evaluation of warm-cool feeling of fabric developed at Technical University of Liberec.
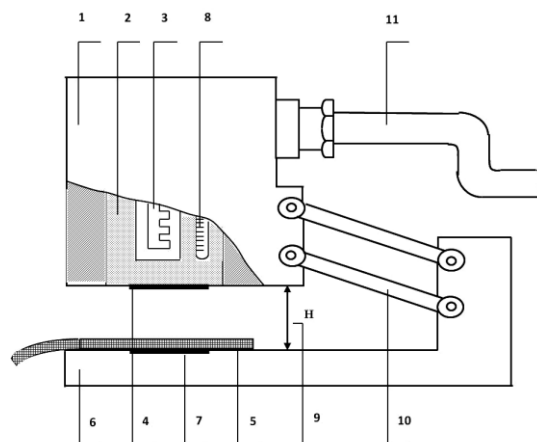
Figure 6. Schematic of alambeta instrument [62].

This computer controlled semi-automatic instrument calculates all the statistic parameters of the measurement. It also shows the instrument auto-diagnostics to avoid faulty instrument operation. The whole measurement procedure, including the measurement of thermal conductivity λ, thermal resistance R, maximum heat transfer rate q_{max}, sample thickness and the results evaluation, lasts less than 3 to 5 mins. As the objective measure of warm-cool feeling of fabrics, so called thermal absorptivity b [$Ws^{1/2}/(m^2K)$] is introduced [62]. The simplified scheme of the instrument is shown on figure 6. The principle of first version of this instrument protected by several patents depends on the application of ultra thin heat flow sensor 4, which is attached to a metal block 2 with constant temperature which differs from the sample temperature. When the measurement starts, the measuring head 1 containing the mentioned heat flow sensor drops down and touches the planar measured sample 5, which is located on the instrument base 6 under the measuring head. In this moment, the surface temperature of the sample suddenly changes and the instrument computer registers the heat flow course. Simultaneously, a photoelectric sensor measures the sample thickness. All the data are then processed in the computer according to an original programme, which involves the mathematical model characterizing the transient temperature field in thin slab subjected to different boundary conditions [19]. To simulate the real conditions of warm-cool feeling evaluation, the instrument measuring head is heated to 32 ºC (see the heater 3 and the thermometer 8), which correspond to the average human skin temperature, while the fabric is kept at the room temperature 22 ºC. Similarly, the time constant of the heat flow sensor, which measures directly the heat flow between the automatically moved measuring head and the fabrics, exhibit similar value (0.07 sec), as the human skin. Thus, the full signal response is achieved within 0.2 sec. The validity of thermal absorptivity as a new warm-cool feeling parameter of fabrics was confirmed by several tests where the results of relative subjective feeling of persons were compared with the values of thermal absorptivity found by means of the alambeta instrument [62]. The thermal properties were tested on alambeta instrument by following ASTM standard D1518. The measurement details are: (a) fabric sample size = (100 × 100) mm; (b) measuring head pressure = 200Pa ± 10%; (c) measuring head temperature = 34 ºC; (d) temperature of fabric =18 to 23 ºC; (e) relative humidity =10 to 80%, and (f) measuring area of head =1 dm^2 [63].

2.6.2   *C-Therm Thermal Conductivity Analyzer (TCi)*

The principle of the apparatus (TCi) is based on conductors in series with respect to the direction of heat flow. The ratio of the temperature drop across the conductors is equal to the

ratio of their thermal resistance. Thus, if the temperature drop across a material of known thermal resistance (standard resistance) and across a test specimen in series is measured, the thermal resistance of the test specimen can be evaluated. The TCi (figure 7) developed by C-Therm Company, measures the thermal conductivity of a small sample using the modified transient plane source (MTPS) method. The TCi consists of a sensor, power control device and computer software as shown in figure 7.

Figure 7. C-Therm (TCi) thermal conductivity analyzer [64].

A spiral-type heating source is located at the centre of the sensor where heat is generated. The generated heat enters the material through the sensor during which a voltage drop occurs rapidly at the heating source.

Table 4. Parameters of TCi thermal conductivity analyzer [65].

Parameters	Range of values
Thermal Conductivity Range	0 to 500 [W/(m K)]
Test Time	0.8 to 5 seconds
Minimum Sample Testing Size	0.67" (17mm) diameter
Maximum Sample Testing Size	Unlimited
Minimum Thickness	Nominally 0.02" (0.5mm), dependent on thermal conductivity of material
Maximum Thickness	Unlimited
Temperature Range	-58 to 392ºF (-50 to 200ºC)
Precision	Better than 1%
Accuracy	Better than 5%
Extra Hook-ups Required	None
Input Power	110-230 VAC 50-60 Hz
Standard test method	EN 61326-2-4:2006

The parameters of TCi thermal conductivity analyzer are given in table 4. The C-Therm TCi thermal conductivity analyzer allows determining accurate values for thermal conductivity and thermal effusivity of material without extensive sample preparation or damage to the sample. This highly accurate technique is based on the transient plane source (TPS) method. The primary difference between the traditional and modified TPS (MTPS) techniques is that the modified method offers a single-side interface compared to the double-sided interface requirements of the traditional version. The MTPS technique has many advantages in comparison to other available testing methods, for example guarded hot plate, hot wire, or hot probe. The non-invasive nature of the C-Therm TCi's MTPS sensors allows testing of materials of any size in situ or in laboratories without destruction of the specimen. Moreover, testing can be done in seconds with consistent and accurate results. The C-Therm TCi consists of a sensor, power control device, and computer software as shown in figure 7. A spiral-type heating source is located at the center of the sensor where heat is generated. The generated heat enters the material through the sensor during which a voltage drop occurs rapidly at the heating source. The thermal conductivity is calculated through the voltage drop data. [66, 67].

2.6.3   *Compression Test and Thickness Measurement Using The KES-FB3*

The KES-FB3 measures properties of compression and thickness. These properties are not dependent on direction and hence measurements in the warp and fill directions are not needed.
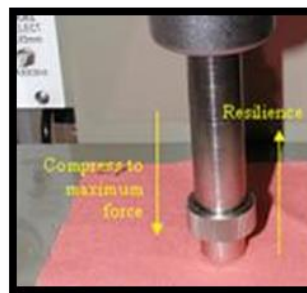
Figure 8. KES-FB3 Compression Tester [68].

The instrument applies a force up to 50 gf/cm^2 to a 2 cm^2 circular area at a constant velocity and measures the thickness with respect to the force per area applied. The device takes measurements during the compression process and the recovery process. Important properties of this instrument include compressibility, compression resilience, and thickness. EMC, denoting compressibility, is a comparison of the initial thickness measurement to the thickness at the maximum applied force. Higher values of EMC denote a greater compressibility. The compression resilience, RC, is the regain in thickness when the force

applied is removed. Larger values of the RC property denote a higher percent recovery from being compressed. Thickness is measured and reported at an applied force of 0.5 gf/cm^2 (see figure 8).

2.6.4   Kawabata (Thermolabo) - Small Hot Plate

KES-FB7 instrument and NT-H1 (where, N stands for NISHIMATSU and TOYONORI) works in accordance with the standard procedure ASTM 1518 and similar principle (surface: 10 cm^2, temperature difference between the two sides: 10 ºC). Thermolabo II evaluates warm or cool feeling through evaluation of q_{max} (Time: 1 min); measurement of thermal conductivity and heat diffusion (Time: 2 to 3 mins) and measurement of heat retention properties (Time: 2 to 5 mins). Kawabata Thermolabo unit is also known as the 'Sweating Guarded Hot Plate' or 'Small Hot Plate', is used for quantitative measurement of the cooling ability and the breathability of the fabric. It is designed to quantitatively measure the thermal comfort properties of the fabric. This test is performed on the Kawabata KES F7 under controlled environment at 21 ºC and 65% R.H shown in figure 9. Thermolabo II is composed of three components namely T-box (For detecting heat and heat retention), B.T box (Hot plate) and Water box (Constant temperature box) as given in figure 9. After the water is circulated through the water box, the sample of 50 x 50 mm is sandwiched between the BT Box (hot plate) and water box (cold plate). The BT Box pressure is set to 6 g/cm^2.The temperature of both plates is controlled. After reaching constant value, the heat flow loss of BT box is read by the panel meter and the thermal conductivity is determined.
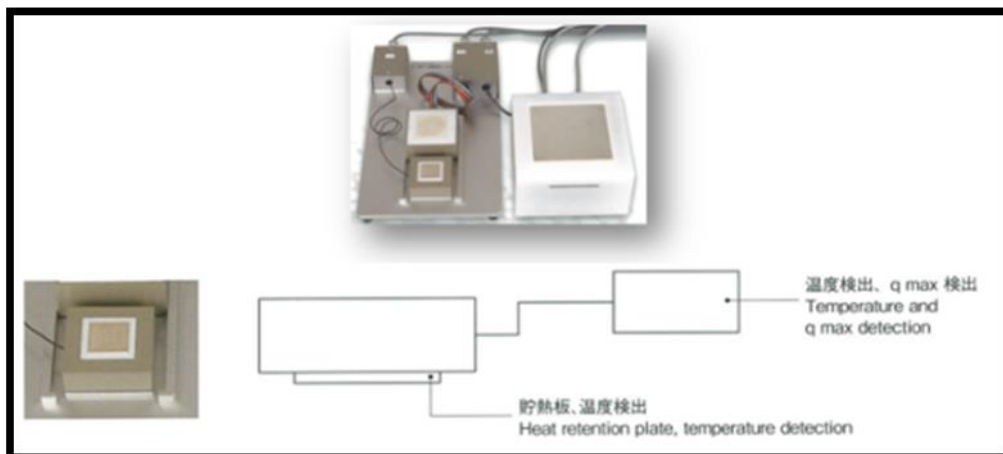
Figure 9. Components of KES Thermolabo II [69, 70].

Kawabata's Thermolabo device is also used to measure the warm/cool sensation of fabrics. When a preheated hot plate (simulation of human skin) is placed on a fabric sample, a heat flux versus time curve is generated. Maximum heat flow (q_{max}) is measured for a fraction of

a second after the hot plate contacts the fabric. This time approximates the warm/cool feeling experienced when fabric is placed on skin. The q_{max} value depends on the heat capacity and conductivity of the fabric and on the area of contact between the skin and fabric surface. Contact area is the most important determinant of how warm or cool a fabric feels to an individual [69, 70].

2.6.5   Measurement of Heat Retention Properties

The sample larger than 10 x 10, maximum of 20 x 20 cm is placed on the sample fitting frame on the B.T. box. Temperature of the B.T hot plate and the wind column shown in figure 10 is usually 10 ºC higher than room temperature.

Figure 10. Image of wind column attached during measurement [69, 70].

The temperature difference ΔT, is adjusted according to the purpose. The temperature of the hot plate of the B.T. box and the heat flow value, Q, on the digital meter is stabilized. Since slight changes in the hot plate have a great influence on the heat flow value, Q, the integrated heat flow value, Q_1, is read between 60 and 180 seconds, The average heat flow value, Q_2, can be displayed on the digital meter by pushing the RES button. The value Q is displayed in the units of W or mW. A constantly changing value Q can be recorded as a voltage signal from the heat flow output terminal. Ideally, measurement should be carried out when equilibrium is reached. The measurement should be completed within a couple of minutes. It is important to note that heat retention measurement is highly sensitive to air conditions such as temperature, air movement, etc. Therefore, good control of such variables will improve the quality of the data obtained. The relative insulation (α) of the sample is calculated by the following equation (2.14);

$$\alpha = \frac{HL_{WO} - HL_w}{HL_{WO}} \text{ x } 100 \text{ [\%]} \tag{2.14}$$

where, HL_{WO} is the heat loss from hot plate to the environment without sample and HL_W is the heat loss from hot plate to the environment through the sample. A standardized sample setting method makes it possible to accurately measure the simultaneous transport of heat and moisture through clothing materials. Stable wind velocities are obtainable, even in low velocity conditions [69, 70].

2.6.6   P.T. Teknik Thermal Manikin

Figure 11. Image of P.T.Teknik thermal manikin, University of Lodz.

Thermal manikin manufactured by P.T.Teknik system shown in figure 12 is used to evaluate whole garments systems (or components of garment systems) for heat and moisture management related to garment insulation and breathability. By measuring these values on a human form, garments are evaluated as they would be worn in the field, accounting for effects of fit, garment construction and design (including trapped air layers). Manikin heat loss measurements are much better approximations for realistic human heat loss than measurements made on the material system alone. Also, measurements can be calculated for individual zones or groups of zones, thus giving the ability to isolate effects of garment fit, design and layering. In addition, the manikin is articulated and has a movement system designed to emulate the pumping action created by walking. The manikin consists of several features designed to work together to evaluate clothing comfort and/or heat stress. Housed in a climate-controlled chamber, the manikin surface is divided into separate sections, each of which has its own sweating, heating, and temperature measuring system. with the exception

of a small portion of the face, the whole manikin surface continuously sweats. Insulation and breathability of garment systems are measured by the following ASTM F 1291 "Standard Method for Measuring the Thermal Insulation of Clothing Using a Heated Manikin" and ASTM F 2370 "Standard Test Method for Measuring the Evaporative Resistance of Clothing Using a Sweating Manikin, respectively". The P.T.Teknik thermal manikin, University of Lodz was used for the study shown in figure 11. The fabric was fixed only to left and right upper arm of the manikin. The results from the manikin were analyzed and calculated by:

$$\text{Thermal resistance (R value) } (m^2 K/W) = \left(\frac{\text{Skin temperature-Environment temperature}}{\text{Heat flow density} \left(W/m^2 \right)} \right) \times \left(\frac{\text{Area of upper arm}}{\text{Area covered by fabric}} \right) \quad (2.15)$$

$$\text{Clo} = \frac{\text{Thermal resistance (R value) } [(m^2 K)/W]}{0.155} \quad (2.16)$$

where, Area of left upper arm = 0.073 m^2, Area of right upper arm = 0.078 m^2 & Area of sample = 0.063 m^2
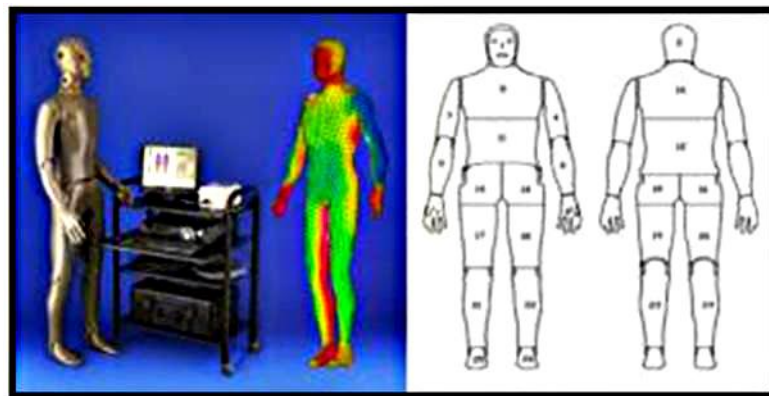
Figure 12. P.T.Teknik Thermal Manikin [71].

Continuous temperature control for the various body segments is accomplished by a process control unit that uses analog signal inputs from separate Resistance Temperature Detectors (RTDs). These evenly distributed RTDs are used instead of point sensors because they provide temperature measurements in a manner such that all areas are equally weighted. Distributed over an entire section, each RTD is embedded just below the surface and provides an average temperature for each section. Software establishes any discrepancy between temperature set point and the input signal, and adjusts power to section heaters as needed. Temperature controls are adjustable, by the operator, for each heater control.

2.6.7   Principles of Particle Image Velocimetry (PIV)

Particle Image Velocimetry (PIV) is a non-intrusive laser optical measurement technique for research and diagnostics into flow, turbulence, micro fluidics, spray atomization and combustion processes. The basic principle involves photographic recording of the motion of microscopic particles that follow the fluid or gas flow. Image processing methods are then used to determine the particle motion, and hence the flow velocity, from the photographic recordings. Provided there are enough particles within the area of flow under investigation, the entire velocity field of the flow can be determined. The near-instantaneous velocity field is of particular importance. PIV therefore has all the advantages of a flow visualization method, but it can also provide valuable quantitative information. Once the velocity field is known, data such as vorticity and strain are easily obtained, and if there are sufficient PIV recordings, even the turbulence intensity can be estimated. The PIV (figure 13) belongs to the family of methods for fluid flow measurement and visualization. It allows measurement in a wide range of flow speeds.
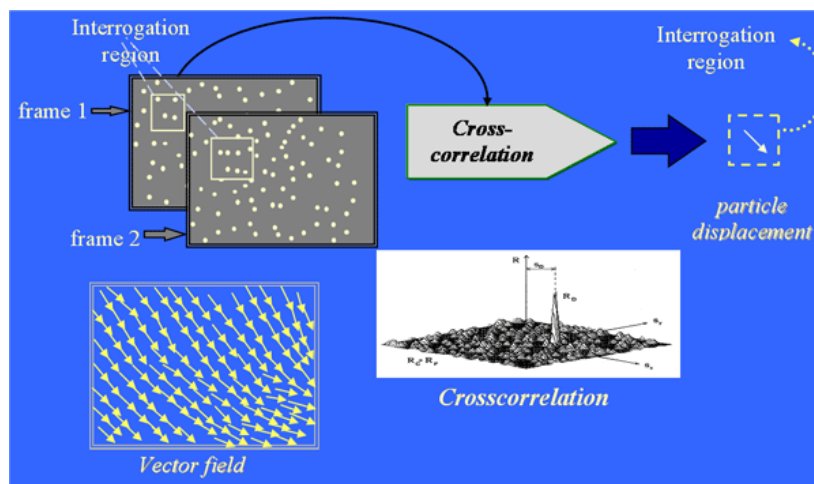
Figure 13. PIV principle [72].

The basic condition for the successful measurements deals with the property of the examined medium. The basic building block of the measuring system is a laser PIV system (Dantec Dynamics). The PIV measurement technique allows obtaining information about the distribution of velocity currents in 2D array in a flowing fluid. In most applications tracer particles have to be added to the flow. These particles have to be illuminated in a plane of the flow at least twice within a short time interval. The motion of the fluid is visualized by the seeding particles that are usually added to the flow. The system displays and analyzes the particles movement in selected planar light cut. Conveniently placed light plane is generated with a powerful laser and optical system component. The position of

particles in the plane of light section is recorded by some device sensitive to light, such as photographic film or a charge-coupled device camera detector. The light scattered by the illuminated particles has to be recorded via a high quality lens either on a single photographical negative or on two separate frames on a special cross correlation CCD sensor. Evaluation thus recorded is based on the fundamental equation expressing relationship between speed, distance, and time, where distance represents the displacement of particles entrained in the fluid flowing in a defined time interval between two laser pulses [73]. The local displacement vector of the images of the tracer particles of the first and second illumination is determined for each area of the interrogation plane by means of statistical methods. In order to be able to handle the great amount of data which can be collected employing the PIV technique, a sophisticated post-processing is required. Therefore nowadays the photographical PIV recording is digitized after development by means of scanners. The output of the CCD sensor is stored directly in real time in the memory of a PC. In PIV, the velocity vectors are derived from sub-sections of the target area of the particle seeded flow by measuring the movement of particles between two light pulses. The flow is illuminated in the target area with a light sheet. The camera lens images the target area onto the sensor array of a digital camera. The camera is able to capture each light pulse in separate image frames. Once a sequence of two light pulses is recorded, the images are divided into small subsections called interrogation areas (IA).

$$C(s) = \iint_{IA} I_1(X) \cdot I_2(X-s)dX$$
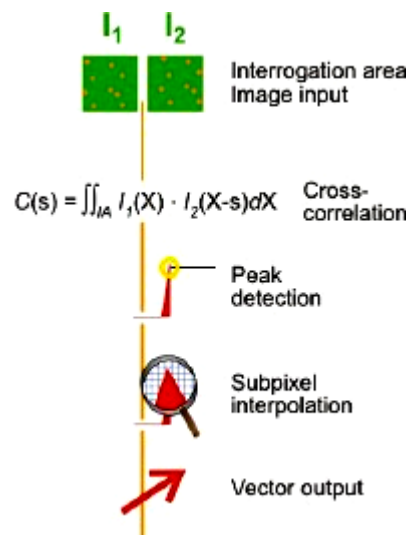
Figure 14. The correlation of the two interrogation areas, I_1 and I_2 [72].

The interrogation areas from each image frame, *I₁* and *I₂*, are cross-correlated with each other, pixel by pixel. The correlation produces a signal peak, identifying the common particle displacement. An accurate measure of the displacement - and thus also the velocity - is achieved with sub-pixel interpolation. A velocity vector map over the whole target area is

obtained by repeating the cross-correlation for each interrogation area over the two image frames captured by the camera. Figure 14 shows correlation of the two interrogation areas, I_1 and I_2, results in the particle displacement, represented by a signal peak in the correlation. For a better understanding of the special technical solution in the field of laser illumination, some general aspects of the PIV technique have to be mentioned in short:

Velocity lag: The need to employ tracer particles for the measurement of the flow velocity requires checking carefully for each experiment whether the particle will faithfully follow the motion of the flow. Experience shows that small particles will follow the flow better even in high speed air flows.

Illumination: For applications in gas flows a high power light source for illumination is required in order that the light scattered by the tiny tracer particles will expose the photographic film or the video sensor. A more powerful light source (e.g. a high energy laser pulse) will allow the use of smaller tracer particles and minimize the problem of the above mentioned velocity lag.

Duration of illumination pulse: The duration of the illumination light pulse must be sufficiently short so that the motion of the particles is "frozen" during the pulse exposure in order to avoid blurring of the images.

Time delay between illumination pulses: Time delay between the illumination pulses has to be long enough to enable the displacement between the images of the tracer particles to be determined with sufficient resolution and short enough to avoid particles with an out-of-plane velocity component leaving the light sheet between subsequent illuminations.

Laser Technique and the Development of PIV During the Past Decades

The development of PIV during the past 20 years has been strongly influenced by the fact that analog recording and evaluation techniques have been replaced by digital techniques. The improvement of computer hardware with respect to processor speed and memory size allows the handling of complete digital PIV recordings by a personal computer. and progressive scan video cameras allow users to store the images of the tracer particles on separate frames for each illumination with a resolution of 1040 x 1320 pixels. A quality equivalent to evaluation of 35 mm photographic films in the past. Besides the use of digital recording and evaluation techniques, the development of reliable high power laser sources was of great influence for the improvement of PIV and its application in air flows. The required high energy light pulse for high speed air flow PIV (as used in the investigation of aircraft aerodynamics) was first made possible by the use of semiconductor lasers. Commercially available Nd:YAG lasers offer sufficient pulse energy of about 100 up to 750

mJ. A further advantage of laser sources is the fact that they emit monochromatic light, which can be bundled into thin light sheets for illuminating and recording the tracer particles without chromatic aberrations. For PIV the fundamental wavelength of 1064 nm is frequency-doubled to a wavelength of 564 nm in visible light. For the PIV measurement shown in figure 14, the parameters were selected after the textile sample directly touches the plate, where the transfer is caused by thermal conduction. The medium (air) above the sample was seeded with olive oil seeding particles for fluid flow visualization. with the increase of free surface temperature of textile sample, the thermal convection started working. One can observe this phenomenon by the fluid motion tracking system enabled by laser [72].
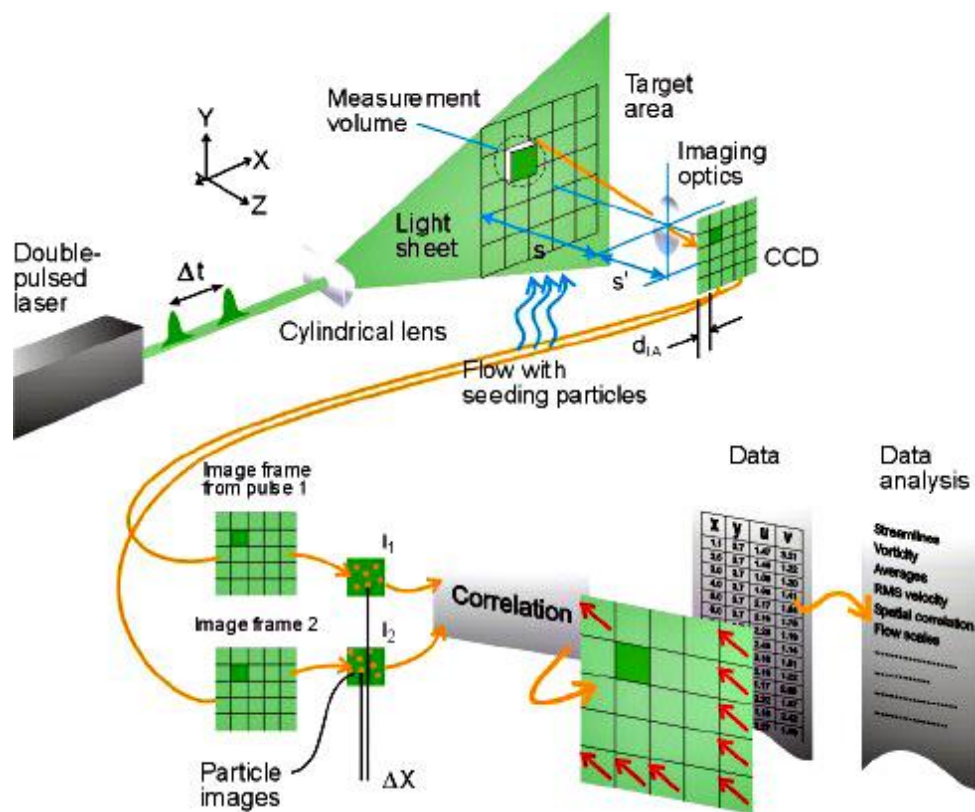
Figure 15. Working principle of PIV-CCD: charge-coupled device [72].

Experimental arrangement of the PIV measurement technique shown in figure 15 consists of (1) Hi-Since 12 bit digital camera, (2) light source - New-Wave Gemini pulsed laser with cylindrical optics expansion of the beam across the board cut, (3) laser beam illuminating the field of observation, (4) testing chamber, (5) textile sample, (6) heating plate, (7) thermocouples, and (8) the PC. The standard test method ASTM D7140M-13 was used.

Features of PIV

The salient features of PIV are (a) The technique is non-intrusive and measures the velocities of micron-sized particles following the flow; (b) Velocity range from zero to

supersonic; (c) Instantaneous velocity vector maps in a cross-section of the flow; (d) All three components may be obtained with the use of a stereoscopic arrangement and (e) With sequences of velocity vector maps, statistics, spatial correlations and other relevant data are available. Results are similar to computational fluid dynamics, i.e. large eddy simulations, and real-time velocity maps are an invaluable tool for fluid dynamics researchers.

PIV Imaging

Recording both light pulses in the same image frame to track the movements of the particles gives a clear visual sense of the flow structure. In air flows, the seeding particles are typically oil drops in the range 1 μm to 5 μm.
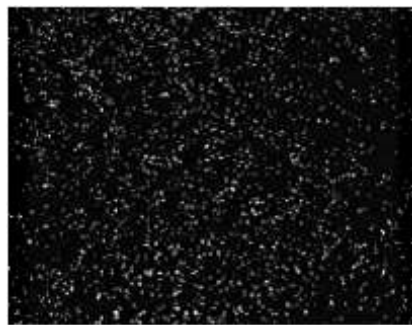
Figure 16. Double-pulsed particle images [72].

For water applications, the seeding is typically polystyrene, polyamide or hollow glass spheres in the range 5 μm to 100 μm. Any particle that follows the flow satisfactorily and scatters enough light to be captured by the camera can be used.

$$\omega = \frac{\partial v}{\partial x} - \frac{\partial u}{\partial y}$$

Vector map and derived vorticity, ω
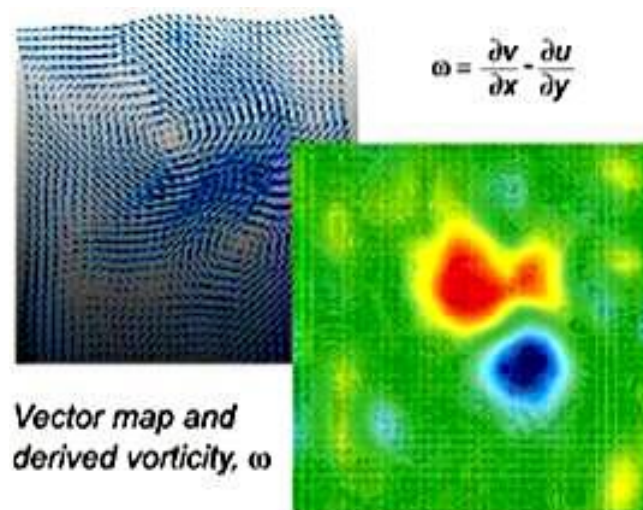
Figure 17. Vector map and derived vorticity [72].

The number of particles in the flow is of some importance in obtaining a good signal peak in the cross-correlation.As a rule of thumb, 10 to 25 particle images should be seen in each interrogation area. When the size of the interrogation area, the magnification of the imaging and the light-sheet thickness are known, the measurement volume can be defined.

2.7 Electrospun Nanofibrous Layers and Thermal Insulation

Recently many researchers have claimed advanced thermal insulation with nanofibrous layers.
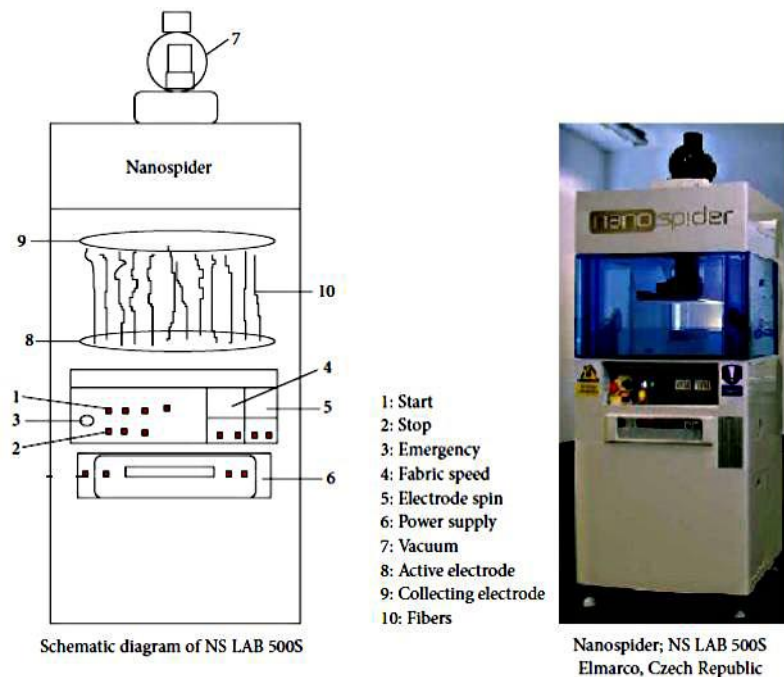
Figure 18. Schematic diagram and photograph of electrospinning setup (NS LAB 500S, Elmarco) [10].

Electrospinning is carried out using nano spider technology as a modified electrospinning technique, Nanospider laboratory machine NS LAB 500S from Elmarco s.r.o (figure 18). Electrospinning is widely accepted as a technique to fabricate submicron polymer fibers. It is a fiber-forming process, where high voltage is used to create an electrically charged jet of polymer solution or melt from the needle. The polymer solidifies as it travels towards the collecting plate, often producing nanometer scale fibers [2-5, 74]. Nanospider shown in figure 19 is a modified electrospinning method which requires the use of a high-voltage electrostatic field to create an electrically charged stream of polymer solution or melt. The innovative idea of nanospider is based on the possibility of producing nanofiber from a thin layer of liquid polymer. In this case, Taylor cones (the source of nanofiber) are created on the surface of a rotating roller, immersed in a polymer solution. Because the Taylor streams

are formed next to each other, throughout the entire length of the roller, this revolutionary idea produced many advantages, such as high productive ability.
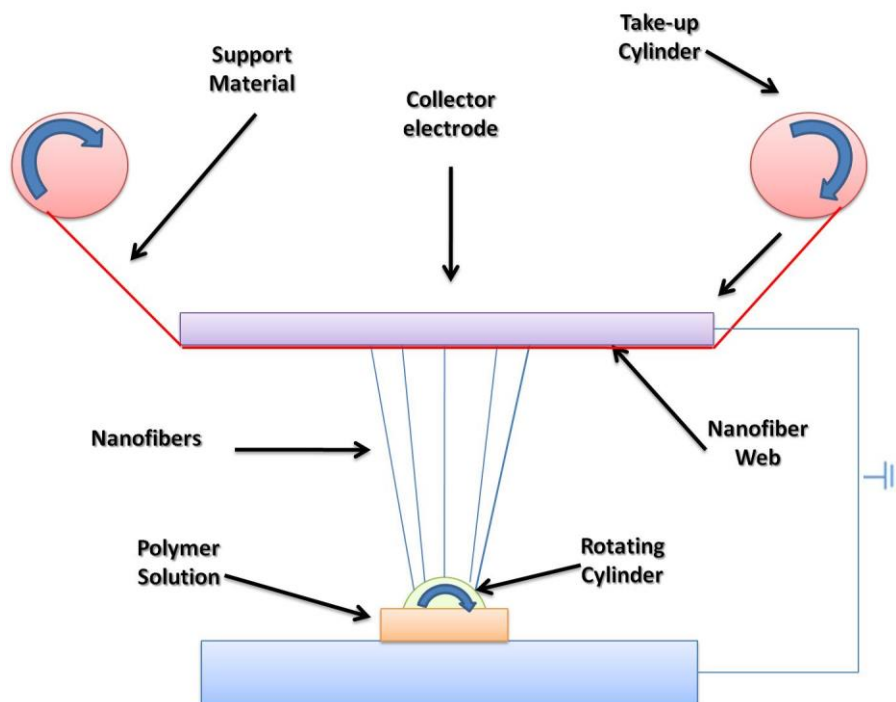
Figure 19. Schematic of electrospinning setup "Nanospider" [75].

This commercial method for production of polymeric nanofiber is used in industrial range. This is a simple and versatile method for production of ultrathin fibers from a variety of materials that include polymers. In addition, Nanospider has the ability to process a wide range of polymers in diameters of 50 to 300 nm into nonwoven webs [23].

2.8 Effect of Variables on Thermal Insulation

The thermal insulating value of a textile material is almost totally dependent on the amount of air in the material. The reason is simply because the thermal insulating value of air is significantly greater than that of fibers. One source [76] gives the thermal insulation of a fiber pad (density of 0.5 g/cm^3) to be about one sixth that of air. Therefore it is logical that the thermal insulating power afforded by a textile material is primarily determined by its thickness and density. Researchers have verified that thermal insulation varies directly as the thickness of the material, whether the variation in thickness was obtained by adding successive layers of the same material [63, 69, 77-82], by altering the thickness of the material by changing the pressure per unit area [77-79] or by testing a range of fabrics with varying thickness [64, 65, 70, 79]. For all practical purposes, the first method holds the density of the material constant while the effect of increasing thickness on thermal insulation

is measured, with the result that the thermal insulation is additive for each successive layer [80-82], if the surface of the material is smooth [83]. The second method increases the density as the thickness of the material is decreased. This results, of course, in a negative correlation between thermal insulation and density [75, 77, 82, 85], to a limit where any further change in density has little or no effect on changing the thermal insulation [81]. However, when Speakman and Chamberlain [77] held the thickness of a mass of loose fibers constant and varied the density from 0.01 to 0.16 g/cm^3, they found that the change in thermal insulation of the mass was insignificant. This apparent discrepancy may be explained in a paper by Peirce and Rees [81]. They stated that the thermal insulating value of a low density batting approaches that of still air. Any change in density of this batting causes a decrease in thermal insulation. When the density of the batting is reduced, convection within and radiation through the batting decreases its insulating power. When the density of the batting is increased, the increase in heat transfer is mainly by conduction through the fibers. Since the fibers have a higher conductivity than air, the thermal insulation again will be decreased. It would appear that the variation in density is not great enough in Speakman and Chamberlain's work to dramatically change the mode of heat transfer and thus give a significant change in thermal insulation. Changes in thermal insulation due to wear, or after laundering or dry cleaning are closely associated with changes in thickness. Wear tends to decrease fabric thickness and therefore tends to decrease thermal insulation. Cleaning the fabric will increase its thickness and thus its thermal insulation if the fabric shrinks or if it is fluffed up during drying or pressing [62, 86-88]. Starching has no effect on thermal insulation [84]. Two factors determine the effect that 'fabric' construction has on thermal insulation. The first factor, of course, is the amount of air contained within the structure. Thus napped and pile fabrics [77, 85], quilted waddings and felts [56], and polyurethane foams [80, 86] have greater thermal insulating power than smooth fabrics. However, the insulation value differed very little when the count of a plain weave fabric was varied from 23 to 50 threads per inch in the warp or from 21 to 43 threads per inch in the weft [87]. The second factor is the direction of fiber arrangement, that is, whether the fibers lie parallel or perpendicular to the fabric surface. Finck [88] showed that thermal insulation was two to three times greater when the fibers were arranged parallel rather than perpendicular to the fabric surface. Bogaty et al's work [78] confirmed these results. In addition, Speakman and Chamberlain [77] found that a parallel fiber arrangement gave a higher insulating value than a disoriented fiber mass. These results support the findings of Gillings et al [89] that the warmth to weight factor of polyester battings is higher

than that of pile fabrics. No relationship has been found between the weight of fabrics and their thermal conductivity [56, 85]. However, Rees [82] pointed out that heavier fabrics would tend to be thicker and so have a higher thermal insulating power than thinner, lighter fabrics. Aelion and Brown [85] found cotton to be a better insulator than wool. In contrast, several researchers [31, 64, 69, 80, 85] found wool to be the best insulator and cotton the worst. In the cases tested by these researchers, the synthetic fibers fell in between these two fibers. It has been shown that it is the space at which the garment is worn from the body rather than the kind of fiber or material from which it is made, which has the greater effect on its value as an insulator. Black and Matthews [87] determined that maximum insulation occurs when there is 0.3 to 0.375 inches of air between the body and the fabric; Rees [82] gives this value to be 0.35 inches and Latham [57] as 0.19 inches. In testing several sets of underwear-outerwear combinations, Fonseca [90] found the underwear layer simply replaced this still air layer between the outer fabric and the body without adding insulation to the ensemble. He concluded that the outer fabric was the deciding factor in determining the thermal characteristics of complete clothing systems. Researchers [60, 62, 71, 82] have discovered this was particularly true if the thermal insulation of the fabrics was measured in a wind, when the thermal insulation drops sharply to a limiting value as the wind velocity increases. This drop is less severe for closely woven fabrics than for open, porous fabrics [82, 91]. Niven [92] found that the drop in thermal insulation was less if the wind was blowing parallel, rather than at right angles, to the sample. Other external atmospheric conditions affect thermal insulation also. For instance, thermal insulation decreases as the temperature increases [63, 82, 89, 90]. Hammel [93] calculated an increase of 0.5 Clo/in. for fur when the temperature was lowered from 20 to -50 ℃. Further, thermal insulation varies inversely with the relative humidity of the air [41, 42] with a relationship approximating a second order equation [79, 94]. Black and Matthews [87] showed that the effect of increasing moisture is most pronounced over the range of 0 to 75% R.H. However, Rees [82] stated that any change in ambient humidity which would be met in wear would have little effect on the thermal insulation of the material, provided there was no evaporation from the fabric surface. Rees statement would agree with Black and Matthew's finding if Rees was referring to ambient conditions in Great Britain where the relative humidity would be above 75% for the majority of the year. Figures have been given for the decrease in thermal insulation with the increase in relative humidity - 10% for wool and 3% for cotton with a 55% increase in relative humidity [82], and a 1% decrease for each 5% increase in water vapor [95]. Further, a linear relationship has been found to exist between thermal insulation

and the moisture content of a fabric [94-96]. Hollies [42] found that thermal insulation is independent of the standard regain of fibers, as measured at 22 °C and 65% R.H. However, all fabrics regardless of fiber content, have approximately the same thermal insulating value when wet [82, 87], this being about three times less than the insulating value of a dry fabric. Finally, when the air, in and around the fur of a pelt, is replaced by the gas Freon, the insulation per unit thickness of the fur is increased about four times [97]. In summary, the factors that influence thermal insulation are thickness, density, porosity, number of layers, wind velocity, temperature and moisture.

2.8.1   *The Air Layer - Effect of Thickness of Air Layers on Thermal Resistance*

All yarn and fabric arrangements consist largely of fiber and air (ignoring most finishes), with fiber dominating in terms of mass and visibility and air dominating in terms of volume. For example, the volume of air present in woven fabrics ranges from 60 to 90% and in knits from 85 to 95%, while products such as quilts are reportedly comprised of as much as 95 to 99% air [98]. As the thermal conductivity of fibers ranges from 5 to 20 times that of air [99, 100], it is the air trapped within the yarn, fabric, and garment (or product) itself that contributes most to the overall thermal resistance. The major contribution of still air to thermal resistance of flat textiles has lead to thickness of materials being used to estimate thermal resistance. However, thickness is only an appropriate predictor if a standard value of thermal resistance per unit thickness is appropriate, and thickness of materials (difficult to determine), is measured accurately. For example, many fabrics considered to be effective insulators, have a high proportion of projecting surface fibers which trap air and instruments commonly used to measure thickness cause compression of the specimen. These factors affect the reliability of the thickness: thermal resistance relationship [101]. The linearity of the relationship between thickness and 'dry' thermal resistance was questioned as early as 1955 and in the case of multiple layers of thin, lightweight materials (and the air layers between them), has been shown to be non-linear under certain conditions [102, 103]. Air layers may form under, between, and over fabric surfaces contributing to the thermal resistance of multiple-layer materials. The properties of these air layers are affected by their thickness, shape, and distribution. When two-dimensional fabrics are wrapped around the human body the geometry of the surface changes, while stacking fabrics one over another may result in additional air being enclosed between fabrics, and not necessarily uniformly distributed. Textile covers are typically non-homogeneous as the proximity of the fabric layers to each other and the number of layers may vary over the surface of body. For

example, the head and hands are often covered only with stable still air (i.e. the boundary layer), which contributes approximately 0.02 to 0.12 [(m^2 K)/W] to the thermal resistance of the body [99, 104]. This boundary layer thus provides some thermal protection to both clothed and nude bodies (although the contribution of the boundary layer to thermal resistance is considerably reduced in moving air). Thermal properties of fabrics with enclosed or underlying air layers have been investigated using laboratory techniques, both flat [100-103], those simulating the 3-dimensional arrangement of materials during use [105, 106], and in actual use [107, 108]. As the size of the air gap increases the relationship between thermal resistance and the number of layers has been shown to become non-linear [102, 109, 110]. Wilson, et al., [110] showed the magnitude of this difference was affected by the thickness of the underlying air gap, the arrangement of the layers, the number of layers, and the distribution of air layers within the assembly. Air gaps between the component layers in form-fitting clothing are considered to increase thermal resistance from 5 to 50% (increases are particularly apparent in relatively small air spaces) [94, 98, 108-110]. In infant bedding, where air spaces of ≤ 180 mm in height have been reported, increases of up to 100% in 'dry' and 300% in 'wet' thermal resistance of dry fabrics have been attributed to the air layer [109, 110]. Using a trace gas method, the introduction of an air layer under a jacket (size and volume not specified) by the use of a spacer showed the exchange of the jacket microclimate air with air from the ambient environment increased by 140 to 300% [111]. Several smaller air spaces have also been shown to provide greater thermal resistance when distributed throughout the bedding than when the same total thickness occurred as one large air space under the first layer [110]. Both the size and distribution of air layers affect thermal resistance.

2.8.2   *Variables Affecting Distribution of Air Layers within Fabrics and Garments*

Investigators have attempted to define variables which affect the distribution and thickness of air spaces within, and thermal resistance of, a garment assembly. Variables such as i) fabric characteristics (including packing density, fabric mass, fiber fineness, yarn count and twist, hairiness, compressibility) [112, 113]; ii) fabric manufacturing processes (such as surface napping and application of finishes); iii) style of garment (including fit, multiple layers) [107], fit and product design [114, 115], and surface area and geometry effects [116] and iv) conditions of use (such as the ambient environment, air movement; and intensity and type of activity of the wearer/user) are some of those that have been evaluated. Many of these issues/variables have been addressed in the literature [99, 117, 118]. However,

garment design [115], the trapping of air, and conditions of use [107, 119, 120] have become the focus of systematic research only from the 1980s.

2.8.3   Convection within Air Spaces

Convection involves the transmission of energy or mass by movement of the medium and occurs as a result of the movement of large masses of molecules in the form of air currents [121]. Air movement occurs as a result of natural or forced convection with the rate of convective heat loss affected by the air velocity and the temperature gradient. The effect of convection in air spaces on thermal resistance has been investigated, generally using thermal hotplates [124-127], humans [122], and articulated manikins [114, 123]. Air spaces $\geq$ 6 to 8 mm are associated with reduced thermal resistance per unit thickness (demonstrated using a guarded hot plate apparatus) [124]. Changes to the thermal resistance of the air space may be due to convection within the space (although losses considered negligible in air spaces $\leq$ 10 to 13 mm thick) [116, 125]. Air spaces > 13 mm have been linked to a significant reduction in thermal resistance of assemblies of various types [109, 110], single- and multiple-layer arrangements of thin fabrics [126] and unspecified surfaces [127].

2.8.4   Thickness, Orientation and Height of Air Layers

Most published test methods used to measure thermal resistance of fabrics attempt to minimize the air space [128] or specify a standard air space (e.g. an air space of 13 mm) [125] in an attempt to control the variability when air spaces are incorporated into the test structure. The effects of introducing either standard or non-controlled air layers, both small (0.2 to 6.3 mm) [125, 129, 130] and large (up to atmosphere) [101-103, 130-132] have been investigated, presumably because of the wish to better approximate real conditions. Results suggest thermal resistance of the fabric and air space differs according to the characteristics of the air gap. For example, gaps may be irregularly shaped, of varying thickness and/or distributed in varying ways throughout the assembly [109, 110], orientated horizontally or vertically [116, 127, 131], and/or open or closed to the ambient environment [110] suggested convection in very large air space, over a critical thickness of horizontal air space, may reduce thermal resistance ('dry') per unit thickness of the air space. A maximum thermal resistance at approximately 20mm was reached and then declined slightly as the thickness of the air space increased. 'Wet' thermal resistance provided by an air space under a standard dry fabric increased to a point (~40 mm) beyond which any further increases in the thickness of the air space did not increase thermal resistance [109]. The orientation and thickness of the air layers appears to also affect the tendency for convective currents to form

within air spaces as does whether the space is open to the ambient environment or enclosed. Differences in heat loss through layers are also dependent on the orientation of the layers. For example, heat transfer in horizontal air layers has been shown to be greater than that occurring in vertical layers [116, 127] and in inclined layers $\geq 70^\circ$ [131]. Fowle provided some insight into the behavior of narrow, vertical layers of air (presumably within enclosed systems) when one vertical surface is heated. Heat transfer through horizontal air spaces was reportedly twice that of vertical ones for air spaces up to 12 mm. The rate of convective heat transfer was independent of the thickness of the layer (or distance between the surfaces) but proportional to the square of the temperature difference between the heated and unheated surfaces and also to the cube of the distance between the two surfaces [127]. At a critical flow speed (which occurred above 20 °C temperature difference and a width of 12 mm) turbulence affected the relationship. This is consistent with the onset of convection [126] at an air space thickness of approximately 13 mm. Fowle [127] considered smooth vertical surfaces, and a closed system was implied (which may account for the differences between these findings and those from several studies on textiles in which heat transfer through horizontal air spaces has been more common). Spencer-Smith also reported greater heat loss in horizontal than vertical air layers between fabrics, using a hot plate and a range of different fabric types (i.e. linen drill, cotton mesh, worsted and blends of 'Leavil' and wool). Differences increased with increasing difference between the surface and the air temperatures (Differences range from 10 to 45 °C). He published findings on the movement of heat through clothing under dry steady-state conditions providing a useful summary of the effect of air layers and their orientation on thermal resistance [116]. Equations for calculating heat loss through clothing layers (in the absence of moisture) under differing conditions are given, although the extent to which they have been validated is unclear. Hollands et. al. [131] investigated the effect of varying the Rayleigh number (sub-critical to 105) of horizontal and inclined air layers (0 to 70º) with a large aspect ratio and which were heated from below. A theoretical result was compared to the experimental data. The theoretical solution predicted Nusselt numbers in good agreement (maximum error approximately 5%) for all experimental data except that obtained for air layers inclined at 700. (Note the theoretical result was confirmed experimentally for air layers inclined at 150 only and the materials used to form the confining surfaces were metallic rather than fabric). Theory suggested that if the fluid flow was independent of the *x* direction, the Nusselt number was a function of the relationship *Ra* cos f (where, *Ra* is the Rayleigh number and *f* the angle of the inclined air layer). From the literature review, it is apparent that not much

study has been conducted to analyze thermal properties of insulation materials at subzero temperatures. There are gaps in detailed comparison of insulation materials to identify the one best suited for thermal insulation applications and a quality assessment of all type of insulation materials. There is also an implied need to explore alternative methods and techniques to those which exist already.

2.9 Silica Aerogel As Insulating Material

Aerogel is one of the highly advanced thermal insulating materials used to treat nonwoven fibrous structures. Aerogel have a very low solid material density ~0.02 to 0.4 g/cm^3 and a very high internal surface area ~900 to 1000 m^2/g. Based on the combination of its solid microstructure, low density, and silica composition, aerogel show great promise as an insulation medium [132]. However, such advanced thermal insulating composite materials are very expensive. Hence their usage is limited mostly to high- performance applications. Because of advances in the thermal performance of aerogel materials, silica aerogel is being considered as a medium to fill the interstitial space among fibers, thereby mechanically obviating any potential internal convection and radiation.

2.9.1   Heat Transfer Phenomenon in Silica Aerogel

The passage of thermal energy through an insulating material occurs through three mechanisms: solid conductivity, gaseous conductivity, and radiative (infrared) transmission. The sum of these three components gives the total thermal conductivity of the material. Solid conductivity is an intrinsic property of a specific material. The improvement of thermal resistance of the fabric can be achieved by decreasing the thermal conductivity. Fricke et al. observed that both the solid conductivity and the gas conductivity were proportional to the density as shown below:

$$\lambda_{gas} \sim \rho^{-0.6} \tag{2.17}$$

$$\lambda_{solid} \sim \rho^{1.5} \tag{2.18}$$

Hummer et al. using these relations derived the following relation for the radiative conductivity, which is a relative equation for the thermal conductivity of opacified silica aerogel:

$$\lambda_{total}(\rho) = \lambda_{solid}\left(\frac{\rho}{\rho_0}\right)^{1.5} + \lambda_{gas}\left(\frac{\rho}{\rho_0}\right)^{-0.6} + \lambda_{rad}\left(\frac{\rho}{\rho_0}\right)^{-1}\left(\frac{T}{T_0}\right)^{3} \tag{2.19}$$

where ρ (kg/m^3) is the density; λ_{total}, λ_{gas}, λ_{solid}, and λ_{rad} [W/(mK] are the total conductivity, the conductivity for gas conduction, the conductivity for solid conduction, and the radiative conductivity, respectively; T (^{o}K) is the temperature, and the index 0 means that parameters are related to a reference material from an aerogel [133]. Aerogel is made of more than 90% of air, having extremely low weight, transparency, and excellent thermal conductivity. Aerogel is an ideal material for thermal insulation due to all these properties [134, 135]. However, silica aerogel possess a very small (~1 to 10%) fraction of solid silica. Additionally, the solids that are present consist of very small particles linked in a three-dimensional network with many "dead-ends". Therefore, thermal transport through the solid portion of silica aerogel occurs through a very tortuous path and is not particularly effective. Further decrease in thermal conductivity of aerogel can be observed if evacuated below 50 hPa; thermal conductivity decreased because of elimination of pore gas. Super insulations with extremely low thermal conductivities can be implemented with evacuated highly porous powder, fiber, or gel spacers. Due to the Knudsen effect, thermal conductivity can become lower than that for the still air, that is, even less than 25 [mW/(m K)] [136].
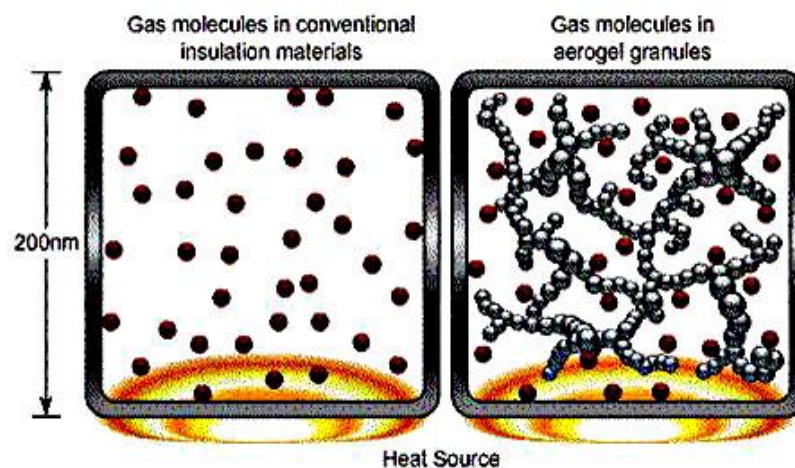
Figure 20. Gas molecules in conventional insulation material and aerogel granules [136].

For example, silica aerogel is a highly porous material with pore diameters in the range of 10 to 100 nm. The porosity is more than 90% with a thermal conductivity lower than that of air, which makes these aerogel a highly insulating material. The space not occupied by solids in an aerogel is normally filled with air (or another gas) unless the material is sealed under vacuum. These gases can also transport thermal energy through the aerogel. The pores of silica aerogel are open and allow the passage of gas through the material. The final mode of thermal transport through silica aerogel involves infrared radiation [133]. Soleimani Dorcheh and Abbasi reported the synthesis of nanostructured silicon based transparent

aerogel with pore diameter 20 to 40 nm [137]. Water molecules do not interact strongly with the hydrophobic aerogel pore walls and therefore will not lose much energy in colliding with the wall and the progress of these molecules will not be significantly slowed. Accordingly, the aerogel possesses high permeation selectivity between water vapor and agent vapors.

2.9.2 *Pore Structure of Silica Aerogel*

Structural features of aerogel have an unusual combination of high porosity and small pore size, making porosity characterization by conventional techniques, such as mercury intrusion, thermoporometry, and nitrogen adsorption/desorption, very difficult. All these techniques are based on the application of capillary pressures on the aerogel network, which may cause large volumetric compressions, leading to incorrect values for pore size and volume [138]. Aerogel are characterized with a very low permeability which can be explained in terms of pore size suitable for transport of water vapors/gases but not for water molecules [139].
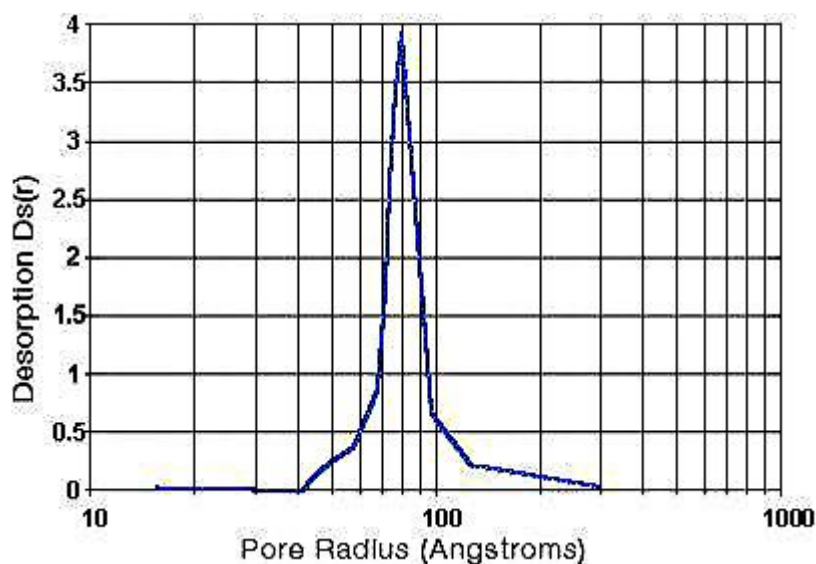
Figure 21. Desorption curve [140].

The International Union of Pure and Applied Chemistry has recommended a classification for porous materials where pores of less than 2 nm in diameter are termed "micropores", those with diameters between 2 and 50 nm are termed "mesopores", and those greater than 50 nm in diameter are termed "macropores". Silica aerogel possess pores of all three sizes. However, the majority of the pores fall in the mesopore regime, with relatively few micropores [140]. It is very important when interpreting porosity data to indicate the method used to determine the data. Because of the limitations of the methods to measure porosity, a major problem in aerogel science remains unresolved. If the mass, density, and total pore volume of an aerogel are measured, it is apparent that there is a substantial amount of

porosity that is not accounted for. This obviously results from the drawbacks of using gas adsorption to determine the pore volume. It is assumed that the "missing porosity" lies in the micro- or macropore regimes, areas not measured effectively by this method. One final important aspect of the aerogel pore network is its "open" nature and interconnectedness. Pores in various materials are either open or closed depending on whether the pore walls are solid or themselves porous (or at least "holey"). A macroscopic example of an open-pored material is a common sponge, while "bubble wrap" packaging is an example of a closed-pore material. In a closed-pore material, gases or liquids cannot enter the pore without breaking the pore walls. This is not the case with an open-pore structure. In this instance, gases or liquids can flow from pore to pore, with limited restriction, and eventually through the entire material. It is this property that makes silica aerogel effective materials for gas phase catalysts, microfiltration membranes, adsorbents, and substrates for chemical vapor infiltration [140].

Chapter 3. Experimental Materials and Methods

3.1 Materials

In this study, 50:50 ratio compositions of six polyester/polyethylene non-woven fabrics treated with aerogel were used. Polyester is the most versatile, most cost effective and most widely used fiber in various applications. It is perfect for any application where a flexible non-woven fabric is required. It is also often supplied as the waterproof material and insulator for the winter clothing. It retains the physical properties when wet and stays extremely stable during humidity changes. This strong and light material resists moisture, staining and chemical attack. Polyethylene has excellent chemical resistant, impact strength and electrical properties, as well as low water absorption, this tough and flexible material is ideal for non-toxic skin contact, and is perfect for clothing. The type of aerogel used was hydrophobic amorphous silica aerogel which is most suitable for application in textile material which provides the super insulating properties of silica aerogel in a flexible form. It is excellent for ambient and sub-ambient insulating applications. The aerogel particles were added during thermal bonding of the non-woven web. The samples were chosen in six different thicknesses as are widely used in most textile insulating applications. These thicknesses are commonly used for insulation of clothing, tents and buildings. Sample H1 is Needle punched struto nonwoven structure having One layer of PP web (Top layer) + One layer of spunbond PP web having melt blown polyamide nanofibers on both sides (Middle layer)+One layer of PP web (Bottom layer). Sample H2 is Needle punched struto nonwoven structure having one layer of PP web (Top layer) + Two layers of spunbond PP web having meltblown polyamide nanofibers on both sides (Middle layer)+One layer of PP web (Bottom layer). Sample M1 was purchased from Elastic Gros Braun patent no. M123A2046 and Sample M2 were purchased from POLARTEC with 100% polyester and 100 gsm alpha insulation. Silica aerogel powder and granules were purchased from Cabot aerogel Corp. Polyurethane (PUR) and Polyvinylidene Flouride (PVDF) was used from the CxI lab (nanocenter, TUL, Czech Republic). To obtain an indication of the effect of areal density on thermal properties, fabrics with comparable densities in different thicknesses and their corresponding weights were measured. The density difference in samples may be attributed to the fabric structure and also in aerogel treated nonwoven fabrics the percentage of aerogel particles present in the fiber. Approximate volume porosity of all aerogel treated samples was around 93%. Since the fabric samples were created from multilayer nonwoven

structures and it is complicated to calculate mean fiber density. Fabric density (kg/m^3) is calculated as ratio of mass per unit area [G (g/m^2)] and thickness [h (m)].

$$Fabric\ density\ =\ \frac{G}{h}\ \ [\text{kg/m}^3] \tag{3.1}$$

Table 5. Description of samples.

Sample No.	Sample description	Thickness [mm]	Weight [g/m²]	Fabric density [kg/m³]
S1	Aerogel treated nonwoven fabrics	3.42 (± 0.37)	272.56 (± 30.68)	79.66 (± 8.80)
S2	Aerogel treated nonwoven fabrics	6.21 (± 0.23)	499.46 (± 49.43)	80.42 (± 8.92)
S3	Aerogel treated nonwoven fabrics	6.61 (± 0.44)	440.70 (± 24.07)	66.73 (± 6.04)
S4	Aerogel treated nonwoven fabrics	8.06 (± 0.17)	535.10 (± 1.29)	66.39 (± 1.36)
S5	Aerogel treated nonwoven fabrics	11.12 (± 0.32)	733.7 (± 5.23)	65.99 (± 1.91)
S6	Aerogel treated nonwoven fabrics	13.80 (± 0.58)	942.70 (± 2.36)	68.33 (± 2.90)
H1	Needle punched struto nonwoven structure	9.34 (± 0.05)	402.01 (± 2.35)	43.06 (± 0.21)
H2	Needle punched struto nonwoven structure	8.05 (± 0.18)	407.50 (± 1.27)	50.64 (± 1.11)
M1	Elastic Gros Braun patent no. M123A2046	1.85 (± 0.24)	101.80 (± 4.57)	55.20 (± 6.76)
M2	POLARTEC with 100% polyester and 100 gsm alpha insulation	1.52 (± 0.16)	104.13 (± 3.26)	68.39 (± 3.57)

Note: "±" *is the upper and lower 95% confidence interval of the mean.*

3.2 Method and Parameters of Sample Preparation

3.2.1 Production of Aerogel Treated Nonwoven Fabric

The aerogel treated nonwoven fabrics were produced by thermal bonding. The confocal microscopic image of aerogel treated nonwoven fabric is shown in figure 22. The fibers for the thermal bonding were selected based on the thermal properties and glass transition temperature. Polyester (T_g - 161.7 ^{o}C for density - 1.3584 g/cc) has the higher glass transition temperature than Polyethylene fibers (T_g - 85 ^{o}C). The properties of amorphous silica aerogel are shown in table 5.
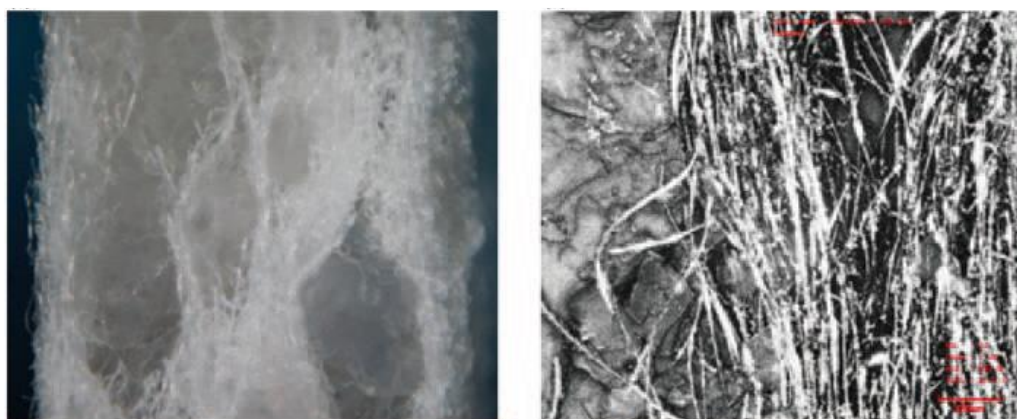
Figure 22. Confocal microscopic image of aerogel treated nonwoven fabric.

Table 6. Properties of amorphous silica aerogel.

S. No.	Properties	Value range
1	Particle size range	0.1 to 0.7mm
2	Pore diameter	~20 nm
3	Particle density	120 to 140 [kg/m^3]
4	Surface chemistry	Fully hydrophobic
5	Thermal conductivity	0.012 [W/(m K)] at 25 ^{o}C

3.2.2 Preparation of Needle Punched Struto Nonwoven Structure

Needle punched struto nonwoven fabrics were produced in our faculty. The polypropylene (PP) web and melt blown polyamide nanofibers were produced separately and were bonded together by needle punched struto nonwoven fabric machine shown in figure 23 and 24.
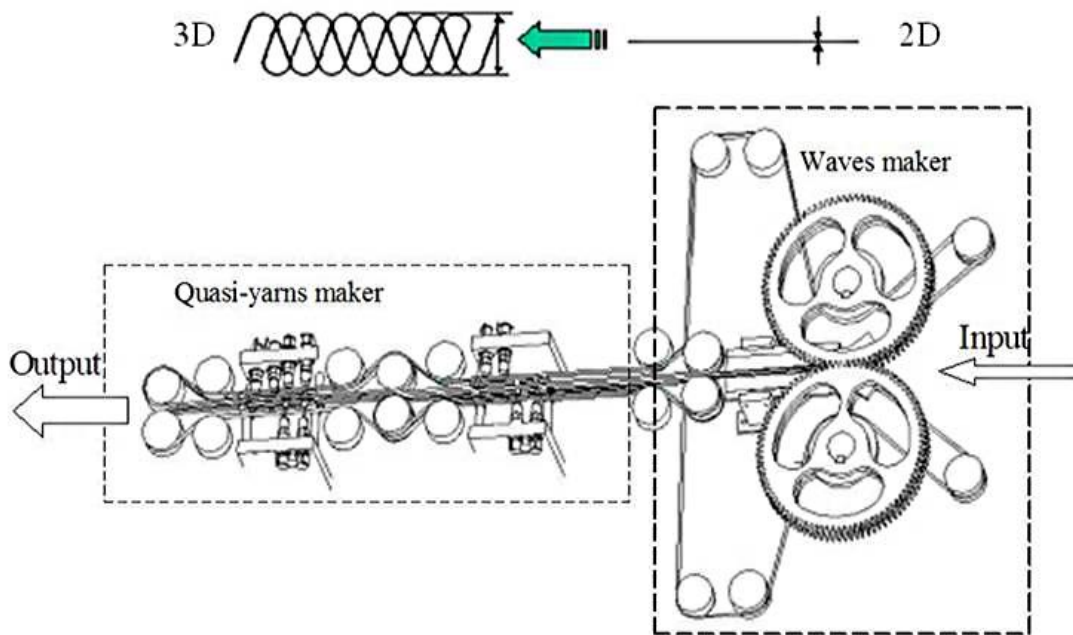
Figure 23. Schematic diagram of needle punched struto nonwoven fabric machine.

Figure 24. Image of needle punched struto nonwoven fabric machine.

The fabric is in the form of corrugated structure where top and bottom layer is polypropylene web and the middle layer consists of melt blown polyamide nanofibers on both sides of spunbond PP web with two different compositions.

3.2.3   Electrospinning of PVDF (Polyvinylidene Flouride) & PUR (Polyeurethane) Nanofibrous Layers

The PUR nanofiber was dissolved in dimethylformamide (DMF) at room temperature at a concentration of 18 wt.% [g/ml] and at the same concentration PVDF also was first stirred for 2 hours and then with SiO_2 aerogel in both powder and granule forms were added.

Table 7. Setting up laboratory equipment for production of PUR nanofibrous layer embedded with aerogel.

Parameters	Specifications
Distance of electrode	175 mm
Wire speed	0.2 [mm/s]
Substrate speed	15 [mm/min]
Carriage speed	380 to 430 [mm/s] on 500 [mm] distance
Substrate	Spunbond polypropylene fabric
Voltage	-10/60 [kV]
Size of the girder	ø 0, 7
Air flow	90/100 [m³h]
Humidity	with dry box

Table 8. Air temperature/humidity and size of the girder specifications of PUR nanofibrous layer embedded with aerogel.

Samples	Air temperature and humidity	Size of the girder
PUR 1	22.7% / 23 °C	ø0, 7
PUR 2	20.3% / 23.6 °C	ø0, 7
PUR 3	20.8% / 23,3 °C	ø0, 7
PUR 4	23.1% / 24.4 °C ; 23.1 % / 24.2 °C	ø0, 7/ ø 0,8/ ø 1,0
PUR 5	23.1% / 24.8 °C (First layer)	ø0, 9
	21.5% / 26 °C (Second layer)	ø0, 9

Table 9. Setting up laboratory equipment for production of PVDF nanofibrous layer embedded with aerogel.

Samples	Substrate speed [mm/min]	Air temperature and humidity	Size of the girder
PVDF 1	30	42.3% / 24.2 °C	ø0, 7
PVDF 2	15	47.0% / 24.1 °C	ø0, 7
PVDF 3	30	43.5% / 24.3 °C	ø0, 7
PVDF 4	15	44.5% / 24.3 °C	ø0, 7
PVDF 5	30	41.5% / 24.3 °C	ø0, 7
PVDF 6	15	38.5% / 24.4 °C	ø 1,2

These mixtures were stirred for 1 to 2 hrs at room temperature prior to electrospinning and were then electrospun at room temperature shown in figure 25. The prepared solution was placed in a cylinder containing active electrode parallel to collecting electrode. The parameters and laboratory set up details are given in table 7, 8 and 9. The fibers were collected on a spunbond polypropylene fabric. The electrospun nanofibrous layers embedded with aerogel sample details are given in table 10 and 11.
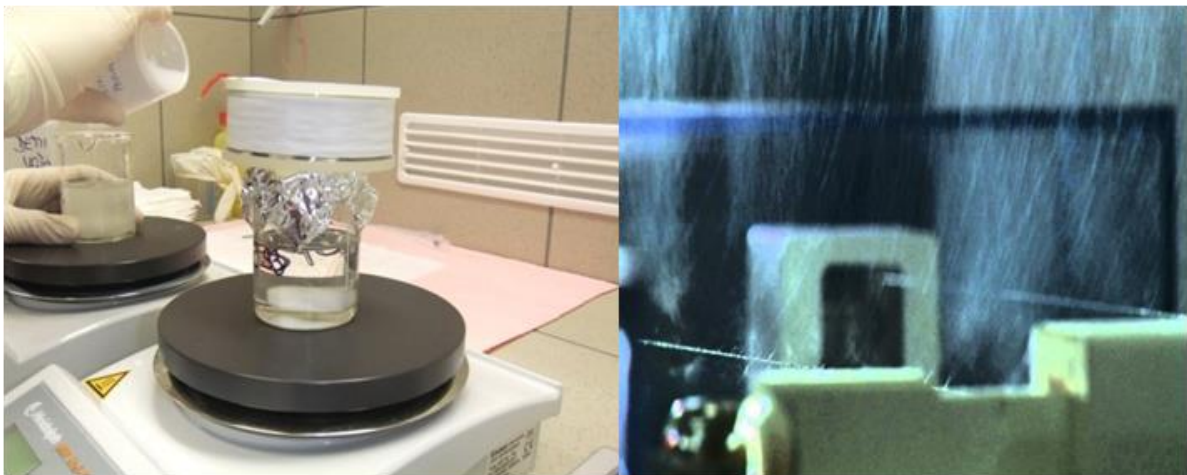
Figure 25. Preparation of solution and closer view of electrospinning of nanofibers.

Table 10. Sample details of electrospun PVDF nanofibrous layer embedded with silica aerogel.

Samples	Type	Sample description (Spun PP +NFA)	Areal density [g/m²]	Thickness [mm]	Themal Conductivity [W m⁻¹ K⁻¹]	Thermal resistance, r [K m² W⁻¹] x 10⁻³
SPUR1	Aerogel nanofibrous layer with Spunbond PP back up	only PUR	34.01 (± 1.71)	0.290 (± 0.014)	0.0336 (± 0.0171)	7.68 (± 0.381)
SPUR2		PUR + aerogel (Powder)	33.11 (± 1.65)	0.254 (± 0.013)	0.0325 (± 0.0064)	8.12 (± 0.410)
SPUR3		PUR + aerogel (Granular)	35.28 (± 1.76)	0.300 (± 0.015)	0.0310 (± 0.0262)	8.88 (± 0.472)
SPUR4		PUR + aerogel (Powder)	35.29 (± 1.65)	0.390 (± 0.020)	0.0326 (± 0.0608)	11.48 (± 0.572)
SPUR5		PUR + aerogel (Granular)	38.58 (± 1.93)	0.370 (± 0.019)	0.0322 (± 0.0091)	11.44 (± 0.072)
PUR1	Aerogel nanofibrous layer	Only PUR	6.01 (± 0.31)	0.083 (± 0.004)	0.0303 (± 0.0512)	3.10 (± 0.255)
PUR2		PUR + aerogel (Powder)	5.11 (± 0.26)	0.089 (± 0.005)	0.0298 (± 0.0730)	5.42 (± 0.072)
PUR3		PUR + aerogel (Granular)	7.28 (± 0.03)	0.112 (± 0.006)	0.0287 (± 0.0047)	5.66 (± 0.208)
PUR4		PUR + aerogel (Powder)	7.29 (± 0.07)	0.206 (± 0.010)	0.0275 (± 0.0177)	7.35 (± 0.084)
PUR5		PUR + aerogel (Granular)	10.58 (± 0.21)	0.248 (± 0.012)	0.0282 (± 0.0232)	8.78 (± 0.092)

Note: "±" *is the upper and lower 95% confidence interval of the mean.*

Table 11. Sample details of electrospun PVDF nanofibrous layer embedded with silica aerogel.

Samples	Type	Sample description (Spun PP +NFA)	Areal density [g/m²]	Thickness [mm]	Themal Conductivity [W m⁻¹ K⁻¹]	Thermal resistance, r [K m² W⁻¹] x 10⁻³
SPVDF1	Aerogel nanofibrous layer with Spunbond PP back up	only PVDF	34.89 (± .79)	0.48 (± 0.045)	0.0304 (± 0.0014)	15.78 (± 0.773)
SPVDF2		only PVDF	38.62 (± 0.93)	0.32 (± 0.036)	0.0280 (± 0.0003)	11.42 (± 0.047)
SPVDF3		PVDF + aerogel (Powder)	34.58 (± 2.73)	0.46 (± 0.048)	0.0303 (± 0.0016)	15.18 (± 0.106)
SPVDF4		PVDF + aerogel (Powder)	44.00 (± 2.38)	0.38 (± 0.091)	0.0301 (± 0.0076)	12.62 (± 0.261)
SPVDF5		PVDF + aerogel (Granular)	37.18 (± 1.26)	0.41 (± 0.025)	0.0317 (± 0.0003)	12.93 (± 0.608)
SPVDF6		PVDF + aerogel (Granular)	39.89 (± 1.95)	0.40 (± 0.102)	0.0290 (± 0.0009)	13.79 (± 0.091)
PVDF1	Aerogel nanofibrous layer	only PVDF	6.80 (± 0.34)	0.11 (± 0.005)	0.0297 (± 0.0006)	3.70 (± 0.083)
PVDF2		only PVDF	10.62 (± 0.43)	0.20 (± 0.012)	0.0240 (± 0.0019)	8.33 (± 0.544)
PVDF3		PVDF + aerogel (Powder)	6.58 (± 0.13)	0.17 (± 0.065)	0.0252 (± 0.0003)	6.74 (± 0.035)
PVDF4		PVDF + aerogel (Powder)	16.00 (± 0.23)	0.05 (± 0.025)	0.0230 (± 0.0022)	2.17 (± 0.188)
PVDF5		PVDF + aerogel (Granular)	9.18 (± 0.60)	0.19 (± 0.033)	0.0236 (± 0.0008)	8.05 (± 0.415)
PVDF6		PVDF + aerogel (Granular)	11.89 (± 0.55)	0.23 (± 0.015)	0.0252 (± 0.0073)	9.12 (± 0.545)

Note: "±" *is the upper and lower 95% confidence interval of the mean.*

3.3 Measurement Methods

Evaluation of various techniques for measurement of thermal conduction, thermal resistance, thermal convection, air permeability, particle size distribution and microscopic analysis was carried out for all the fabric samples. Before conducting the measurements, all samples were conditioned at standard atmospheric conditions (20 ± 2 °C, $65 \pm 2\%$ R.H) for 24 h. The averages of 20 measurements for each sample were taken, and mean values of the thermal properties were calculated. To confirm repeatability, measurements were performed thrice at an interval of 30 days for all the samples. The precision of the instrument was measured up to two decimal places for the same fabric that was tested in similar conditions and the accuracy was approximately 14%. The new testing instruments are proposed to measure the thermal properties of fabrics. The calibration of the apparatus and the data acquisition procedure are considered in detail in order to measure thermal conductivity and thermal resistance constants of the tested fabric samples.
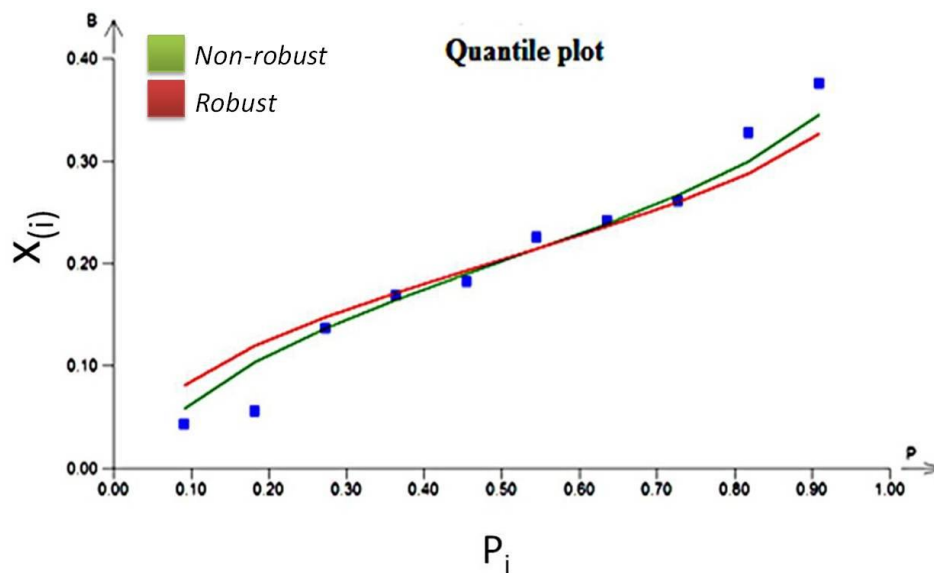
Figure 26. Quantile plot.

The quantile plot is used in this study where it permits the identification of any peculiarities of the shape of the sample distribution, which might be symmetrical or skewed to higher or lower values. Figure 26 shows the quantile plot with the cumulative (order) probability P_i in x-axis and the order statistic $x_{(i)}$ in y-axis and also shows empirical quantiles and the inverse cumulative distribution function (the quantile function, QF) of the fitted normal distribution. The green curve corresponds to the normal QF with the classical estimates of the parameters (non-robust or standard), the red curve corresponds to the median based estimates of the parameters (robust). The data better fits the green curve which corresponds to the normal QF with the classical estimates of the parameters, where mean was chosen as an estimate of the

mean value [141]. The upper and lower (±) 95% confidence interval of the mean is specified for the values in the tables. The tested data were statistically analyzed using data analysis software ORIGIN LAB (origin pro 8), MATLAB & QC Expert.

3.3.1   Scanning Electron Microscope (SEM) and Confocal Microscope

The non-woven fabric samples were characterized using SEM (VEGA TESCAN Inc. USA) at 30 kV and confocal microscope (OLYMPUS Confocal Scanning IR Laser Microscope, LEXT LS3000-IR). SEM provides detailed high resolution images of the samples by a focused electron beam across the surface and detecting secondary or backscattered electron signal. It provides images with magnifications up to ~ x 50, 000 allowing sub micron-scale features to be seen i.e. well beyond the range of optical microscopes. It is useful for characterization of particulates and defects in the material and examination of grain structure and segregation effects in the fabric structure.

3.3.2   Gas/Vapor Adsorption

This is the most widely available and utilized method for determining aerogel porosity. In this technique a gas, usually nitrogen, at its boiling point, is adsorbed on the solid sample. The amount of gas adsorbed depends of the size of the pores within the sample and on the partial pressure of the gas relative to its saturation pressure. By measuring the volume of gas adsorbed at a particular partial pressure, the Brunauer, Emmit and Teller (BET) equation gives the specific surface area of the material. At high partial pressures, where there is hysteresis in the adsorption/desorption curves (called "isotherms"), the kelvin equation gives the pore size distribution of the sample. The pore size distribution shown above was determined using a 40-point nitrogen adsorption/desorption analysis. Gas adsorption methods are generally applicable to pore in the mesopore range. However, microporosity information can be inferred through mathematical analyses such as t-plots or the Dubinin-Radushevich method. Gas adsorption cannot effectively determine macropores. For a detailed description of this procedure, see the IUPAC guidelines for "Reporting Physisorption Data for Gas/Solid Systems" in Pure and Applied Chemistry, volume 57, page 603, (1985). Autosorb IQ MP Quantachrome Instrument, USA was used to evaluate the method of adsorption of nitrogen at liquid nitrogen temperature and the evaluation was performed by the software provided by AsiQwin Quantachrome Instruments using gas adsorption/desorption method. According to the firmware, a standard procedure was used for determining the specific surface area by adsorption of nitrogen using multipoint BET method and the analysis of nitrogen adsorption/desorption curve at liquid nitrogen

temperature. The specific surface area was evaluated based on the BET theory of five points (multi-point BET p/p_o = 0.1 - 0.3), the guaranteed accuracy of the method is 0, x m^2/g (for surfaces above 100 m^2/g x m^2/g). The volume of micropores (d < 2 nm) were determined by t-plot by de Boer. The volume and size distribution of mesopores (d = 2 to 50 nm) was determined using the BJH desorption of the curve. The total volume of pores with a diameter below 40 nm was determined from the desorption curves for the partial pressure of p/p_o = 0.95. Specific surface areas and volumes are relative to the weight of the sample after degassing (without adsorbed moisture and other volatile impurities).

3.3.3   *Air Permeability Measuring Instrument*

The principle of FX 3300 air permeability instrument depends on the measurement of air flow passing through the fabric at a certain pressure gradient *Δp*. In this instrument any part of the fabric can be placed between the sensing circular clamps (discs) without the garment destruction. As the fabric is fixed firmly on its circumference (to prevent the air from escaping), the fabric dimensions do not play any role. There is also enough space between the clamps and the instrument frame, which allows the measurement on large samples.

3.4 Measurement of Thermal Properties

3.4.1   *Modified Particle Image Velocimetry - PIV Setup*

Particle Image Velocimetry (PIV) is a whole-flow-field technique providing instantaneous velocity vector measurements in a cross-section of a flow. Two velocity components are measured, but use of a stereoscopic approach permits all three velocity components to be recorded, resulting in instantaneous 3D velocity vectors for the whole area. The use of modern digital cameras and dedicated computing hardware, results in real-time velocity maps. In normal PIV systems, the chamber set-up was very big and the hot plate was not used to determine the thermal properties. In our research, the chamber was made with the dimensions of 10 x 10 cm wide and 70 cm height. Three different set-ups were custom built to measure the velocity profile above the fabric sample shown in figure 27. The first set-up was placing the fabric sample directly on the hot plate. The second and third set-up was to place the fabric sample 2 and 5 cm above the hot plate respectively.
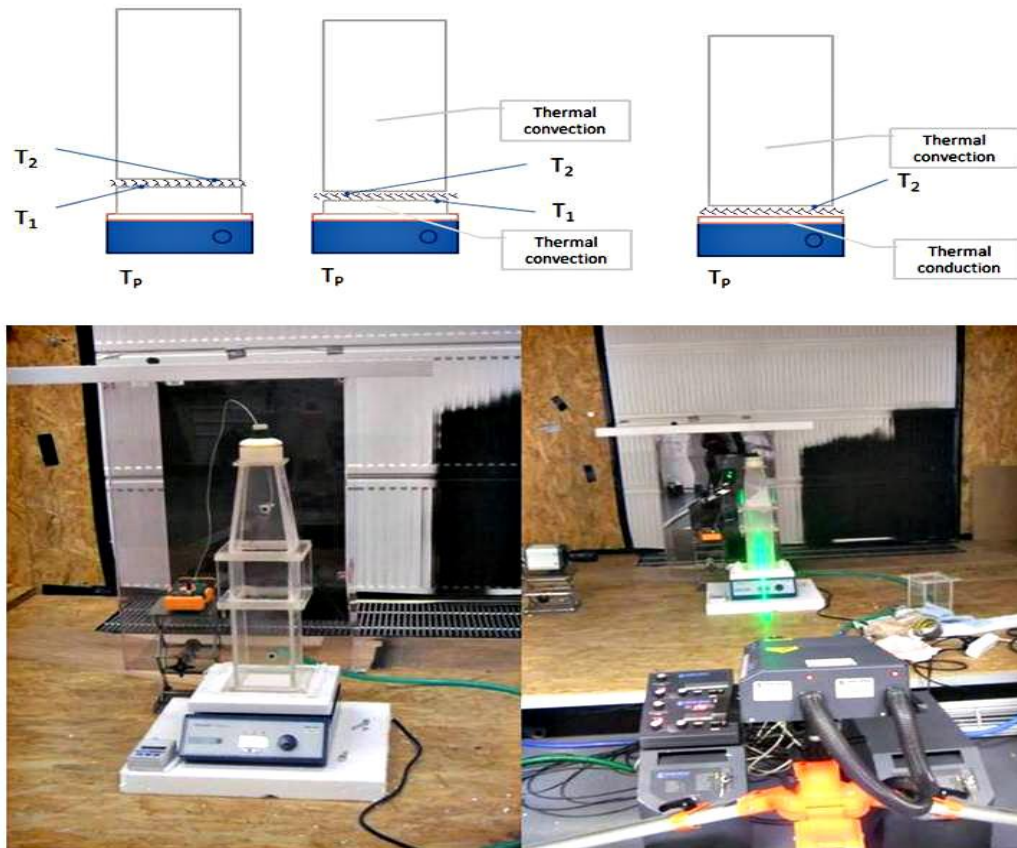
Figure 27. Experimental set-up for PIV measurements.

After the test is performed with the tracer particles for the heat flow, the image captured by the CCD camera is saved in the system. First, the images are divided into small windows called interrogation regions. Using a statistical method called cross-correlation, the displacement of each window from frame 1 to frame 2 is determined from the peak point in the cross correlation function. The most probable displacement over the time interval is the average velocity vector in one interrogation window, i.e. $\Delta x / \Delta t \approx v$, shown in figure 28. By repeating these calculations, the velocity field of the entire image area is obtained.
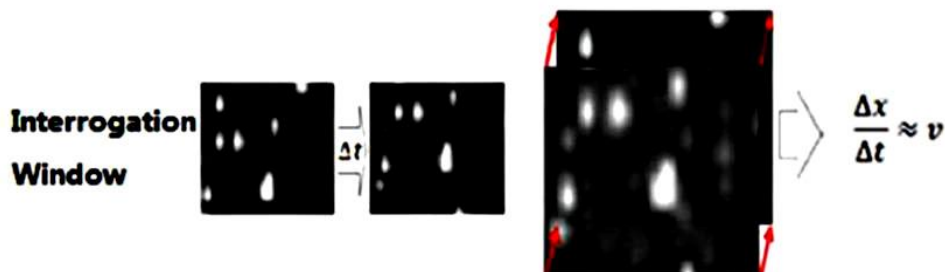
Figure 28. Average velocity vector of one interrogation window obtained by cross correlation [72].

Details of the PIV technique, including the tracer particle size, light source, light sheet optics, digital image recording, post-process data analysis and mathematical background of the statistical PIV evaluation can be found in the state of the art section [142].

3.4.2 *Custom Built Steady State Thermal Measurement Instrument*

The newly fabricated instrument works according to transmission of heat in the steady-state condition as described in BS 4745:1971. Single-plate heating method was used as reference to fabricate this instrument. In single-plate method (figure 29), the specimen under test is placed on the heated lower plate covered with 100% cotton as an outer fabric, since the issue of thermal contact is also very important. Fixed pressure (10 g/cm^2) was applied on the test specimen during the measurement which ensures good contact without deformation of textile structure. The surface temperature of the outer fabric is measured using the infrared thermometer.
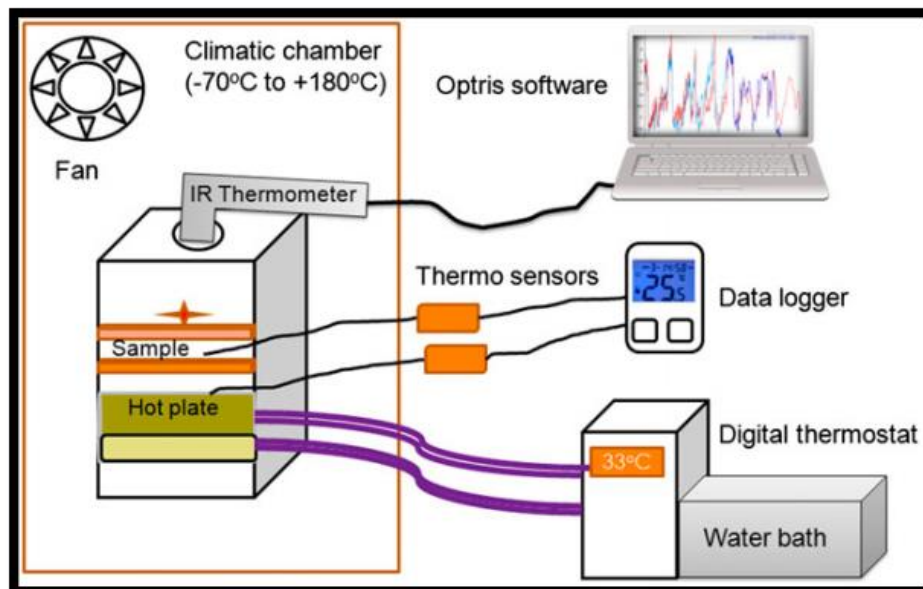
Figure 29. Schematic diagram of custom-built instrument for measuring thermal properties.
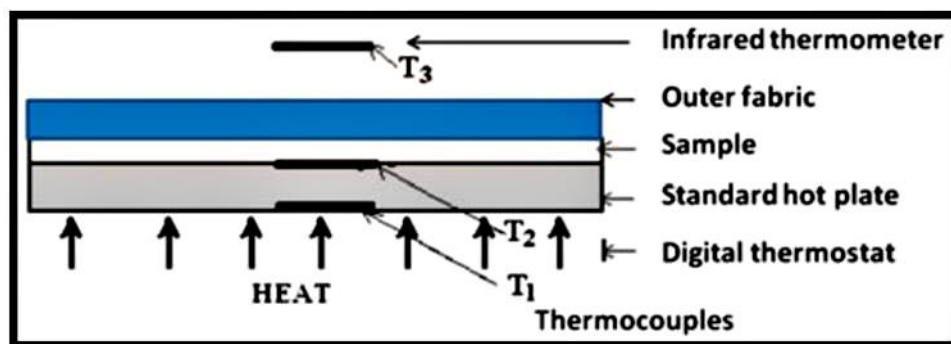
Figure 30. Schematic diagram of the newly fabricated instrument (single-plate method).

The instrument was used to determine the temperatures at various positions on the aerogel-treated fabric. From these measurements, the thermal conductivity and thermal resistance were calculated. The sample was placed in a climatized temperature system (chamber) which operates with the temperature range from (−70 to +180 °C). The instrument measures the heat transport through textile material. The test specimen was placed on the cylindrical hot plate which is connected to the digital thermostat water bath where the skin temperature is maintained at ~33 °C as shown in figure 29. The test specimen was placed on the hot plate and the outer fabric (100% plain woven cotton fabric) was placed over the test specimen applying 10 g weight on each side. Two thermocouples and heat flow sensors were used to measure temperature variations. First one (T_1) is fixed on the surface of the test specimen which touches the hot plate and the second one (T_2) is fixed on the surface which is covered by the outer fabric. The hot plate was adjusted to constant skin temperature and the climatic temperature system was adjusted to a controlled constant differential temperature. The heat flow sensors act on both the surfaces of the fabric. with the help of thermocouples, the temperature difference between the upper surface and the inner side of the test specimen can be measured. The Infrared thermometer was used to measure the temperature variations on the surface of the outer fabric. The fundamental measuring principle implies the measuring and processing of the heat flows with dependence to time. The instrument measures parameters: (1) Temperature on the surface of the test specimen which is in contact with the skin (T_1), (2) Temperature on the surface of the fabric which is in contact with the outer fabric (T_2), (3) Temperature inside the climatic temperature chamber which is set as the environmental temperature from (+25 to −25 °C) (T_3) and (4) Temperature on the surface of the outer fabric which is sensed by infrared thermometer (T_4).

3.4.3   *Development of Heat Convection Instrument (Laboratory Set-Up)*

The thermal property of fabrics under heat convection was evaluated by a laboratory model device developed in department of material engineering, Technical University of Liberec, shown in figure 31. This device consists of one air tunnel, sample holder, heater, several sensors, data acquisition module and laptop. The thermocouples are attached to one to heater and the other to the fabric, and the anemometers are on both sides of fabric, data acquisition module connects sensors with PC. The air flow goes through the testing sample, the temperatures of both sides of the fabric can be real-time monitored and saved in laptop. The output of heater was around 60 °C at 2.5 m/s.
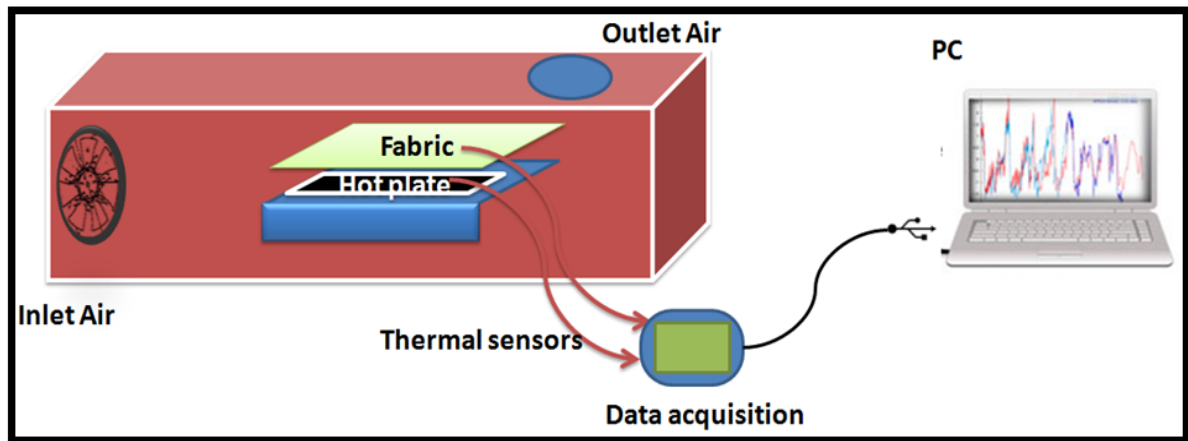
Figure 31. Schematic of laboratory model thermal convection instrument.

Flow Profile by Convection

Heat energy transfers between a solid and a fluid when there is a temperature difference between them. This is known as "convection heat transfer". The temperature of the solid due to an external field such as fluid buoyancy can induce a fluid motion. This is known as "natural convection" and it is a strong function of the temperature difference between the solid and the fluid. Blowing air over the solid by using external devices such as fans, pumps and even heat generation within the object can also generate a fluid motion which is known as "forced convection". Fluid mechanics plays a major role in determining convection heat transfer.

Reynolds Number (Re)

Two-dimensional flow analysis over a flat object serves well to illustrate several key concepts in forced convection heat transfer. As given in equation (2.7), the viscosity of the fluid μ requires that the fluid of density ρ, have zero velocity at the surface of the object. As a result a boundary layer exists where the fluid velocity changes from u_∞ in the free stream (far from the object) to zero at the object. Within this boundary layer, the flow is initially laminar but can proceed to turbulence once the Reynolds Number Re of the flow is sufficiently high. The transition from laminar to turbulent flow over a flat object of length L. For the current study it has been assumed that the fabric specimen maintains its temperature at constant position T_w, making this problem isothermal. Laminar flow takes the interest in this study, so it is assumed that the specimen length L is sufficiently short such that turbulent flow is never triggered (i.e. $Re < 3 \times 10^5$).

Nusselt Number (Nu)

In heat transfer at a surface within a fluid, the Nusselt number (Nu) is the ratio of convective to conductive heat transfer across the boundary. In this context, convection includes both

advection and conduction and it is a dimensionless number. The conductive component is measured under the same conditions as the heat convection but with a (hypothetically) stagnant fluid which is defined by the equation (2.9).

Prandtl Number (Pr)

The Prandtl Number *Pr* is a non-dimensional ratio of the viscous boundary layer thickness to the thermal boundary layer thickness which is defined by the equation (2.8).

3.5 Computational Simulation of Heat Transfer

3.5.1 *Simulating Convective Heat Transfer through Aerogel Treated Nonwovens Using ANSYS*

Before a model is set, it passes through several stages. Thermal analysis is one of them and plays a very important role in product development. Various products such as engines, refrigerators, heat exchangers and so on are designed based on the results of this analysis.

Thermal analysis is used to determine the temperature distribution and related thermal quantities in the model. In this analysis, all heat transfer modes, namely conduction, convection and radiation are analyzed. The output from a thermal analysis are (1)Temperature distribution; (2)Amount of heat loss or gain; (3) Thermal gradients and (4) Thermal fluxes. This analysis is used in many engineering industries such as automobile, piping, electronic, power generation, and so on. In ANSYS workbench, two types of thermal analysis can be carried out, namely Steady-State and transient Thermal Analysis. The following are the basic steps required to perform the thermal analysis:

1. Set the analysis preference.
2. Create or import solid model.
3. Define element attributes (element types, real constants, and material properties.
4. Mesh the solid model.
5. Specify the analysis type, analysis options, and the loads to be applied.
6. Solve the analysis problem.
7. Post-process results.

The steady-state thermal analysis may be either linear or non-linear, with respect to material properties that depend on temperature. The thermal properties of most of the materials do vary with temperature; therefore the analysis usually is non-linear. Including radiation effects or temperature-dependent convection in a model also makes the analysis nonlinear. The steps to solve a problem relate to the thermal analysis are the same as that of the structural analysis, except a few steps such as selecting the element-type, applying the load,

and post processing results. In the transient thermal analysis, the system is studied under varying thermal loads with respect to time. The temperatures can be derived varying with time, thermal gradients and thermal fluxes in a transient thermal analysis. The transient thermal analysis takes more time compared to other analysis types. It is necessary to understand the basic mechanism of the problem to reduce the time involved in getting the solution. For example, if the problem contains nonlinearity, then you first need to understand how they affect the response of structures by doing the steady-state thermal analysis. Owing to the highly random structure of non-wovens/sheet/batt, a unit cell was considered. Individual fibers were modeled, each having a circular cross-section and a random shape.
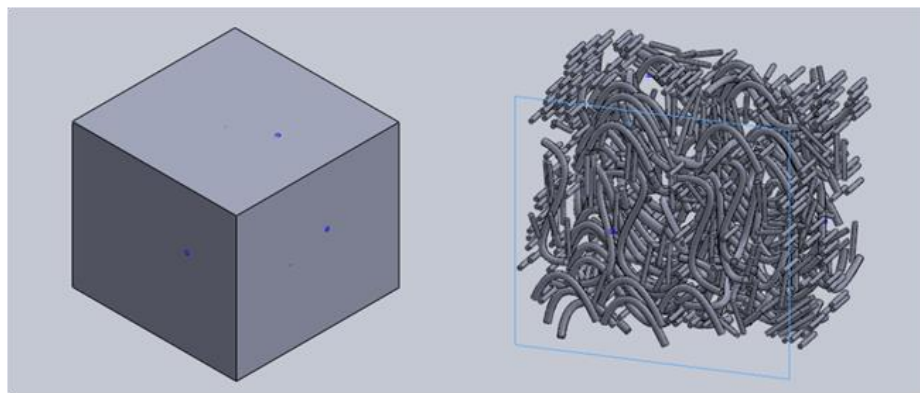
Figure 32. Unit cell model of nonwoven.

For this, a spline (a curve) was made, and the profile of a circle was swept over the spline to create the fiber. The modeled fibers were assembled together to create a nonwoven structure, such that the fibers occupy 26.27% space inside the unit cell, so as to give 73.73% porosity to the fabric as shown in figure 32. This assembly of fibers was saved as a PART file so that it could be used as a component in the further complex assembly.
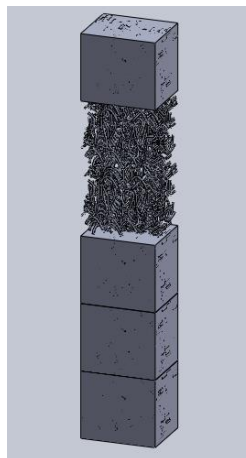
Figure 33. Whole width of the fabric.
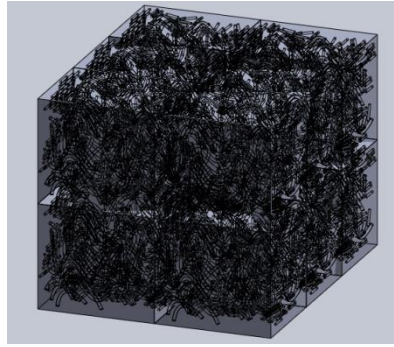
Figure 34. Macroscale image of the nonwoven fabric.

A chain of unit cells, about 3.5 mm long, was assembled using the 'mate' function to give a more realistic view of the fabric – this was simulated in Ansys Workbench 14. A model view of the structure of the non-woven fabric developed has been shown in figure 34.
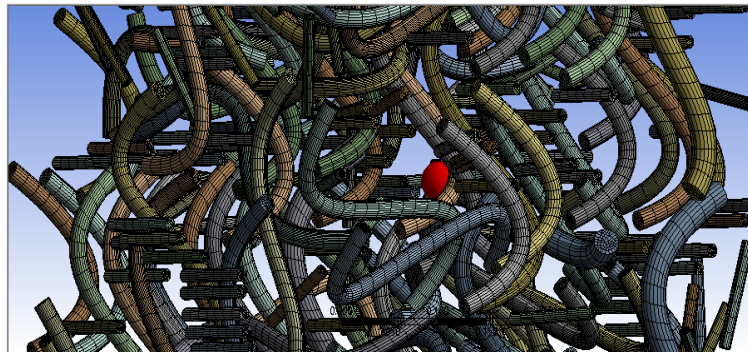
Figure 35. Meshing of elements in the unit cell.

3.5.2 *Simulation of Convective Heat Transfer Through Aerogel Treated Nonwovens Using COMSOL*

A unit cell to represent the fabric sample was modeled in solidworks. The fiber percentage in the unit cell was approximately 26.5%. Most of the fiber parts were aligned in the machine direction and very few in other directions as shown in figure 36.
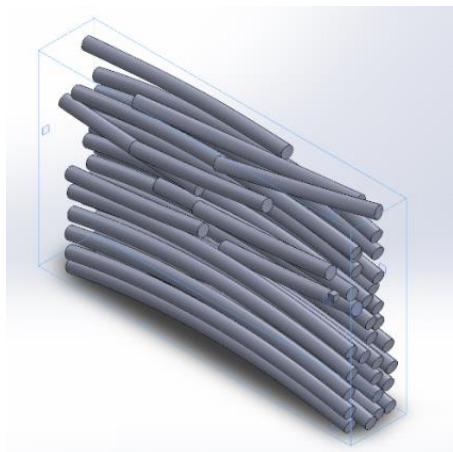
Figure 36. Fiber alignment in the unit cell.

The simulation of heat transfer through the fabric unit cell was done in Comsol, which uses Finite Element Method (FEM) to do the simulations. The input given was heat capacity, density, thermal conductivity for both fiber and surrounding fluid and the viscosity and the ratio of heat capacity at constant pressure and constant volume (gamma). Since the fluid responsible for the convection taking place was the same for both aerogel and free air, the viscosity, density and gamma values were the same for both simulations. The thermal conductivity and the heat capacity for both fluids were different. In the model used, most of the heat transfer was because of the convection by the fluid and conduction between air and fiber, very less due to the conduction in fibers itself since none of the fibers in the model touch each other. The conjugate heat transfer module, which combines the heat transfer through solids module and heat transfer through fluids module, was used. The heat transfer in solids module considers the fact that conduction is more prominent and the heat transfer in fluids module considers convection to be more prominent. This module couples the heat transfer module with the fluid flow module. The simulation was done assuming laminar and compressible flow and results obtained were for the steady state. One of the faces of the fabric was given a constant temperature of 329.19 K and the outside temperature was taken to be 263.15 K. This was done for 4 cases: (1) Aerogel as the fluid in the fabric with forced convection (2.5 m/s wind at the outer surface); (2) Aerogel as the fluid in the fabric without forced convection. (3) Air as the fluid in the fabric with forced convection (2.5 m/s wind at the outer surface) and (4) Air as the fluid in the fabric without forced convection
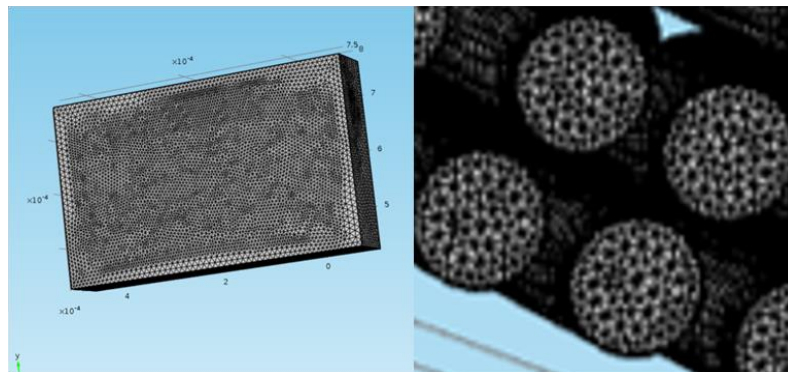
Figure 37. Meshing of the unit cell.

The model was meshed and various boundary conditions were given as shown in figure 37. For both with and without forced convection cases, one face was given a temperature of 329.19 K and initial temperature of the whole fabric was given as 263.15 K. For the forced convection case, the opposite face was given a convective flux with convection factor 23.76 [W/(m^2 K)] (2.5 m/s wind) and 263.15 K outside temperature.For the case without forced

convection, the opposite face was given an open boundary condition with outside temperature of 263.15 K. The meshing parameters are as given in Table 12.

Table 12. Meshing Parameters

Parameter	Value
Maximum size given	5.7 e^{-5} m
Minimum size given	1.03 e^{-5} m
Boundary layer thickness	5.7 e^{-6} m
Number of mesh elements total	1816188.

Chapter 4. Results & Discussion

4.1 Microscopic Analysis of Samples

4.1.1 Aerogel Treated Nonwoven Sample

Results for the characterization of aerogel treated nonwoven fabrics and needle punched struto nonwoven structure samples by SEM, Confocal/optical microscopy, DSC, FTIR and BET analysis as confirmation techniques are discussed.

The aerogel deposition in the fabric between the fibers was also observed. Figure 22 shows the images taken from confocal microscope. The aerogel particles present between the fibers can be seen clearly from the images. The inter-fiber spaces are clearly visible. The micro spacing between fibers is filled with aerogel particles. It can be seen that the aerogel is covering surface of individual fibers and is uniformly distributed in the structure. SEM images are shown in figure 38. The aerogel deposition on the fibers can be clearly observed. These images provide a more clear understanding of the deposition of silica aerogel particles on the fiber surface. Fiber arrangement plays a vital role in deciding the density and thus the porosity of nonwoven fabrics. The fabric is in the form of corrugated structure where top and bottom layer is polypropylene web and the middle layer consists of melt blown polyamide nanofibers on both sides of spunbond PP web shown in figure 39.
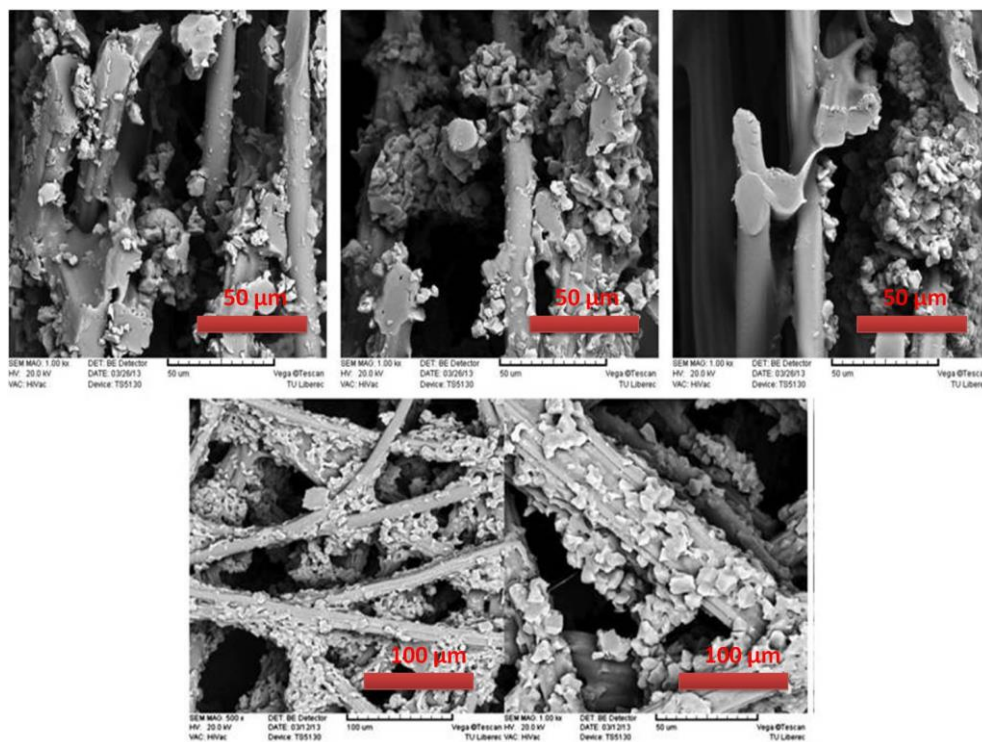
Figure 38. Scanning electron microscope images of aerogel-treated non-woven fabrics.

4.1.2   Needlepunched Struto Nonwoven Sample

The struto fabric shown in the figure 39 is in the form of corrugated structure where top and bottom layer is of polypropylene web and the middle layer consists of melt blown polyamide nanofibers on both sides of spunbond PP web with two different compositions.

Figure 39. Needle punched struto nonwoven structure.

4.1.3   Microstructures of Nanofibrous Layer with Aerogel

Figure 40 and 41 shows the morphologies and microstructures of electrospun PUR & PVDF nanofibrous layers. The electrospun nanofibrous layers have better integrity and flexibility. The different microstructures could be observed with and without aerogel particles present which were electrospun from the solutions with the concentration of 18wt.%.

PUR 3   PUR 4

PUR 1 (cross section)   PUR 2(cross section)

PUR 3(cross section)   PUR 4(cross section)
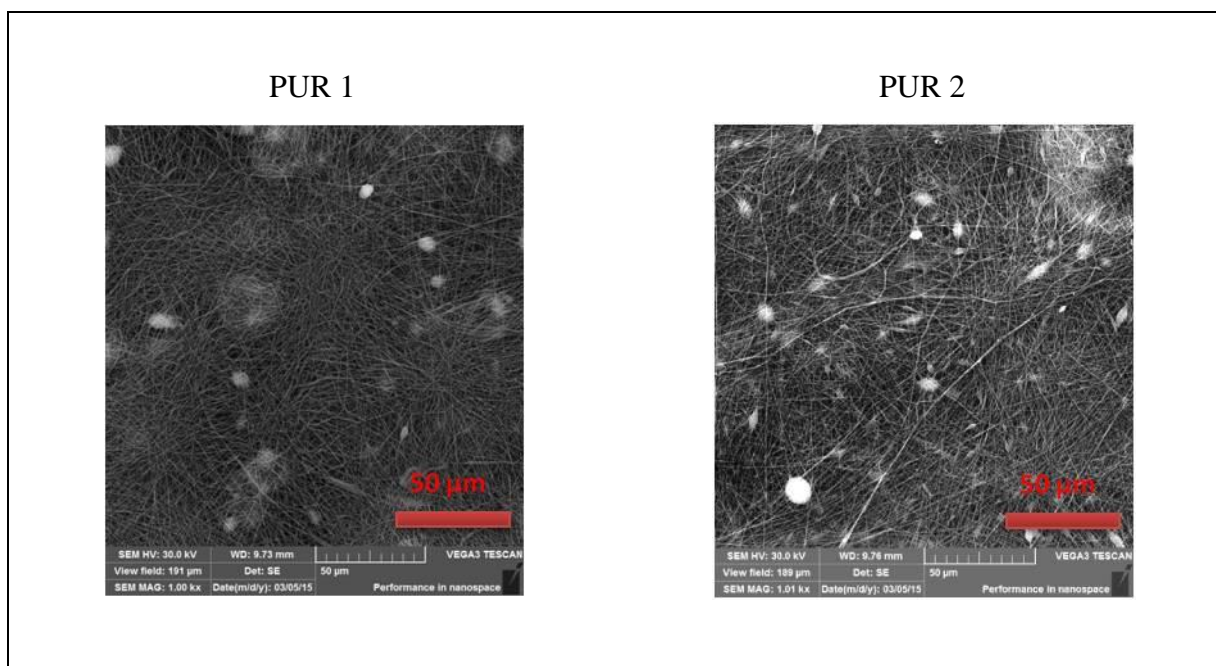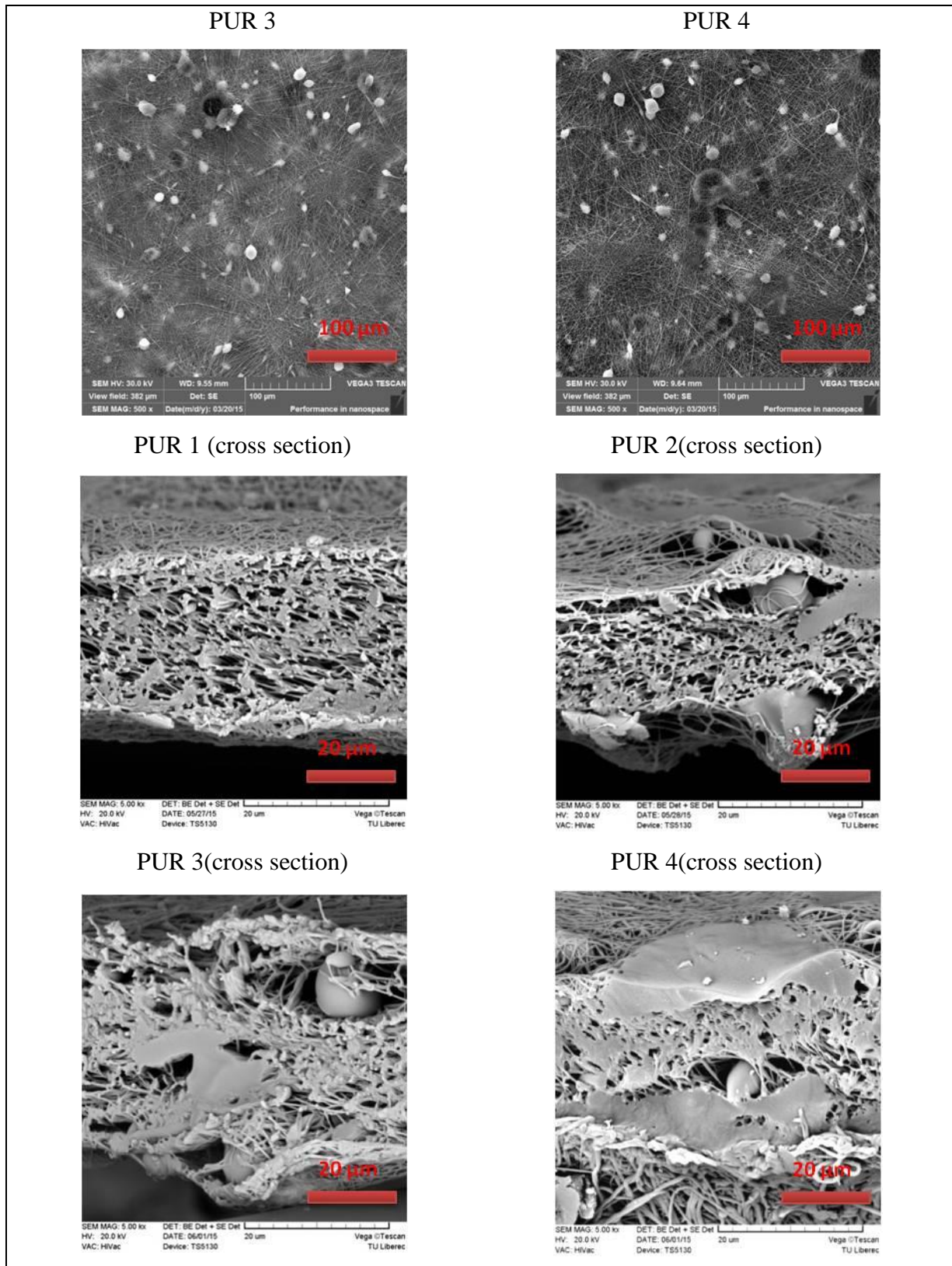
Figure 40. Morphology and microstructure of electrospun PUR nanofibrous layers embedded with SiO_2 aerogel from 18 wt.%.

PVDF 1

PVDF 2

PVDF 3

PVDF 4

PVDF 5

PVDF 6
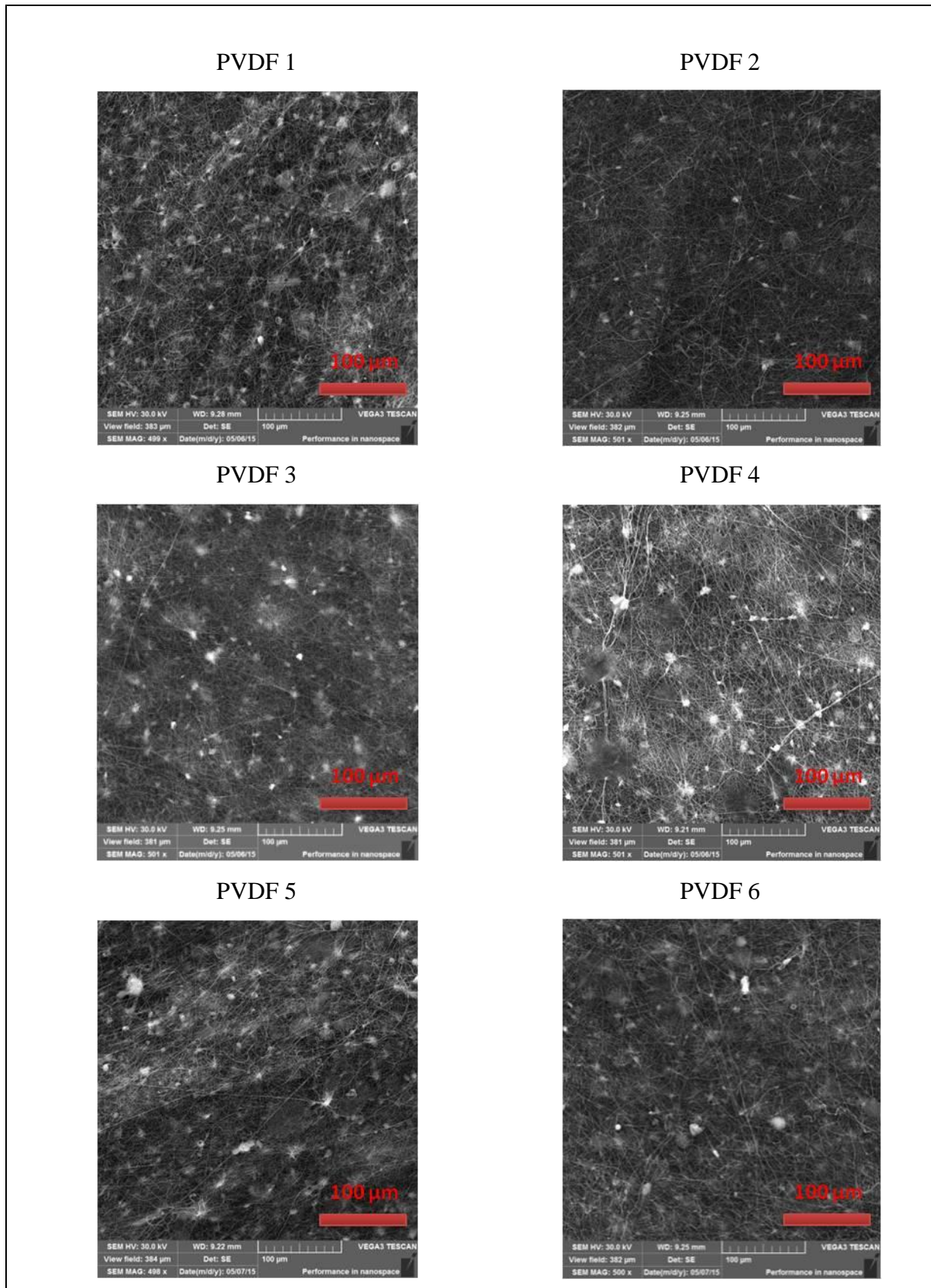
Figure 41. Morphology and microstructure of electrospun PVDF nanofibrous layers embedded with SiO_2 aerogel from 18 wt.%.

4.2 FTIR Analysis of SiO₂ Aerogel Particles

The presence of SiO_2 in the nonwoven fabric specimen was characterized by Fourier transform infrared spectroscopy (FTIR) as shown in figure 42.
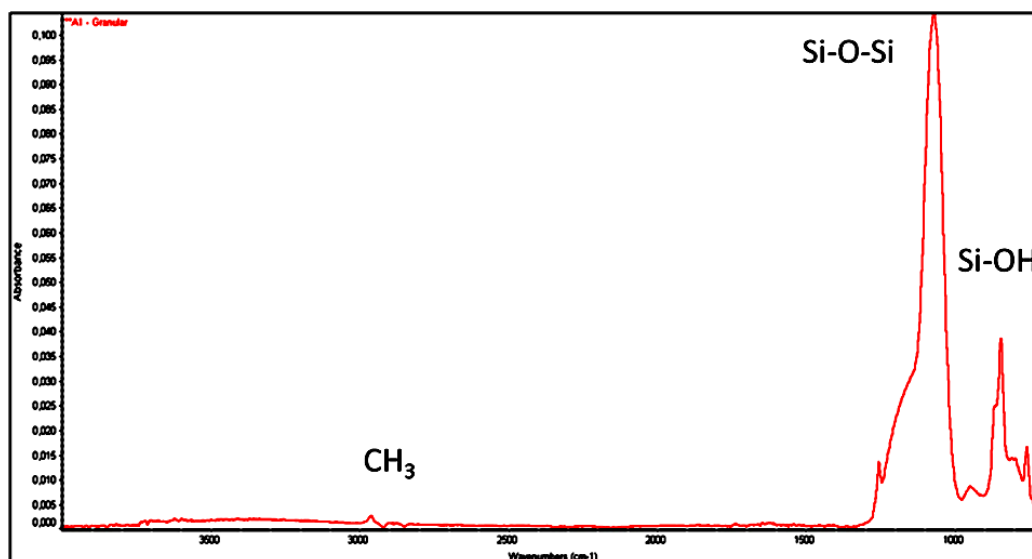
Figure 42. FTIR image of aerogel particle in granular form.

The peaks at 1071.57 and 1071.12 cm^{-1} are ascribed to the Si-O-Si bending vibration, that at 1100 cm^{-1} to the Si-O stretching vibration and the peaks at 2881.89 and 2779.47 are attributed to CH$_3$ stretching vibrations. The other peaks at 971.18, 957.41, 797.70 and 792.91are attributed to Si-OH vibrations.

4.3 Gas Adsorption/Desorption of SiO₂ Aerogel Particles

The pore structure of silica aerogel is difficult to describe by geometry. The International Union of Pure and Applied Chemistry has recommended a classification for porous materials where pores of less than 2 nm in diameter are termed "micropores", those with diameters between 2 and 50 nm are termed "mesopores", and those greater than 50 nm in diameter are termed "macropores". Silica aerogel possess pores of all three sizes. However, the majority of the pores fall in the mesopore regime, with relatively few micropores [143-145]. It is very important when interpreting porosity data to indicate the method used to determine the data. Nitrogen adsorption/desorption method was used for determining aerogel porosity. In this technique a gas, usually nitrogen, at its boiling point, is adsorbed on the solid sample. The amount of gas adsorbed depends on the size of the pores within the sample and on the partial pressure of the gas relative to its saturation pressure. By measuring the volume of gas adsorbed at a particular partial pressure, the Brunauer, Emmit and Teller (BET) equation gives the specific surface area of the material. At high partial pressures,

where there is hysteresis in the adsorption/desorption curves (called "isotherms"); the Kelvin equation gives the pore size distribution of the sample. The pore size distribution shown in figure 43 was determined using a 40-point nitrogen adsorption/desorption analysis. Gas adsorption methods are generally applicable to pore in the mesopore range. However, microporosity information is inferred through mathematical analyses such as t-plots method. Gas adsorption cannot effectively determine macropores.
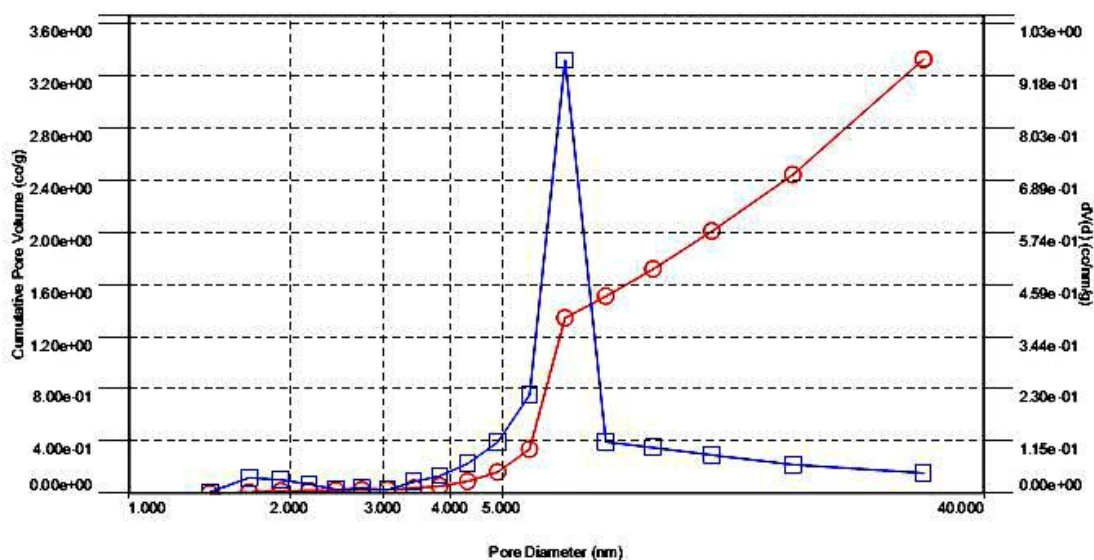
Figure 43. Distribution curve of pore diameter and cumulative pore volume curve for aerogel sample.

The nitrogen sorption experiments performed for the methyl functionalized silica aerogel resulted into specific surface areas. Amorphous silica aerogel in granular form was measured for the surface area and porosity. The measured total specific surface (BET) area *A* was 783 m^2/g (correlation coefficient of 0.9999) and total pore volume (d < 40 nm) $V_v =$ 2.686 cm^3/g. The micropores diameter was d < 2 nm which was measured by t-plot method according to de Boer. The specific surface area *'A'* micro was 0 m^2/g and the pore volume *V* micro was 0 cm^3/g. The mesopores measured by BJH method from the desorption branch of the isotherm is shown in figure 43, the assumption is cylindrical pores. Figure 43 shows distribution curve of pore diameter and cumulative pore volume curve for aerogel sample (assuming cylindrical pores) from the desorption branch of the isotherm; x-axis is pore diameter in nm.

4.4 Flow Rate Dependence on Pressure of Insulation Materials

Air permeability is the measure of airflow passed through a given area of a fabric. This parameter influences the thermal comfort properties of fabrics to a large extent. It is

generally accepted that the air permeability of a fabric depends on its air porosity, which in turn influences its openness. with more porosity, more permeable fabric is obtained.

Equation y = a + b*x		Value	t-test Significance ("Yes" or "No")	Adj. R-Square	F-test Significance ("Yes" or "No")
S1	Intercept	462.811	Yes	0.9884	Yes
	Slope	3.2702	Yes		
S2	Intercept	277.867	Yes	0.9911	Yes
	Slope	2.37027	Yes		
S3	Intercept	355.383	Yes	0.9885	Yes
	Slope	2.40963	Yes		
S4	Intercept	223.972	Yes	0.9901	Yes
	Slope	2.0685	Yes		
S5	Intercept	153.028	Yes	0.9945	Yes
	Slope	1.75217	Yes		
S6	Intercept	206.833	Yes	0.9916	Yes
	Slope	1.82567	Yes		
H1	Intercept	23.2222	Yes	0.9949	Yes
	Slope	1.274	Yes		
H2	Intercept	88.0278	Yes	0.9903	Yes
	Slope	1.16417	Yes		
M1	Intercept	1063.89	Yes	0.9891	Yes
	Slope	8.89	Yes		
M2	Intercept	1569.72	Yes	0.9771	Yes
	Slope	14.1183	Yes		

Figure 44. Flow rate dependence on pressure.

Statistical analysis results show that the there is a significance on the air permeability values of the aerogel treated nonwoven fabrics (p = 0.003). Figure 44 shows the air permeability with respect to different pressure levels of the fabrics. The result indicates that air permeability is directly proportional to the pressure level. On comparison of ten fabrics, the air permeability is higher in the case of sample M2. It may be due to the fact that air permeability is related to porous structure of the fabric and is directly proportional to percentage of porosity of the fabric. It was also noticed that when the pressure level increased, the flow rate also increased. Irrespective of different pressure levels, the air permeability was low for samples S1 to H2. It may be attributed to the layered structure and high porosity.

4.5 Thermal Properties of Insulation Materials – Results from Alambeta and TCi

The thermal conductivity of air is constant at a certain temperature; heat transfer in a fabric may be subject to some variations depending on the different thermal conductivities of the component fibers. The volumetric proportion of fibers in a fabric is represented by the fabric density, which relates to the volumetric proportion of air trapped in the fabric (or fabric porosity).

Equation y = a + b*x	Value	t-test Significance ("Yes" or "No")	Adj. R-Square	F-test Significance ("Yes" or "No")
Intercept	0.0768	Yes	0.82673	Yes
Slope	-6.486E-4	Yes		
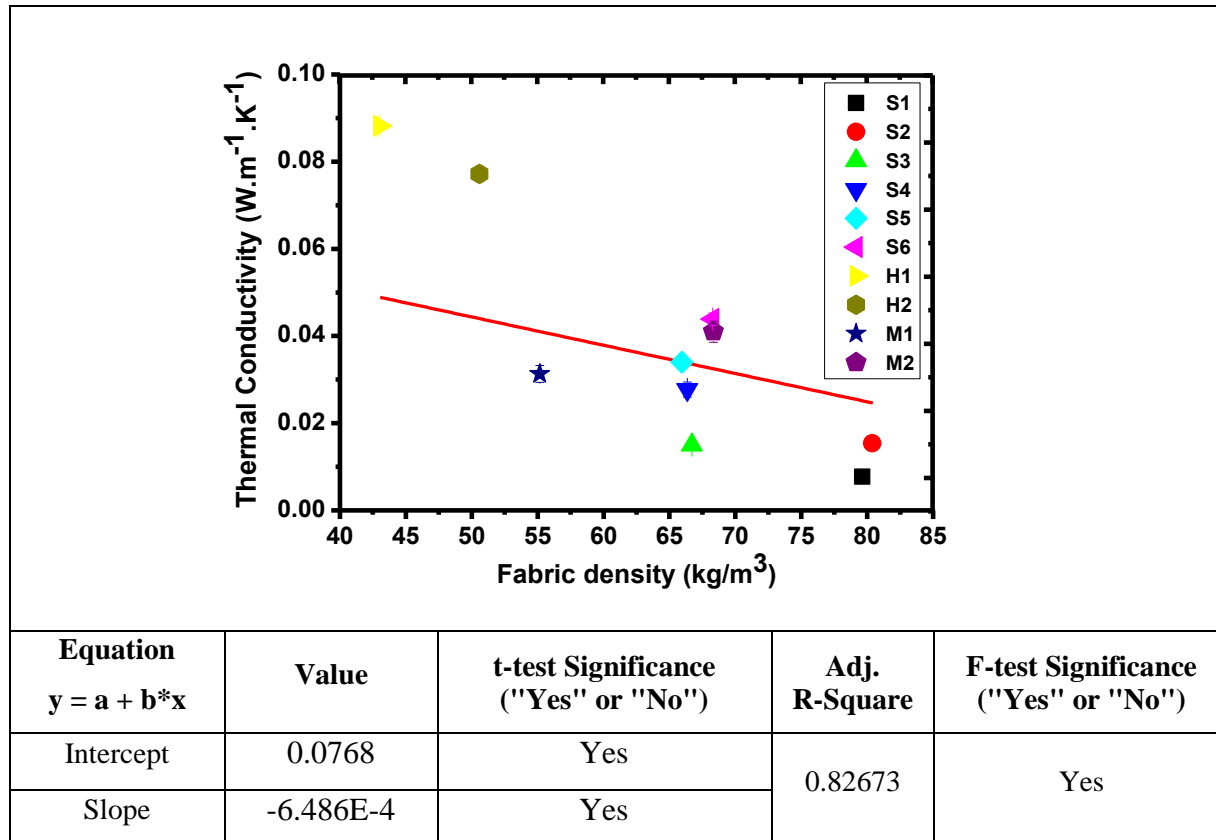
Figure 45. Thermal conductivity (Alambeta).

For nonwoven fabrics, the density is the primary factor contributing to the heat transfer through fabrics. Figure 45 shows the comparison between thermal conductivity calculated for constituent fibrous material**.** Figure 46 shows the effect of different pressure levels on thermal conductivity. The thermal conductivity of nonwoven fabrics depends on many factors including environmental temperature, thermal conductivity of the solid polymer materials and fabric dimensional and structural parameters such as fabric density, fabric porosity, and fiber arrangement. The analysis of variance (ANOVA) results shows that the fabric density affects the thermal conductivity values of the aerogel treated nonwoven fabric ($p = 0.006$).

Pressure (Pa)	Equation y=a + b*x	Value	t-test Significance ("Yes" or "No")	Adj. R-Square	F-test Significance ("Yes" or "No")
200	Intercept	0.05939	Yes	0.54399	Yes
	Slope	-3.1034E-4	Yes		
1000	Intercept	0.0696	Yes	0.56655	Yes
	Slope	-4.319E-4	Yes		
2000	Intercept	0.01	Yes	0.52221	Yes
	Slope	1.553E-4	Yes		
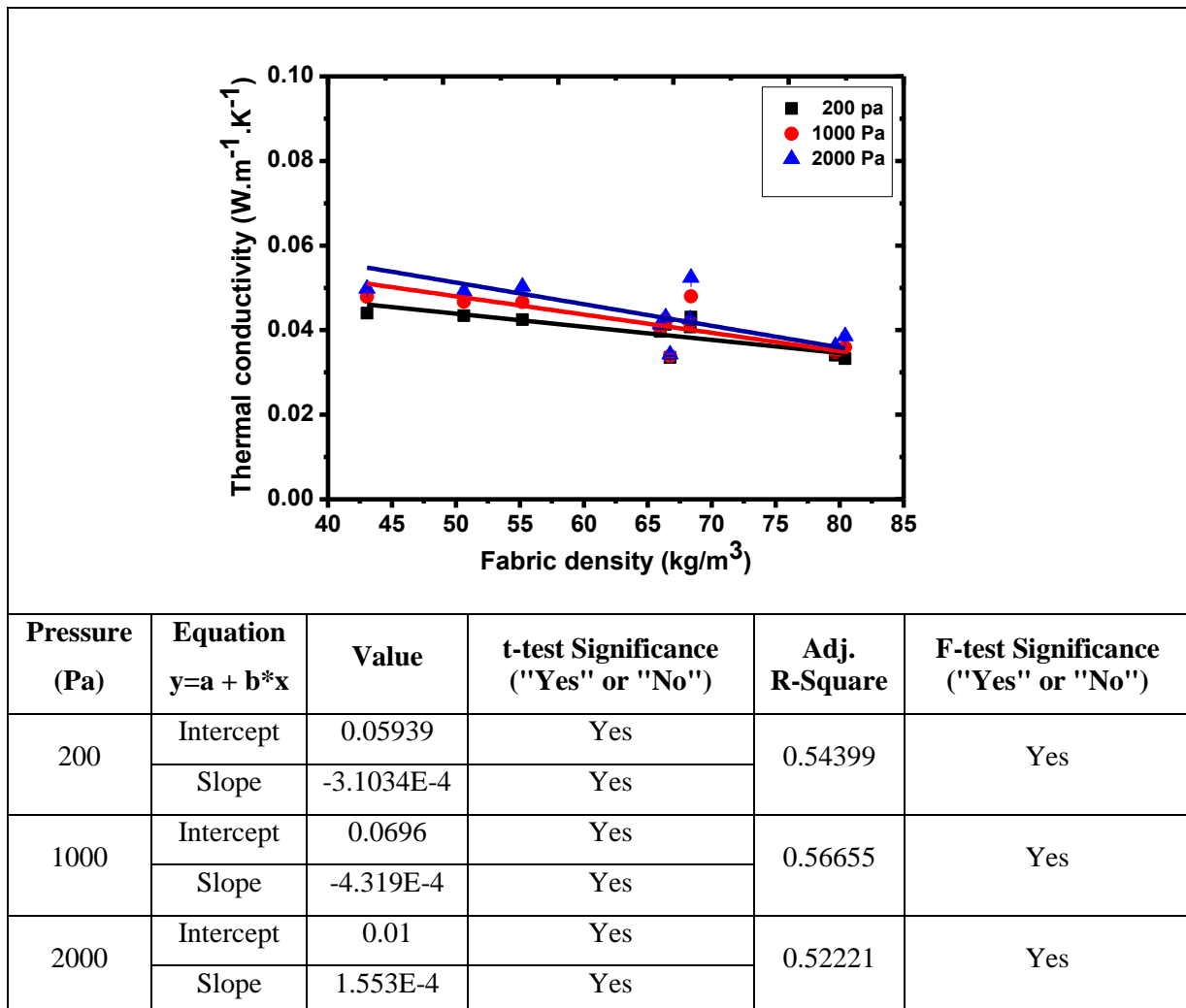
Figure 46. Thermal conductivity (TCi instrument).

Thermal resistance is a function of the thickness and thermal conductivity of a fabric, and is a very important parameter from the view point of thermal insulation, and is proportional to the fabric structure also. The original thickness measurements for the three fabrics were under relaxed conditions.

Equation y = a + b*x	Value	t-test Significance ("Yes" or "No")	Adj. R-Square	F-test Significance ("Yes" or "No")
Intercept	0.03327	Yes	0.88623	Yes
Slope	0.02437	Yes		
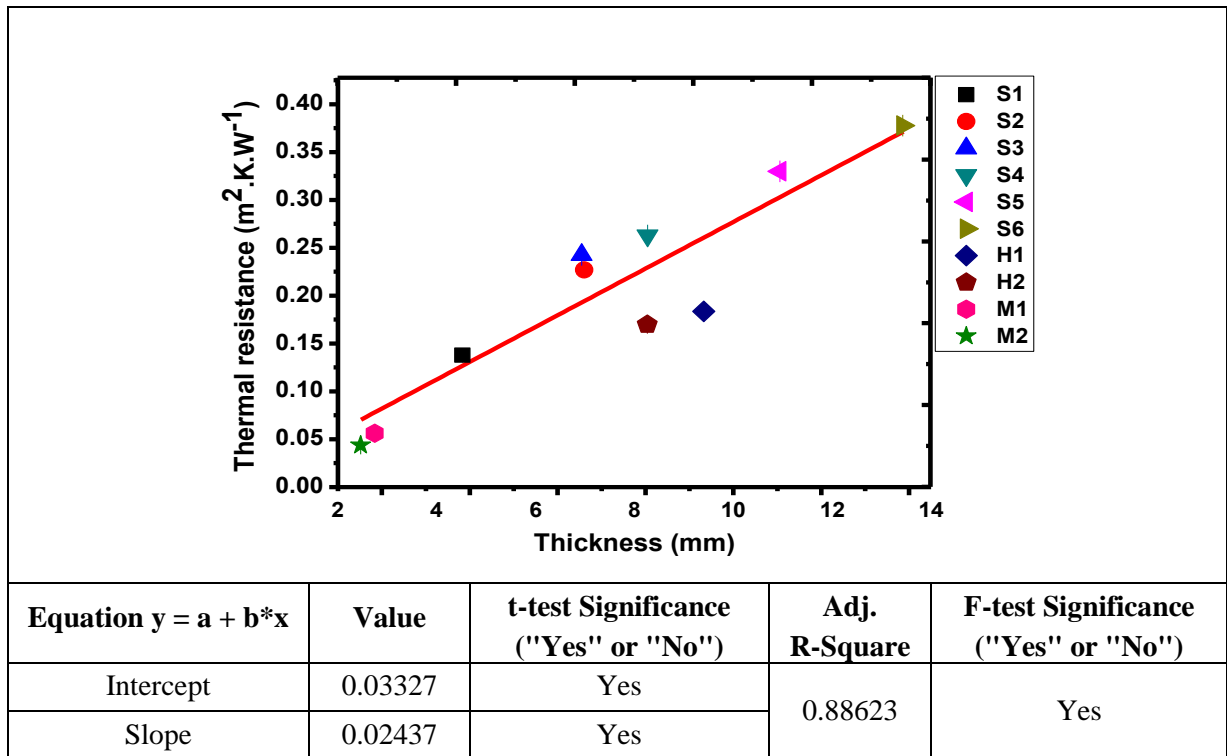
Figure 47. Thermal resistance (Alambeta).

Pressure (Pa)	Equation y = a + b*x	Value	t-test Significance ("Yes" or "No")	Adj. R-Square	F-test Significance ("Yes" or "No")
200	Intercept	10.8561	Yes	0.96209	Yes
200	Slope	23.812	Yes		
1000	Intercept	7.7868	Yes	0.95056	Yes
1000	Slope	23.1872	Yes		
2000	Intercept	4.03978	Yes	0.94735	Yes
2000	Slope	22.9534	Yes		
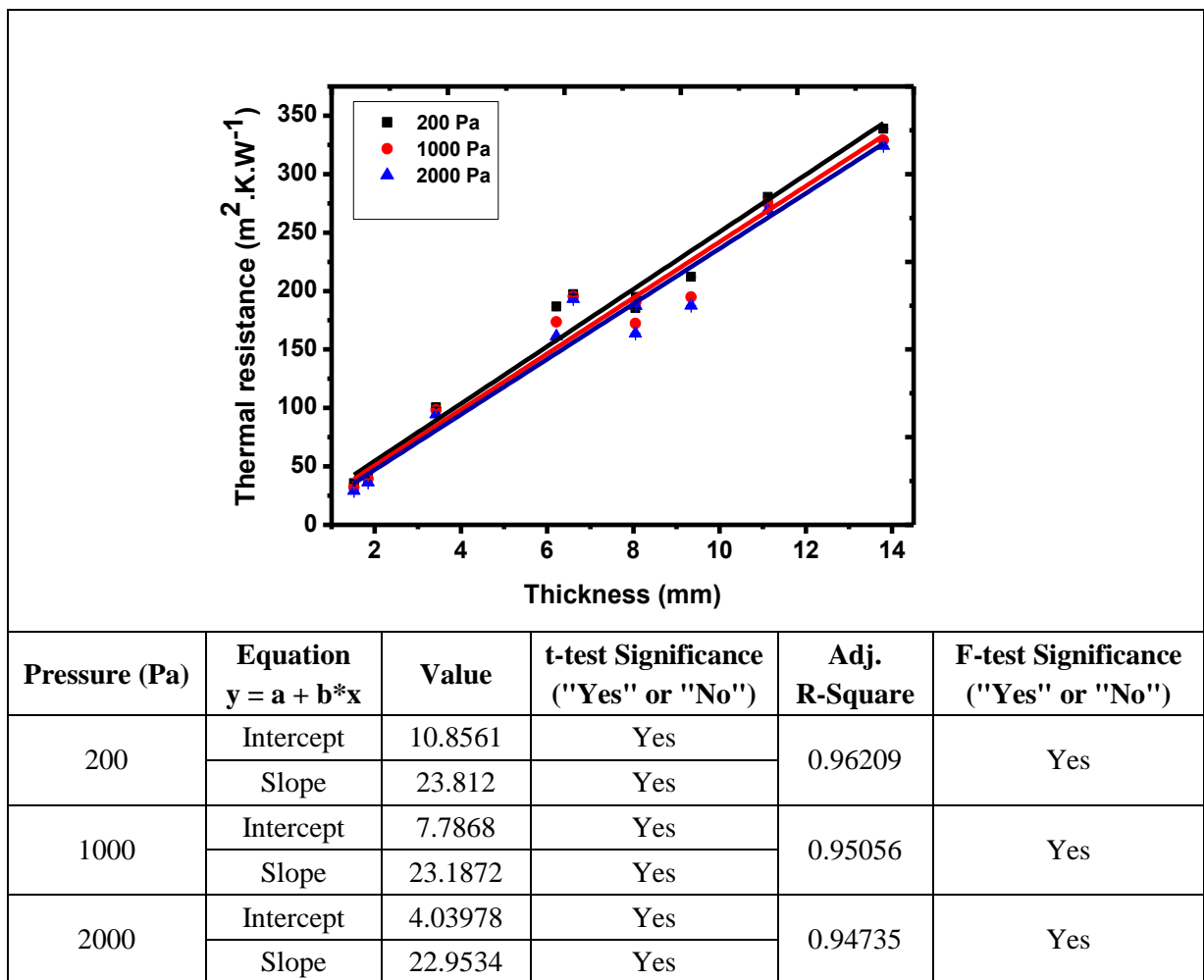
Figure 48. Thermal resistance (TCi).

Figure 47 indicates that the thermal resistance of sample S1, S2, H1, H2, M1 & M2 is lower than the samples S4, S5 and S6. It was observed that samples with higher thickness had higher thermal resistance. Figure 48 shows the effect of various pressure levels have an impact on thermal resistance. The various pressure levels didn't have much impact on the thermal resistance of the fabrics. Due to increase in thickness, there is an increase in thermal insulation and the decrease of heat losses are due to the space insulated by the fabric. This may be attributed to aerogel particles in the fabric. In the ideal case when all samples have same thermal conductivity, line in figure 47 & 48 should have intercept equal to 0 and slope equal to 1/thermal conductivity. It is interesting that line calculated by least squares is following this assumption and approximately all tested samples have the similar thermal conductivity. The statistical analysis shows that the fabric thickness has a highly significant influence on the thermal resistance ($p = 0.006$).

4.6 Evaluation of Thermal Properties by Custom Built Equipment

4.6.1   Effect of Temperature Variations

The environmental temperature versus the thermal conductivity of the fabric is shown in figure 49. The temperature variations at each point varied for the test specimens with the change in climatic chamber temperature (environmental temperature). The temperature gradient was higher for the lower temperatures (sub-zero temperatures). The temperature of materials is determined with thermal energy in the form of kinetic energy of disordered molecular movement [146]. Temperature gradient is an important factor for calculating the thermal conductivity of the test specimens. This difference in temperature gradient may be attributed to the aerogel present in the non-woven fabric. Aerogel is the main component in the non-woven fabric structure blocking air pockets inside its highly porous structure which provides thermal insulation and thereby considered to be beneficial for such applications. From the figure 49, it is found that the fabric temperature variations increase rapidly during initial stage of the exposure. This may be because of the temperature difference between the fabric sample and the exposed air is high in the early stage of the exposure process. As the temperature stabilizes, the variations decreased. It can be observed that the temperature difference between the inner surface and outer surface of test specimen increased as the sample thickness increased. A bulkier sample with lower density and more air pores inside proved to be more efficient in insulating the flow of heat from the hot plate to outer environment. It means that a human body can maintain the skin temperature for a longer time with insulating material of higher thickness having higher porosity. Aerogel treated

samples performed better in thermal insulation as compared to other samples at extreme temperatures.

Equation y = a + b*x		Value	t-test Significance ("Yes" or "No")	Adj. R-Square	F-test Significance ("Yes" or "No")
S1	Intercept	2.04E-02	No	0.97512	No
	Slope	1.79E-05	Yes		
S2	Intercept	3.55E-02	No	0.98335	No
	Slope	4.60E-05	Yes		
S3	Intercept	3.75E-02	No	0.95683	No
	Slope	5.57E-05	Yes		
S4	Intercept	4.56E-02	No	0.98013	Yes
	Slope	6.34E-05	Yes		
S5	Intercept	6.30E-02	No	0.95588	Yes
	Slope	1.24E-04	Yes		
S6	Intercept	7.79E-02	No	0.95152	No
	Slope	1.63E-04	Yes		
H1	Intercept	5.36E-02	No	0.88935	Yes
	Slope	8.90E-05	Yes		
H2	Intercept	4.64E-02	No	0.8557	Yes
	Slope	6.18E-05	Yes		

Figure 49. Thermal conductivity (custom built Instrument).

Thermal conductivity increases with fabric density and also for constant thickness of fabric; and below density of 60 kg/m^3, increase in fabric thickness causes increased thermal insulation and reduction in fabric temperature variations (up to an optimum level). The increase in weight-to-thickness ratio causes increase in effective thermal conductivity due to increase in fiber-to-fiber contact and packing density. It causes increase in tortuosity i.e.

mean free path for photons to be travelled and so less heat flows through the channels in nonwoven fabric [147, 148]. Regardless of the shape of the material, aerogel-treated non-woven fabric acts as an insulating layer with a conductivity that is constant. From figure 49, it can be seen that the thermal conductivity of the samples didn't show significant difference with respect to environmental temperature. Due to the open pore structure and irregular pore network of the aerogel present in fabric, solid and gaseous thermal conductivity is reduced. This reduction is due to the Knudsen effect, where the excited gas molecules that are entering the open pore structure of the silica aerogel collide with the surface of the aerogel and transfer their energy to the surface [149]. This reduces the gaseous movement, thus limiting the silica aerogel's gaseous thermal conductivity. Gaseous thermal conductivity can also be reduced by 33% by placing the aerogel under vacuum [150]. Sample S1 showed lower conductivity compared to other samples due to a relatively higher percentage of aerogel content.

4.6.2   *Determination of Thermal Resistance at Various Temperatures*

Figure 50 demonstrates how the environmental temperature affects the result in an almost linear relation between fabric thickness (expressed as volume of insulation material per unit of fabric area) and insulation [107]. Uniform distribution of heat provides the best insulation in the extreme cold conditions. Thermal insulation increases with thickness due to increased quantity of enclosed air, whereas if thickness is maintained constant, then thermal insulation decreases with increase in weight as quantity of enclosed air is reduced [151]. The thermal insulation value of porous, low-density non-woven fabric is affected by compression and hence the layered structure of aerogel treated non-woven fabric gives better insulation because of good compression recoverability. It can be observed that samples S2, S3, S4, S5 and S6 have higher resistance when compared to sample S1, H1 and H2. Thus, it can be stated that thickness and aerogel present had more profound effect on insulation compared to the material composition. One interesting observation is that the thermal resistance is higher at lower temperatures, in spite of having almost similar conductivity at all temperatures 51). This is mainly attributed to the nature of nanopores of air in the structure which are capable of higher insulation at much higher temperature gradient. However, after certain level of stabilization, their heat insulation capacity goes down and the resistance is also visibly lower. It was examined by one-way analysis of variance (ANOVA) with 95% confidence level. A significant difference ($p < 0.05$) has been observed. The analysis of variance (ANOVA) result reported as an F-statistic and its associated degrees of freedom with

significance limit (p value). Here, the ANOVA F-statistic is a ratio of variation between groups and variation within group.

Equation $y = a + b*x$		Value	t-test Significance ("Yes" or "No")	Adj. R-Square	F-test Significance ("Yes" or "No")
S1	Intercept	167.706	Yes	0.95341	Yes
	Slope	-0.12625	Yes		
S2	Intercept	175.065	Yes	0.97943	Yes
	Slope	-0.21106	Yes		
S3	Intercept	176.624	Yes	0.98399	Yes
	Slope	-0.22967	Yes		
S4	Intercept	188.057	Yes	0.9644	Yes
	Slope	-0.50901	Yes		
S5	Intercept	244.508	Yes	0.99203	Yes
	Slope	-0.3156	Yes		
S6	Intercept	258.008	Yes	0.89139	Yes
	Slope	-0.3765	Yes		
H1	Intercept	201.423	Yes	0.88663	Yes
	Slope	-0.2303	Yes		
H2	Intercept	163.646	Yes	0.87687	Yes
	Slope	-0.22741	Yes		

Figure 50. Thermal resistance (custom built instrument).

A large F is evidence against H_0 (null hypothesis), since it indicates that there is more difference between groups than within groups. ANOVA was done to analyze the results with 95% confidence level. A significant difference ($p < 0.05$) has been observed in the thermal resistance and conductivity properties of the nonwoven fabrics with different thicknesses.

4.7 Thermal Insulation of Insulative Materials from KES Instrument

From the figures 51 & 52, the fabrics measured in both KES thermolabo II and NT-H1 shows higher value of thermal conductivity for Sample S1 where the thickness of the assembly depends on the fabric density and the structure of the fabric.

Samples	Equation $y = a + b*x$	Value	t-test Significance ("Yes" or "No")	Adj. R-Square	F-test Significance ("Yes" or "No")
S1	Intercept	0.01112	Yes	0.73012	Yes
	Slope	3.30E-05	Yes		
S2	Intercept	0.01384	Yes	0.58249	Yes
	Slope	3.67E-05	Yes		
S3	Intercept	0.01485	Yes	0.67442	Yes
	Slope	4.60E-05	Yes		
S4	Intercept	0.01737	Yes	0.71875	Yes
	Slope	5.52E-05	Yes		
S5	Intercept	0.01472	Yes	0.79578	Yes
	Slope	4.36E-05	Yes		
S6	Intercept	0.01793	Yes	0.56237	Yes
	Slope	4.20E-05	Yes		

Figure 51. Thermal conductivity of fabrics (KES Thermolabo II).

Samples	Equation y = a + b*x	Value	t-test Significance ("Yes" or "No")	Adj. R-Square	F-test Significance ("Yes" or "No")
S1	Intercept	0.01183	Yes	0.76658	Yes
	Slope	2.80E-05	Yes		
S2	Intercept	1.49E-02	Yes	0.37774	Yes
	Slope	2.96E-05	Yes		
S3	Intercept	1.60E-02	Yes	0.53396	Yes
	Slope	3.47E-05	Yes		
S4	Intercept	0.01928	Yes	0.29455	Yes
	Slope	5.28E-05	Yes		
S5	Intercept	0.01618	Yes	0.46135	Yes
	Slope	3.41E-05	Yes		
S6	Intercept	0.01919	Yes	0.2976	Yes
	Slope	5.15E-05	Yes		

Figure 52. Thermal conductivity of fabrics (NT-H1).

Samples	Equation y=a + b*x	Value	t-test Significance ("Yes" or "No")	Adj. R-Square	F-test Significance ("Yes" or "No")
S1	Intercept	32.2125	Yes	0.6761	Yes
	Slope	-0.07534	Yes		
S2	Intercept	51.8101	Yes	0.5772	Yes
	Slope	-0.10951	Yes		
S3	Intercept	46.0984	Yes	0.6655	Yes
	Slope	-0.11048	Yes		
S4	Intercept	78.29634	Yes	0.7325	Yes
	Slope	-0.18517	Yes		
S5	Intercept	45.84196	Yes	0.7691	Yes
	Slope	-0.10694	Yes		
S6	Intercept	75.195	Yes	0.5666	Yes
	Slope	-0.13985	Yes		

Figure 53. Thermal resistance of fabrics (KES Thermolabo II).

Aerogel content present in the fabrics plays a major role and gives better thermal conductivity. Thermal resistance is a very important parameter from the point of view of thermal insulation, and is proportional to the fabric structure. Due to increase in thickness, it can be observed from figures 53 & 54, the increase of thermal insulation, and in the same way the decrease of heat losses for the space insulated by the fabrics.

Samples	Equation y=a + b*x	Value	t-test Significance ("Yes" or "No")	Adj. R-Square	F-test Significance ("Yes" or "No")
S1	Intercept	30.12817	Yes	0.77106	Yes
	Slope	-0.05555	Yes		
S2	Intercept	47.80054	Yes	0.35019	Yes
	Slope	-0.0733	Yes		
S3	Intercept	42.68925	Yes	0.51927	Yes
	Slope	-0.07141	Yes		
S4	Intercept	70.46511	Yes	0.23037	Yes
	Slope	-0.13584	Yes		
S5	Intercept	41.6434	Yes	0.43068	Yes
	Slope	-0.06921	Yes		
S6	Intercept	69.72783	Yes	0.21029	Yes
	Slope	-0.13109	Yes		

Figure 54. Thermal resistance of fabrics (NT-H1).

4.7.1   *Effect of Aerogel on Thermal Insulation of Fabrics*

The influence of wind speed on the thermal insulation properties of the fabrics has been studied. It is expressed as a percentage which represents the reduction in the rate of heat loss due to the insulation, relative to the heat loss from the surface. If figures 55 and 56 are considered, it can be observed that heat retention properties is always more important for

fabrics in colder environments; besides there is a linear relationship with the air flow velocity. The fabrics with high porosity will prevent air passage and then reduce convection heat loss.

Samples	Equation y=a + b*x	Value	t-test Significance ("Yes" or "No")	Adj. R-Square	F-test Significance ("Yes" or "No")
S1	Intercept	64.8493	Yes	0.931	Yes
	Slope	0.1209	Yes		
S2	Intercept	77.802	Yes	0.907	Yes
	Slope	0.0831	Yes		
S3	Intercept	74.452	Yes	0.876	Yes
	Slope	0.0946	Yes		
S4	Intercept	85.342	Yes	0.838	Yes
	Slope	0.0503	Yes		
S5	Intercept	75.766	Yes	0.870	Yes
	Slope	0.0778	Yes		
S6	Intercept	84.834	Yes	0.815	Yes
	Slope	0.0572	Yes		

Figure 55. Thermal Insulation of fabrics (KES Thermolabo II).

Samples	Equation $y = a + b*x$	Value	t-test Significance ("Yes" or "No")	Adj. R-Square	F-test Significance ("Yes" or "No")
S1	Intercept	63.4279	Yes	0.84936	Yes
	Slope	0.11556	Yes		
S2	Intercept	76.85152	Yes	0.70859	Yes
	Slope	0.07969	Yes		
S3	Intercept	74.10457	Yes	0.75576	Yes
	Slope	0.08615	Yes		
S4	Intercept	84.28019	Yes	0.51355	Yes
	Slope	0.0481	Yes		
S5	Intercept	73.44883	Yes	0.76595	Yes
	Slope	0.08883	Yes		
S6	Intercept	84.13632	Yes	0.49233	Yes
	Slope	0.04936	Yes		

Figure 56. Thermal Insulation of fabrics (NT-H1).

It is observed from figure 55 and 56 that with the increase in aerogel content, the thermal insulation rate increases with increase in wind velocity. This may be attributed to higher thickness of the fabric having higher aerogel content. All data were analyzed and found to fit the linear regression model. The residuals approximates (independent random errors) and goodness of fit (coefficient of determination, R^2), were calculated to see how closely values obtained from fitting a model match the dependent variable the model is intended to predict. The calculated results showed closer fit to data (goodness of fit was closer to 1 ($R^2 = 1$).

4.8 Correlation of TCi and Alambeta at Room Temperature

The TCi and alambeta instrument were correlated based on the results of thermal conductivity and thermal resistance measured at room temperatures. Results of thermal conductivity of both the instruments were found to be well correlated ($R^2 > 0.62$) as shown in figure 57 (*R*-squared is a statistical measure of how close the data are to the fitted regression line). Due to the dominance of low conductivities of enclosed air in the porous structure of the samples, fabric conductivity is mostly constant for fabrics of various thicknesses. Therefore, heat insulation is proportional to the thickness of the fabric.

Equation y = a + b*x	Value	t-test significance "Yes" or "No"	Adj. R-Square	F-test Significance "Yes" or "No"
Intercept	0.0257	Yes	0.6192	Yes
Slope	0.3965	Yes		
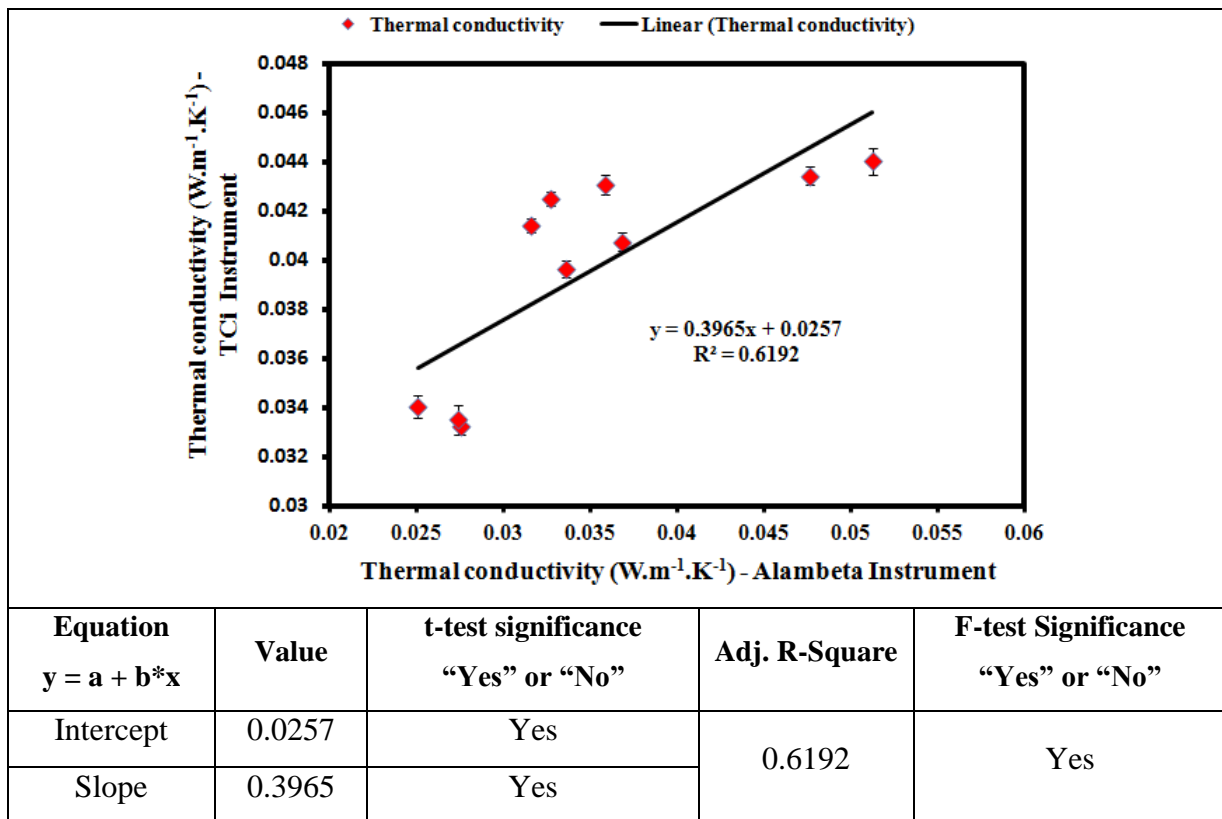
Figure 57. Correlation of thermal conductivity.

The total thermal resistance to transfer of heat from the body to the surrounding has three effective components namely, resistance to heat transfer from the material surface to surrounding, thermal resistance of clothing material itself and thermal resistance of the air trapped inside the fabric. The correlation of the two instruments for thermal resistance is shown in figure 58. The thermal resistances of both instruments correlate well with the value of around $R^2 > 0.9258$. The correlation proves that the two instruments are suitable for measuring the thermal properties only at room temperatures. Figure 59 shows the thermal conductivity of variances versus the thermal conductivity means using a log-log-scale for thermal conductivity with at least 20 reading.

Equation y = a + b*x	Value	t-test Significance "Yes" or "No"	Adj. R-Square	F-test Significance "Yes" or "No"
Intercept	4.1415	Yes	0.9258	Yes
Slope	0.8593	Yes		
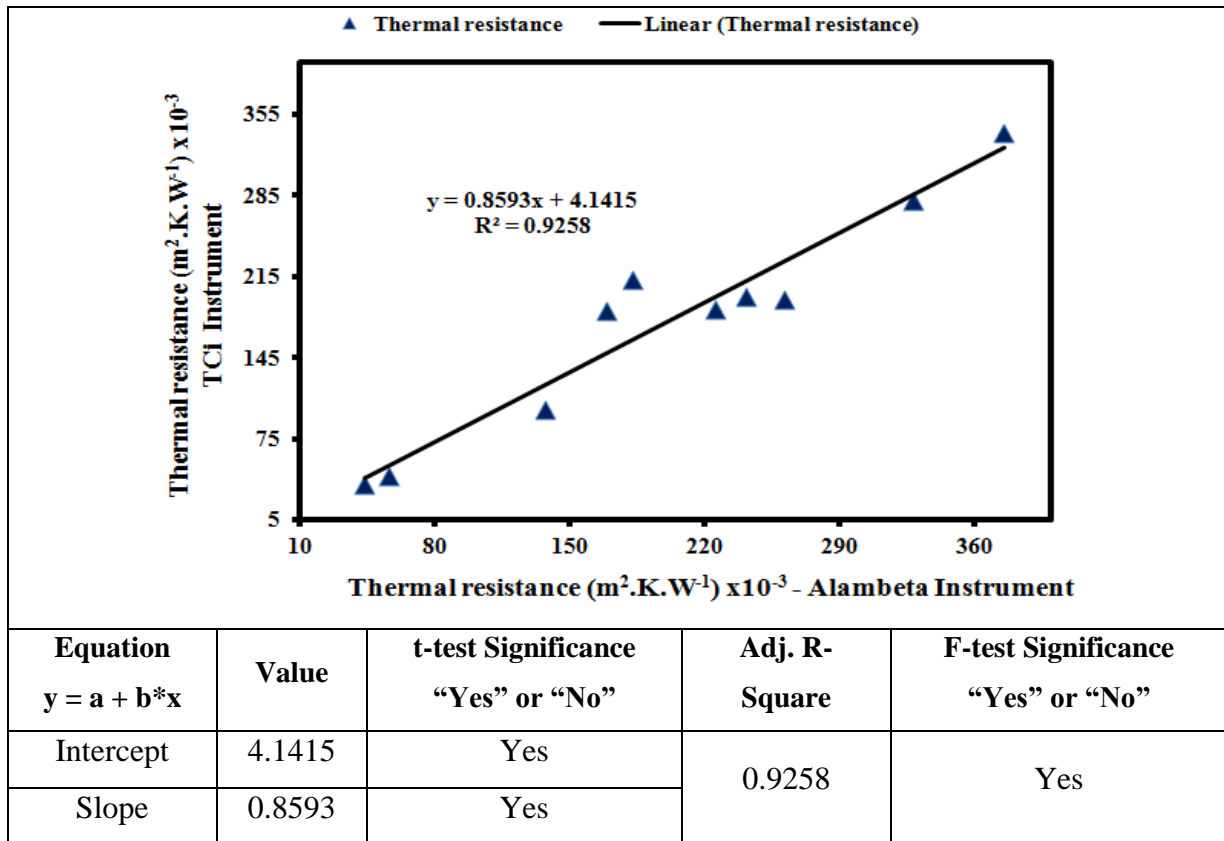
Figure 58. Correlation of thermal resistance.
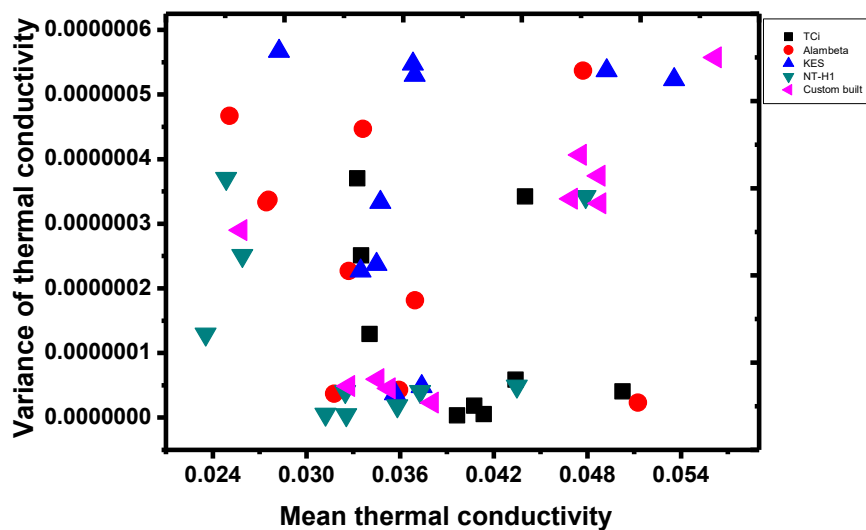
Figure 59. Mean-variance relationship of thermal conductivity.

From figure 59, it can be observed that most of the points lie, indicating that the variance is independent on mean i.e., no significant function of variance on mean. Still, the assumption of proportionality brings as much closer to the data than the assumption of constant variance.

4.9 Validation of Theoretical Model with Experimental Data

The correlations between experimental and theoretical model data are show in the figures 60 to 65. Theoretical model data was correlated with the measured data of three instruments namely, alambeta, TCi and custom built instrument. The theoretical model data were calculated as per the formulae given below. The thermal conductivity of parallel arrangement λ_{hP} (higher limit) is equal to,

$$\lambda_{hP} = P \ \lambda_a + (1-P) \ \lambda_f \tag{4.1}$$

For serial arrangements is thermal conductivity λ_{hS} (lower limit) defined as

$$\lambda_{hs} = \frac{\lambda_a \ \lambda_f}{P \ \lambda_f + (1-P) \ \lambda_a} \tag{4.2}$$

Actual composition of a fibers and air phases can be presented by linear combination of parallel and series structures [152]. The compromise is to compute the mean thermal conductivity of hollow fiber λ_h as arithmetic mean between upper and lower limit.

$$\lambda_h = \frac{\lambda_{hP} + \lambda_{hS}}{2} \tag{4.3}$$

The parallel/series structure gives a firsthand prediction and would give reasonable prediction accuracy for practical application due to its simplicity. The theoretical model and experimental data are shown in table 13. From the figure 60 to 65, it can be seen that the correlation between the theoretical and experimental values of thermal resistance were around $R^2 = 0.8$ for alambeta and custom built instrument. Around $R^2 = 0.9$ was for TCi instrument. Since the correlation between the theoretical calculation and the experimental values are good, it can be concluded that the data generated from the experiments are theoretically compatible.

Table 13. Theoretical model and experimental data.

Sample no.	Fabric density [kg/m³]	λ_{hp}	λ_{hs}	Thermal conductivity λ_h, [W m^{-1} K^{-1}]				Thermal resistance R, [m² K W^{-1}]			
				Calculated	Experimental			Calculated	Experimental		
					TCi	*Alambeta*	*Custom built*		*TCi*	*Alambeta*	*Custom built*
S1	79.66 (± 8.80)	0.0394	0.0255	0.0324	0.0340 (±0.0017)	0.0251 (±0.0013)	0.0317 (±0.0067)	0.1053	0.1006 (+0.0050)	0.1368 (+0.0068)	0.1687 (+0.0840)
S2	80.42 (± 9.00)	0.0396	0.0256	0.0325	0.0333 (±0.0017)	0.0276 (±0.0019)	0.0344 (±0.0023)	0.1907	0.1868 (±0.0093)	0.2252 (±0.0112)	0.1702 (±0.0085)
S3	66.73 (± 6.00)	0.0370	0.0253	0.0311	0.0335 (±0.0034)	0.0274 (±0.0024)	0.0366 (±0.0038)	0.2122	0.1972 (±0.0086)	0.2410 (±0.0120)	0.1810 (±0.0090)
S4	66.39 (± 1.36)	0.0369	0.0253	0.0311	0.0414 (±0.0021)	0.0315 (±0.0015)	0.0379 (±0.0019)	0.2591	0.1948 (±0.0007)	0.2611 (±0.0130)	0.2219 (±0.0113)
S5	65.99 (± 1.91)	0.0368	0.0253	0.0310	0.0396 (±0.0053)	0.0336 (±0.0047)	0.0439 (±0.0072)	0.3580	0.2805 (±0.0147)	0.3278 (±0.0163)	0.2886 (±0.0144)
S6	68.33 (± 2.90)	0.0373	0.0253	0.0313	0.0407 (±0.0067)	0.0368 (±0.0018)	0.0444 (±0.0035)	0.4408	0.3387 (±0.0163)	0.3753 (±0.0187)	0.3291 (±0.0164)
H1	43.06 (± 0.21)	0.0358	0.0255	0.0306	0.0440 (±0.0071)	0.0312 (±0.0026)	0.0438 (±0.0079)	0.3047	0.2122 (±0.0107)	0.1824 (±0.0091)	0.1672 (±0.0083)
H2	50.64 (± 1.11)	0.0372	0.0256	0.0313	0.0434 (±0.0075)	0.0326 (±0.0017)	0.0449 (±0.0032)	0.2563	0.1854 (±0.0921)	0.1686 (±0.0084)	0.1678 (±0.0079)
M1	55.20 (± 6.76)	0.0320	0.0251	0.0285	0.0420 (±0.0021)	0.0328 (±0.0016)	0.0424 (±0.0021)	0.0647	0.0430 (±0.0015)	0.0558 (±0.0072)	0.0557 (±0.0029)
M2	68.39 (± 3.14)	0.0339	0.0253	0.0296	0.0430 (±0.0022)	0.0359 (±0.0018)	0.0482 (±0.0024)	0.0514	0.0360 (±0.0018)	0.0433 (±0.0217)	0.0563 (±0.0082)

Note: "*±*" *is the upper and lower 95% confidence interval of the mean*

Equation y = a + b*x	Value	t-test Significance "Yes" or "No"	Adj. R-Square	F-test Significance "Yes" or "No"
Intercept	0.08637	Yes	0.22841	Yes
Slope	-1.77495	Yes		
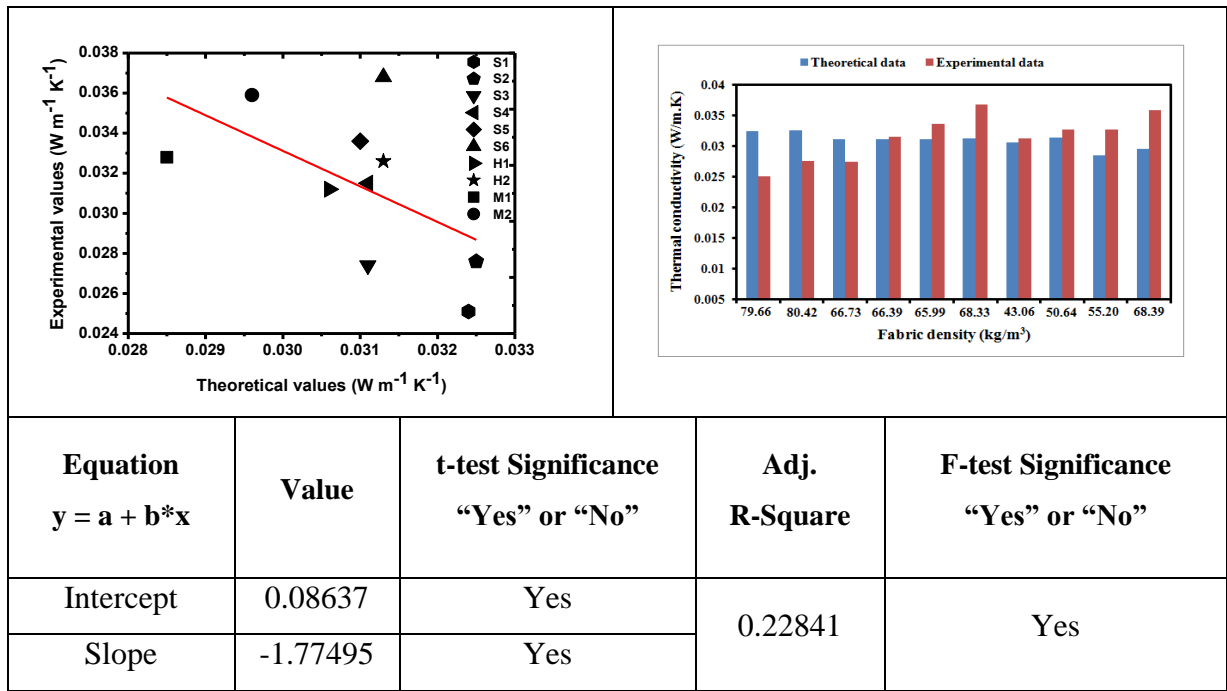
Figure 60. Thermal conductivity - alambeta (Experimental data Vs Theoretical model data).

Equation y = a + b*x	Value	t-test Significance "Yes" or "No"	Adj. R-Square	F-test Significance "Yes" or "No"
Intercept	0.11247	Yes	0.35864	Yes
Slope	-2.35333	Yes		
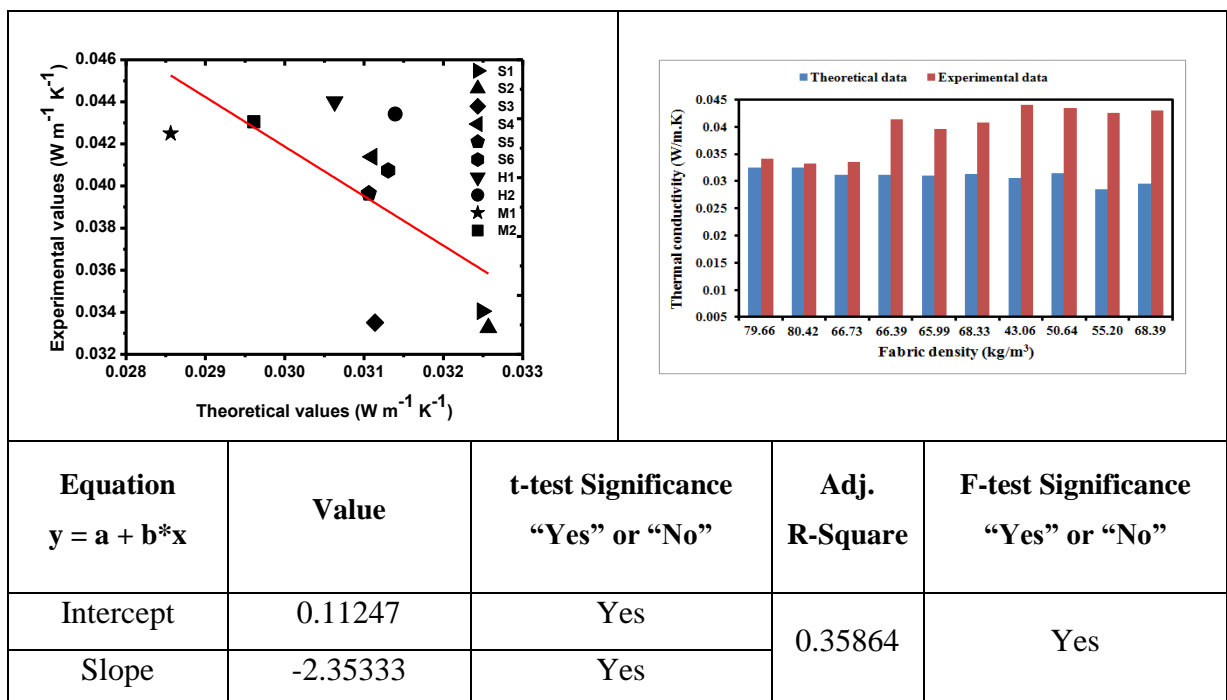
Figure 61. Thermal conductivity - TCi (Experimental data Vs Theoretical model data).

Equation y = a + b*x	Value	t-test Significance "Yes" or "No"	Adj. R-Square	F-test Significance "Yes" or "No"
Intercept	0.12894	Yes	0.33619	Yes
Slope	-2.84383	Yes		
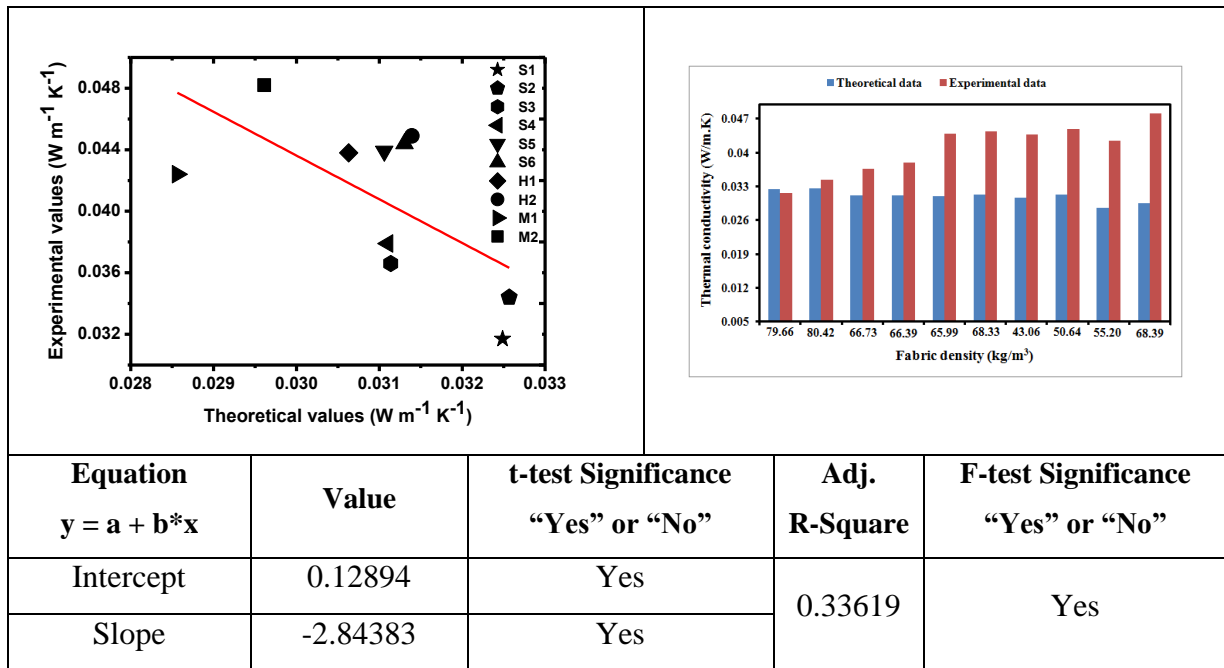
Figure 62. Thermal conductivity - custom built instrument (Experimental Vs Theoretical model data).

The thermal resistance values obtained from theoretical and experimental values are compared as shown in figures 63 to 65.

Equation y = a + b*x	Value	t-test Significance "Yes" or "No"	Adj. R-Square	F-test Significance "Yes" or "No"
Intercept	0.02907	Yes	0.80196	Yes
Slope	0.76971	Yes		
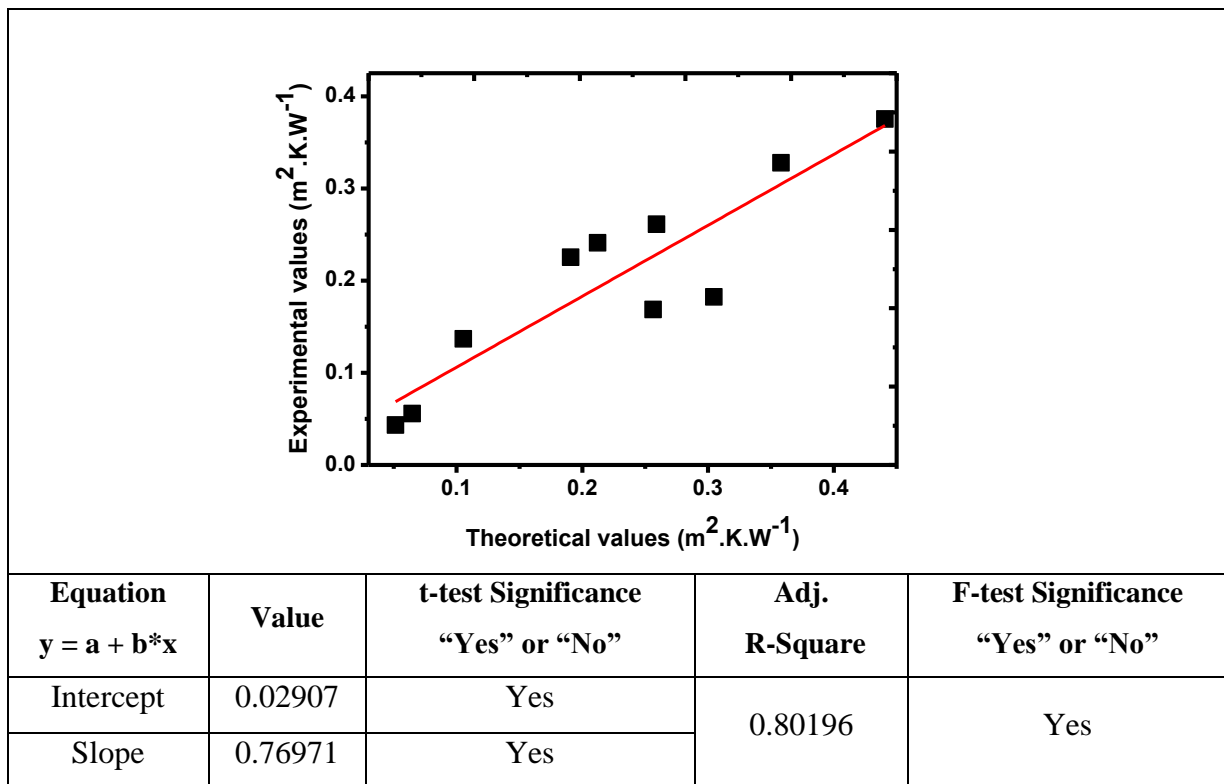
Figure 63. Thermal resistance - alambeta (Experimental Vs Theoretical model data).

Equation y = a + b*x	Value	t-test Significance "Yes" or "No"	Adj. R-Square	F-test Significance "Yes" or "No"
Intercept	0.01136	Yes	0.95212	Yes
Slope	0.74071	Yes		
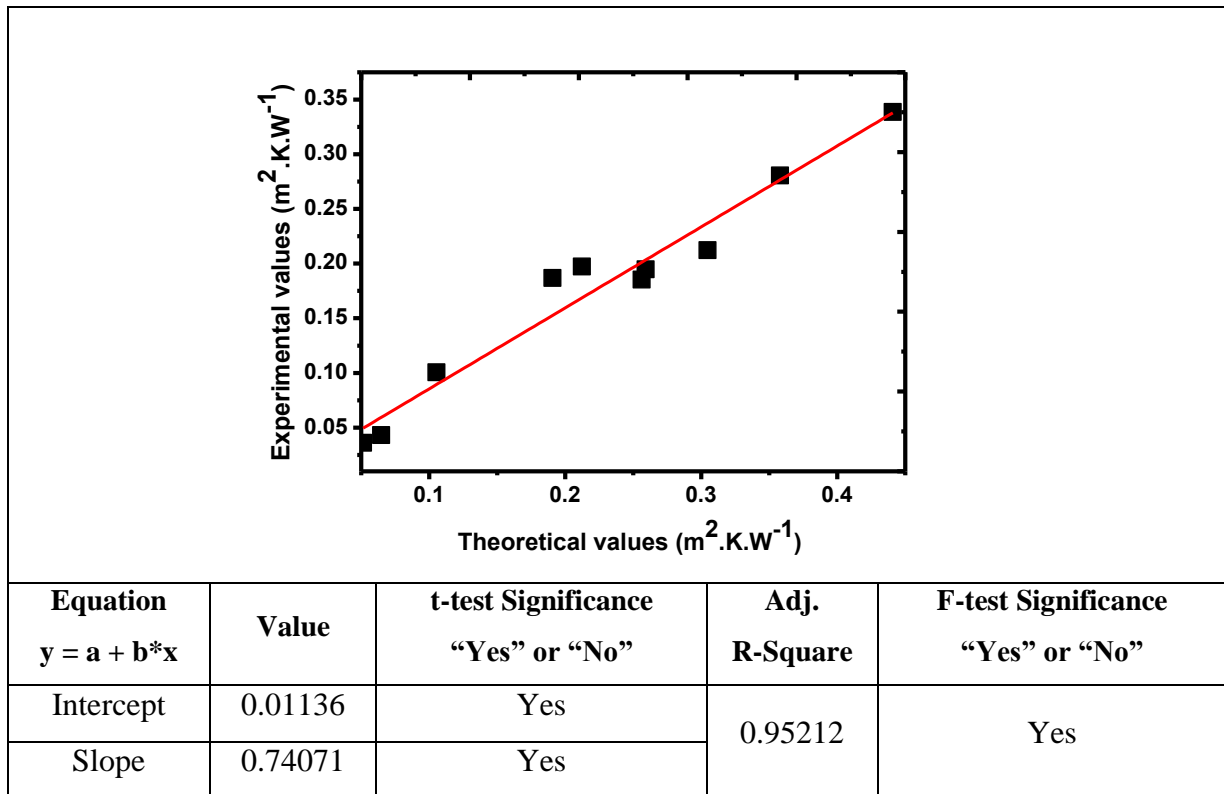
Figure 64. Thermal resistance - TCi (Experimental Vs Theoretical model data).

Equation y = a + b*x	Value	t-test Significance "Yes" or "No"	Adj. R-Square	F-test Significance "Yes" or "No"
Intercept	0.04112	Yes	0.81121	Yes
Slope	0.62202	Yes		

Figure 65. Thermal resistance - Custom built instrument (Experimental Vs Theoretical model data).

111

4.10   Assessment of Thermal Properties Using a Thermal Manikin

In this section, the thermal insulation values obtained from the cold protective fabrics, the aerogel treated nonwoven fabrics and needle punched nonwoven fabrics are presented. The discussion is focused on the resistance and clothing insulation results. Table 14 shows the results of the calculation of total and effective clothing insulation for selected ensembles obtained in tests on the thermal manikin. Both graphical representations highlight a comparative analysis of different insulation materials. The results obtained with the parallel method are globally followed and the parallel methods scenario was repeated in all the ensembles tested. In addition, it is important to underline that the highest differences between the calculations methods are seen to correspond to the cold protective ensemble. The mean values and standard deviation for the total (I_T and I_T *(human)*) and effective (I_{clo} and I_{clo} *(human)*) clothing thermal insulation were calculated on the basis of all experimental sessions. The differences between the mean clothing thermal insulation determined on the thermal manikin for fabrics were statistically significant (coefficient of significance = 0.02 to 0.03). The difference was about 13%; higher insulation was obtained for the aerogel treated nonwoven fabrics. The aerogel treated nonwoven fabrics insulation was around 2.05 clo.

4.10.1 Calculation of Manikin Results

Methods for the calculation of clothing insulation depend on the operating mode of the manikins. Only the parallel method should be used to calculate clothing insulation using insulation values from the individual segments when manikins are operated in UST (Uniform skin temperature) mode. The serial method should be used when manikins are operated in UHF mode. Ideally, in UHF (Uniform heat flux) mode, skin temperatures should be uniform to minimize heat transf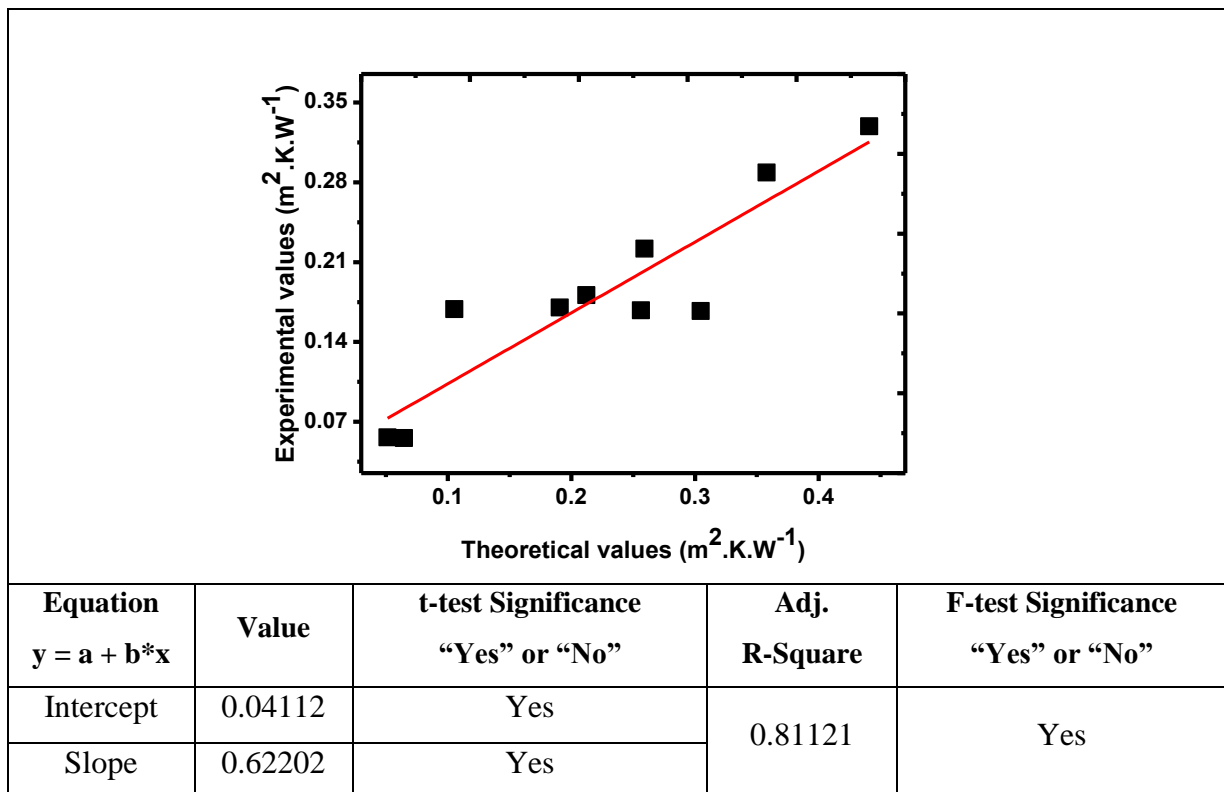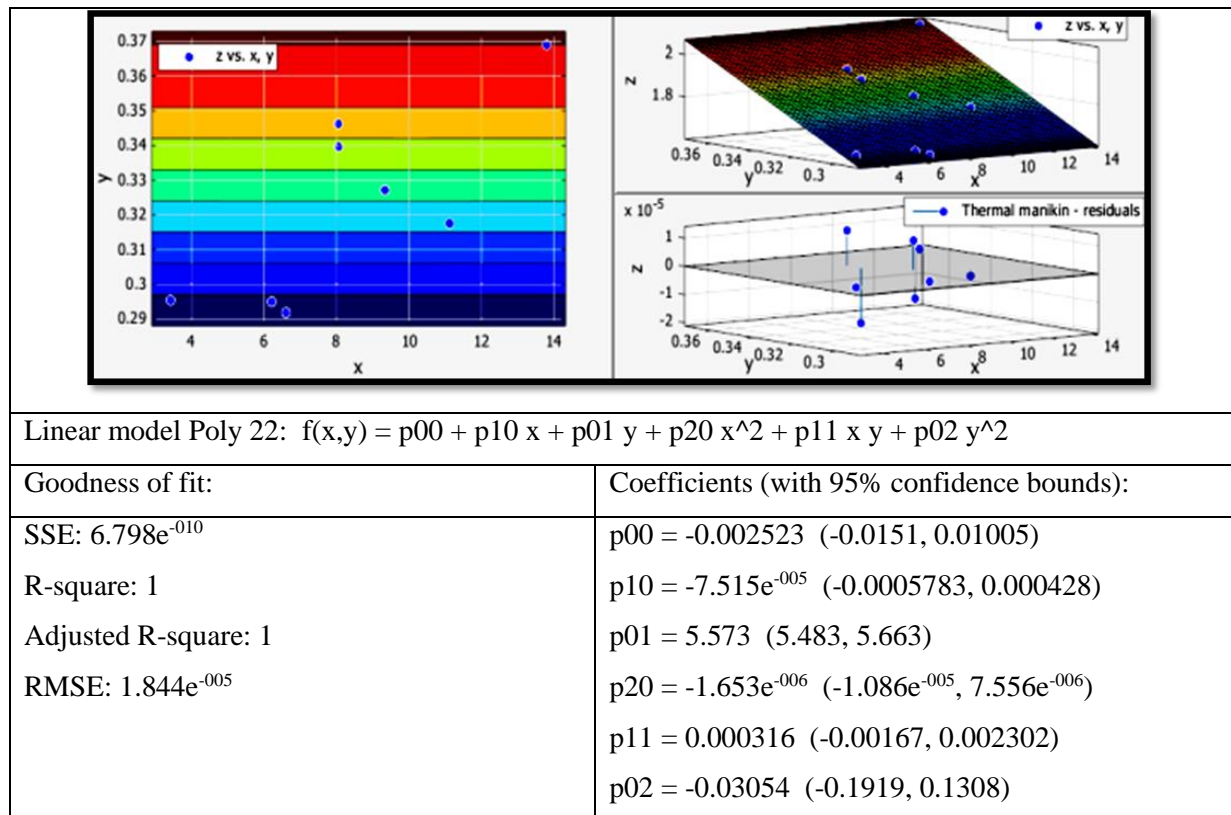er among segments, and in that case, the parallel method is a viable option. The serial It in UST mode does not yield total insulation that accurately represents the insulation performance of the clothing, and the resulting apparent insulation values will be misleading. Heat Loss Potential [W/m^2] is calculated for a standard environment by combining both the dry and sweating components of heat loss measured in their respective states. Since different fabric layers and reinforcements are used in clothing systems, resultant data from sweating manikin tests provide a powerful basis for understanding how to optimize the materials and clothing design to minimize heat loss from the full ensemble. Table 14 shows the results of the calculation of *R*-value & *Clo* value for selected ensembles obtained in tests on the thermal manikin.

Table 14. Thermal Manikin results.

Samples	Thickness [mm]	q, heat flux, [W/m²]	R-value [(m² K)/W]	Clo value
S1	3.424 (± 0.167)	50.520 (±2.273)	0.295 (±0.073)	1.6410 (±0.0738)
S2	6.212 (± 0.029)	44.100 (±1.985)	0.295 (±0.067)	1.6390 (±0.0738)
S3	6.608 (± 0.136)	43.140 (±1.941)	0.292 (±0.073)	1.6220 (±0.0737)
S4	8.060 (± 0.066)	40.150 (±1.807)	0.340 (±0.048)	1.8870 (±0.0849)
S5	11.120 (± 0.024)	41.120 (±1.850)	0.318 (±0.088)	1.7640 (±0.0794)
S6	13.800 (± 0.182)	39.170 (±1.763)	0.369 (±0.067)	2.0500 (±0.0923)
H1	9.336 (± 0.545)	82.000 (±3.690)	0.327 (±0.057)	1.8180 (±0.0818)
H2	8.048 (± 0.577)	80.000 (±2.902)	0.346 (±0.072)	1.9230 (±0.0113)

Linear model Poly 22: $f(x,y) = p00 + p10\,x + p01\,y + p20\,x^2 + p11\,x\,y + p02\,y^2$	
Goodness of fit:	Coefficients (with 95% confidence bounds):
SSE: $6.798e^{-010}$	$p00 = -0.002523$ $(-0.0151, 0.01005)$
R-square: 1	$p10 = -7.515e^{-005}$ $(-0.0005783, 0.000428)$
Adjusted R-square: 1	$p01 = 5.573$ $(5.483, 5.663)$
RMSE: $1.844e^{-005}$	$p20 = -1.653e^{-006}$ $(-1.086e^{-005}, 7.556e^{-006})$
	$p11 = 0.000316$ $(-0.00167, 0.002302)$
	$p02 = -0.03054$ $(-0.1919, 0.1308)$

Figure 66. 3D fit model (Thermal manikin) where x = Thickness [mm], y = R-Value [(m² K)/W] & z = Clo value.

Linear model Poly22: f(x,y) = p00 + p10 x + p01 y + p20 x^2 + p11 x y + p02 y^2	
Goodness of fit:	Coefficients (with 95% confidence bounds):
SSE: 0.000474 R-square: 0.9137 Adjusted R-square: 0.6979 RMSE: 0.01539	p00 = 6.683 (-6.816, 20.18) p10 = -0.09256 (-0.3402, 0.155) p01 = -0.1301 (-0.3412, 0.08104) p20 = 0.000412 (-0.00079, 0.001614) p11 = 0.0007745 (-0.0009191, 0.002468) p02 = 0.000713 (-0.0002566, 0.001683)
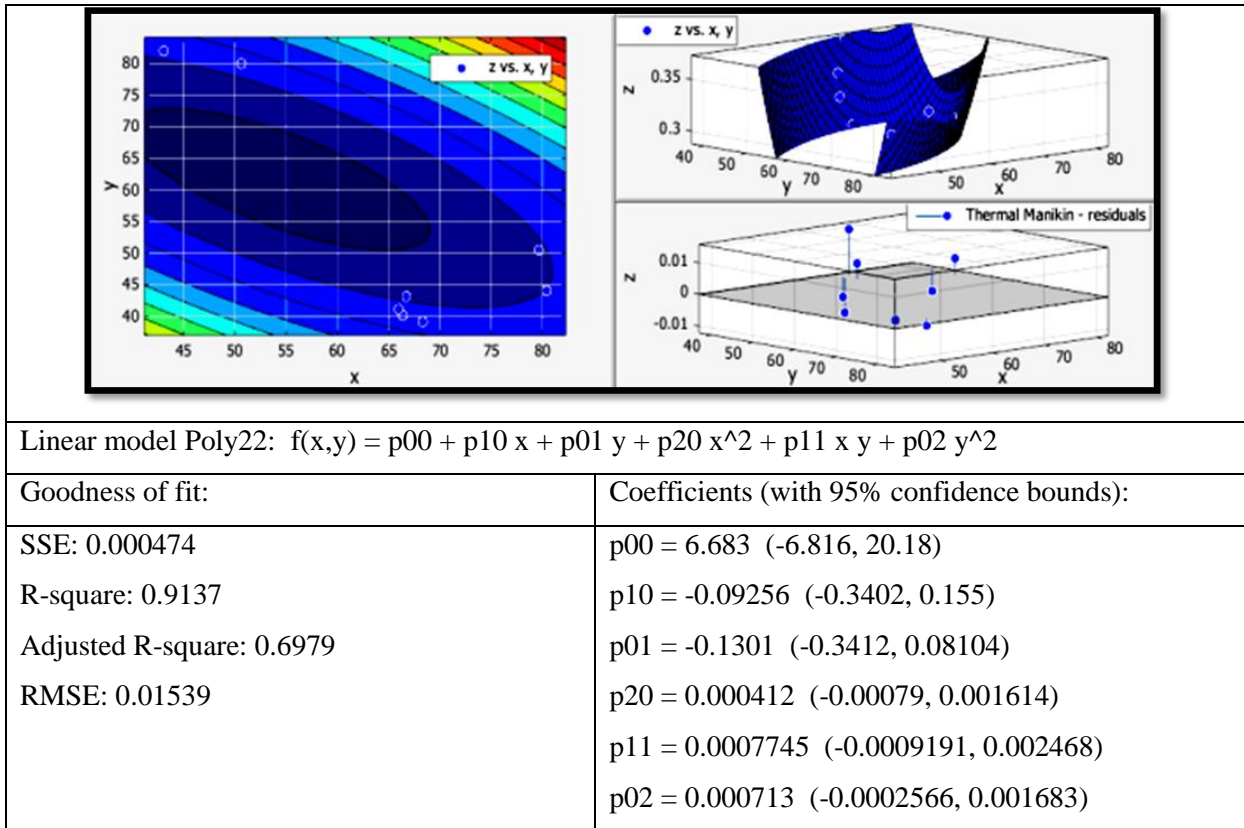
Figure 67. 3D fit model (Thermal manikin) where x = Fabric density [kg/m^3], y = Heat flux [W/m^2] & z = R-value [(m^2 K)/W].

The L-R plot is an influential scatter plot that is effective in distinguishing between high leverage points and outliers. The L-R plot combines the leverage values and the residuals in a single scatter plot. The leverage value p_{ii} (y-axis) versus the squared normalized residuals a_i^2 (x-axis). The scatter points on the L-R plot lie within the triangle. As can be seen from the figure 68, the data points are falling in the lower left corner and only one point are just above the blue hyperbolic curve. These few data points which are out of the triangle will not have much influence. There are no outliers or high leverage points are found in the dataset. It can be said that the data points are substantially influential.
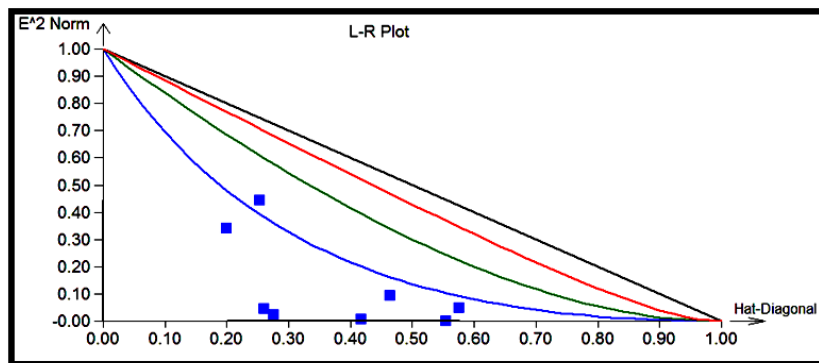
Figure 68. L-R Plot (Areal density, Heat flux & Thermal resistance) - Thermal manikin.

Q-Q plot is used for residual normality check. One advantage of the QQ-graph, compared to the statistics describing skewness, kurtosis etc. is that one can visually check whether the lack of normal appearance (nonlinearity) is caused by just a few points or whether it is a general tendency shared by all data. From the figure 69, it can be seen that the data points are normally distributed (Gaussian) residuals which are plotted close to the line. All random variables in the sequence have the same finite variance.
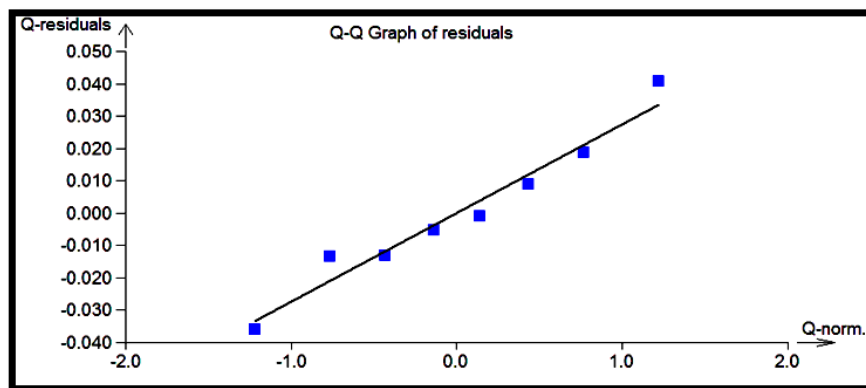
Figure 69. Q-Q plot for residual normality check.
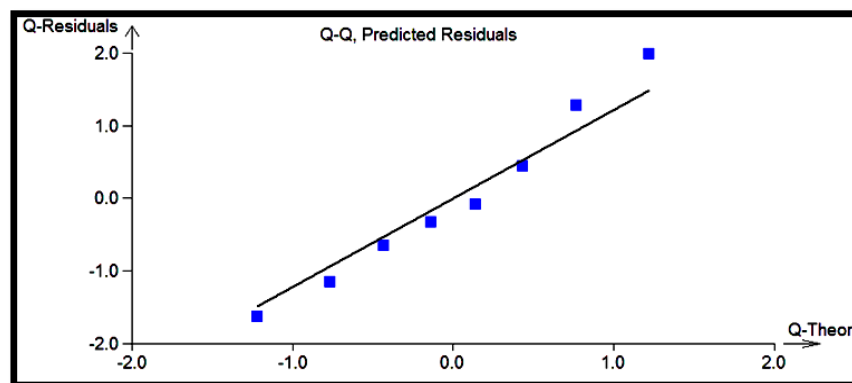
Figure 70. Q-Q Predicted Residuals.

Table 15. Statistical characteristics of regression.

Multiple correlation coeff. R	0.988
Determination coeff. R^2	0.975
Predicted correl. coeff. R_p	0.834
Mean quadratic error of prediction MEP	0.039

Predicted correlation coefficient, useful in the context of data containing outliers. Predicted correlation coefficient, R_p shows that the higher R_p (closer to one), the better is the sample quantile approximated by the theoretical quantile. The R_p can be looked at when comparing how good is the fit of different distributional types. It is anticipated that the calculation

115

models will improve the level of accuracy with regard to measurements of heat exchange between the human and the environment. The models are based on the data obtained from thermal manikin tests; that is, the real distributions of temperatures on a human like skin for given testing ensembles. It should also be pointed out that the insulation value is determined by a number of other factors, such as air velocity and body movement, which considerably decrease the thermal insulation of clothing ensembles, particularly in tests on the thermal manikin.

Table 16. Testing of the regression triplet (DATA+MODEL+METHOD) [141].

Fisher-Snedecor test for model significance	**Scott's test of multicollinearity**
Computed F-statistic : 98.96	Computed SC statistic : 0.73
Quantile F (1-α, m-1, n-m) : 5.786	Conclusion: Model exhibits multicollinearity!
Probability : 9.529295558E-005	
Conclusion: Model is significant	
Cook-Weisberg test of heteroscedasticity	**Jarque-Berra test for normality**
Computed CW Statistic : 0.361	Computed JB statistic: 0.781
Quantile χ^2 (1-α,1): 3.841	Quantile χ^2 (1-α,2) : 5.99
Probability : 0.548	Probability : 0.677
Conclusion: Residuals exhibit homoscedasticity.	Conclusion: Normality of residuals is accepted.
Wald's test for autocorrelation	**Durbin-Watson's test for autocorrelation**
Computed WA statsitic : 2.372	Computed DW statistic: -1
Quantile χ^2 (1-α,1): 3.841	Critical values of DW : 2
Probability : 0.123	Conclusion: Negative autocorrelation is not proved.
Conclusion: Autocorrelation is insignificant	

4.11   Convective Heat Transfer by Forced Convection - Laboratory setup Instrument

To predict the contribution of convective heat transmission on total thermal transmission characteristics of fabrics, the thermal resistances of fabrics were measured under forced convection mode. From the statistical analysis, it can be seen that the thermal transmission through multilayered fabrics significantly differs under convective mode of heat transfer. It can be observed from table 17 that the thermal resistance of all the fabrics under forced convection mode shows high thermal resistance. In this study, since the dry heat transmission is under consideration, the evaporative heat transmission is neglected. Due to the temperature gradient between test plate and the ambient air the density of air present within the textile material varies gradually from test plate to ambient air. Due to the

variation in density, the air moves from the region of higher density to that of lower density, i.e. from the region adjacent to the test plate to the region adjacent to the ambient air layer [153]. The thermal resistance during forced convection in general is lower than that of natural convection, because of higher air speed. So the heat transfer through fabric is generally higher. The thermal transmission during forced convection takes place due to the movement of air and the heat transfer coefficient depends on the air velocity [154-156]. It can be observed from table 17 that aerogel treated nonwoven fabrics has highest thermal resistance.

Table 17. Results of laboratory set-up instrument.

Samples	Temperature Gradient (Convection) ℃	Heat Transfer Coefficient [W/(m² K)]	Thermal conductivity [W/(m K)]	Thermal resistance [(m² K)/W] x10⁻³
S1	14.5	26.31 (±1.32)	0.0440 (±0.0022)	77.46 (±3.87)
S2	9.0	30.60 (±1.53)	0.0360 (±0.0018)	172.07 (±8.60)
S3	8.3	28.52 (±1.45)	0.0310 (±0.0016)	214.54 (±10.76)
S4	10.0	27.07 (±1.36)	0.0330 (±0.0017)	244.24 (±12.21)
S5	12.5	25.81 (±1.30)	0.0420 (±0.0021)	264.76 (±13.24)
S6	7.5	29.25 (±1.46)	0.0290 (±0.0015)	477.51 (±23.88)
H1	6.8	38.38 (±1.92)	0.0430 (±0.0042)	218.64 (±10.93)
H2	6.5	32.71 (±1.64)	0.0390 (±0.0027)	258.78 (±12.94)

Note: "±" *is the upper and lower 95% confidence interval of the mean.*

The needle punched struto nonwoven fabrics show least thermal resistance value. The higher thermal resistance in aerogel treated nonwoven fabric is mainly due to presence of higher amount of air within the structure. The thermal resistance differs with respective to thickness of the fabrics used in the study. From the statistical analysis, it is observed that the type of fabric significantly affects the thermal resistance of multilayered fabrics. The effect of type of fabric on thermal resistance is statistically significant at 95% confidence interval. The thermal transmission at this situation is solely governed by the thermal resistance of the

component fabric layer. The only difference between the fabrics H1 and H2 is the middle layer, i.e. meltblown polyamide nanofiber NF1 and NF2, respectively. It is also evident from table 17 that in general the thermal resistance of fabric H1 and H2 are lower than the S1 to S6. The reason for this is that the middle layer of the S1 to S6 fabric consist of aerogel with relatively higher thermal resistance than needle punched struto nonwoven fabric (H1 and H2). Convective heat transfer coefficient depends on air velocity, which defines the type of the convection [157]:

- for small air flow velocities (V_a < 1 m/s) there is a free convection type, for which:

$$h_c = 3.5 + 5.2 \ V_a \tag{4.4}$$

- for higher velocities (Va > 1 m/s), the forced convection is as follows:

$$h_c = 8.7 \ V_a \tag{4.5}$$

Since fabrics were measured in forced convection mode, the heat transfer coefficient is calculated with air velocity 2.5 m/s. By substituting the air velocity in the equation 4.5, the heat transfer coefficient for forced convection is 21.75 W/(m^{2}K).

Probability-Probability (P-P) plot compares data distribution with several theoretical models, using the empirical cumulative distribution function and cumulative distribution function of normal (solid blue curve), Laplace, and uniform distributions. A model which fits data well should plot approximately as the y = x line. From the figure 71 the data fit well with y = x line except sample H1 (conduction) which proves that the other samples have better fit. The plots are used to distinguish among symmetrical distributions according to their kurtosis.
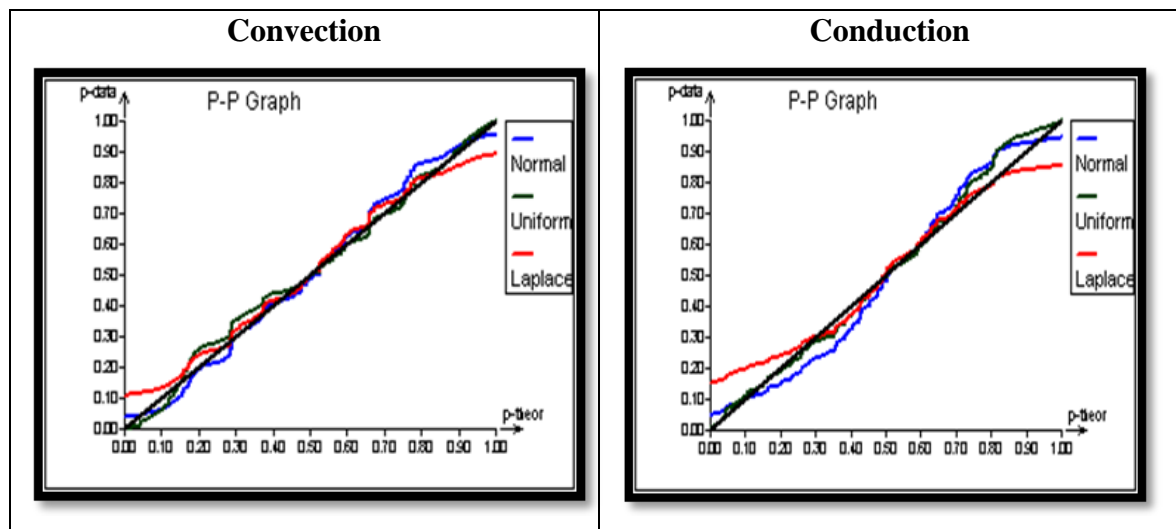

Figure 71. Probability-Probability (P-P) plot of convection and conduction heat transfer.

The parameters and values shown in table 18 are calculated for the fluid flow profile above the fabric samples. From these dimensionless numbers the type of flow can be found. For any given condition of velocity profile, it is the relative magnitude of v/α which determines the magnitude of convective heat transfer.

Table 18. Calculated parameters of the fluid flow profile.

The length of the specimen	$L = 15$ cm
Area of the specimen	$A = 120$ cm^2
Air free-stream velocity	$u_\infty = 2.5$ m s^{-1}
Air free-stream temperature	$T_\infty = -10$ °C
Air viscosity	$\mu = 0.017$ cP
Air density	$\rho = 1.29$ kg m^{-2} K^{-1}
Air specific heat	$c_p = 1.005$ kJ kg^{-1} K^{-1}
Thermal conductivity of air	$k = 0.025$ W m^{-1} K^{-1}
Reynolds Number	$Re = 2.84$ x 10^3
Prandtl Number	$Pr = 0.683$
Nusselt Number	$Nu = 139.8$
Heat Transfer Coefficient	$h_c = 23.3$ W m^{-2} K^{-1}

Correlations between three important dimensionless (empirically obtained) numbers can be used to estimate the value of heat transfer coefficient. The convective heat transfer coefficient h_c strongly depends on the fluid properties and *roughness* of the solid surface, and the type of the fluid flow (*laminar* or *turbulent*).
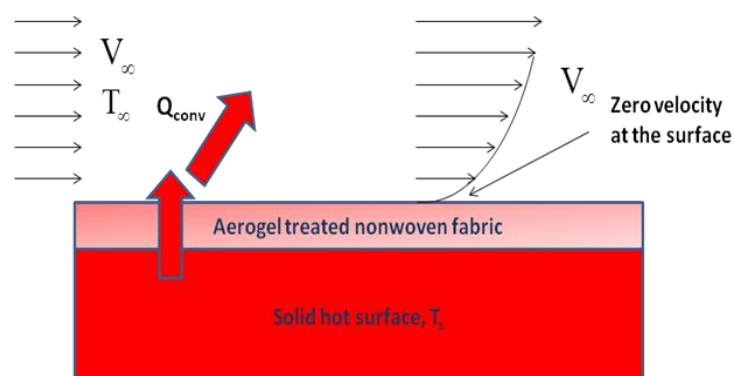

Figure 72. Forced convection.

As shown in the figure 72, it is assumed that the velocity of the fluid is zero at the wall; this assumption is called no slip condition. As a result, the heat transfer from the solid surface to

the fluid layer adjacent to the surface is by pure conduction, since the fluid is motionless. The velocity and the temperature of the fluid approaching the fabric are uniform at U_∞ and T_∞. The fluid can be considered as adjacent layers on top of each others.
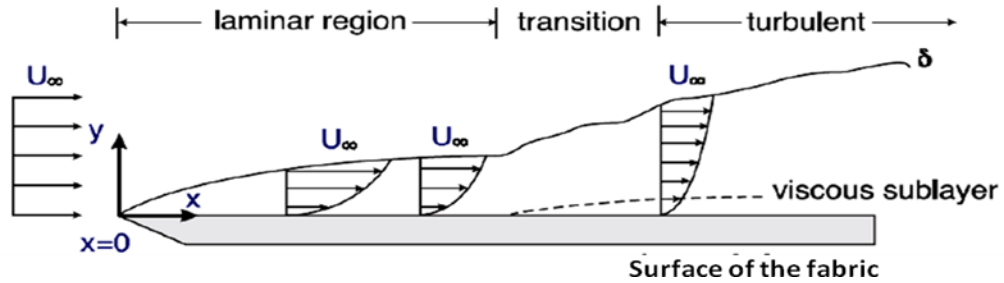
Figure 73. Velocity boundary layer.

Assuming no-slip condition at the wall, the velocity of the fluid layer at the wall is zero. The motionless layer slows down the particles of the neighboring fluid layers as a result of friction between the two adjacent layers. The presence of the fabric is felt up to some distance from the fabric beyond which the fluid velocity U_∞ remains unchanged. This region is called *velocity boundary layer* as shown in figure 73. Similar to velocity boundary layer, a thermal boundary layer as shown in the figure 74 develops when a fluid at specific temperature flows over a surface which is at different temperature.
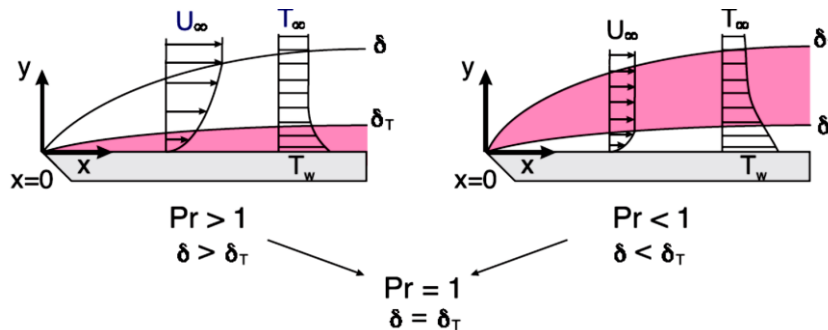
Figure 74. Thermal boundary layer.

The thickness of the thermal boundary layer δt is defined as the distance at which:

$$\frac{T - T_s}{T_\infty - T_s} = 0.99 \tag{4.6}$$

The relative thickness of the velocity and the thermal boundary layers is described by the Prandtl number. For low Prandtl number fluids, heat diffuses much faster than momentum flow ($Pr = v/\alpha << 1$) and the velocity boundary layer is fully contained within the thermal boundary layer. On the other hand, for high Prandtl number fluids, i.e. oils, heat diffuses

much slower than the momentum and the thermal boundary layer is contained within the velocity boundary layer.

4.12   Fluid Flow by Thermal Convection using Particle Image Velocimetry

Vector and scalar maps of the fluid flow developed by thermal convection above the textile sample were plotted for different temperature gradients. The vector maps are colored to highlight the acceleration zones. The scalar maps were put in one scaling and could be compared. Scalar maps are used to display the on-screen multiple data derived from the velocity fields. The x and y axis scales in vector and scalar maps illustrate the magnitude and direction of the out-of-plane velocity component.
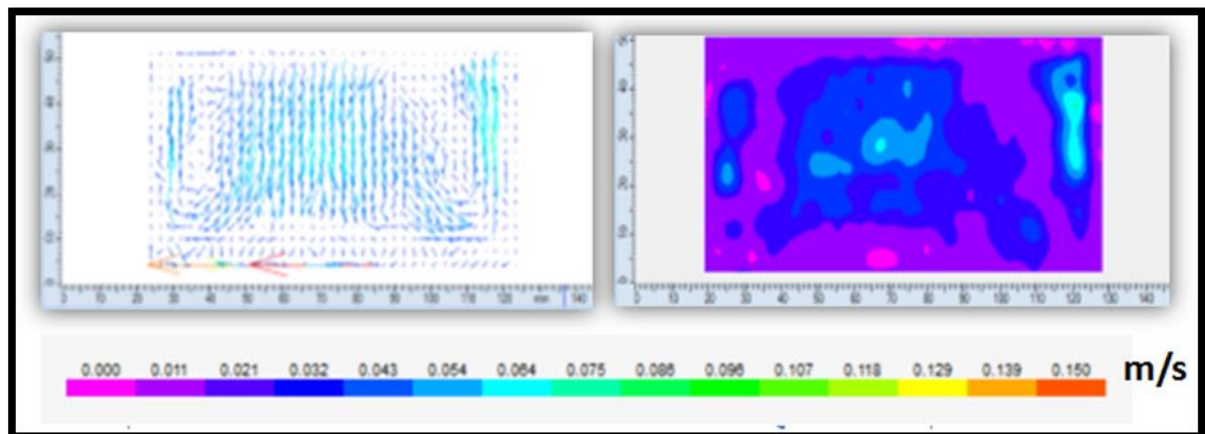
Figure 75. Vector and scalar maps for temperature gradient 21.5 °C.
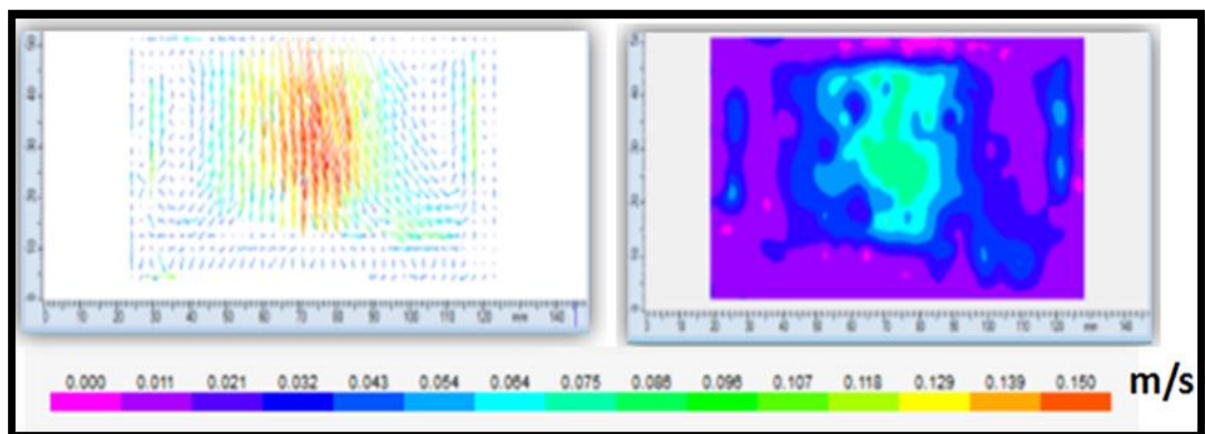
Figure 76. Vector and scalar maps for temperature gradient 23.8 °C.
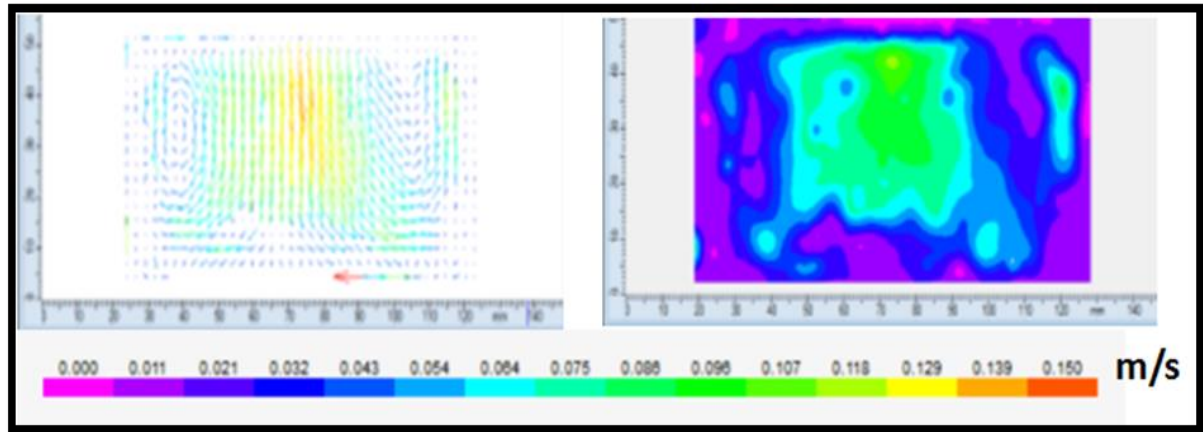
Figure 77. Vector and scalar maps for temperature gradient 37.5 ℃.
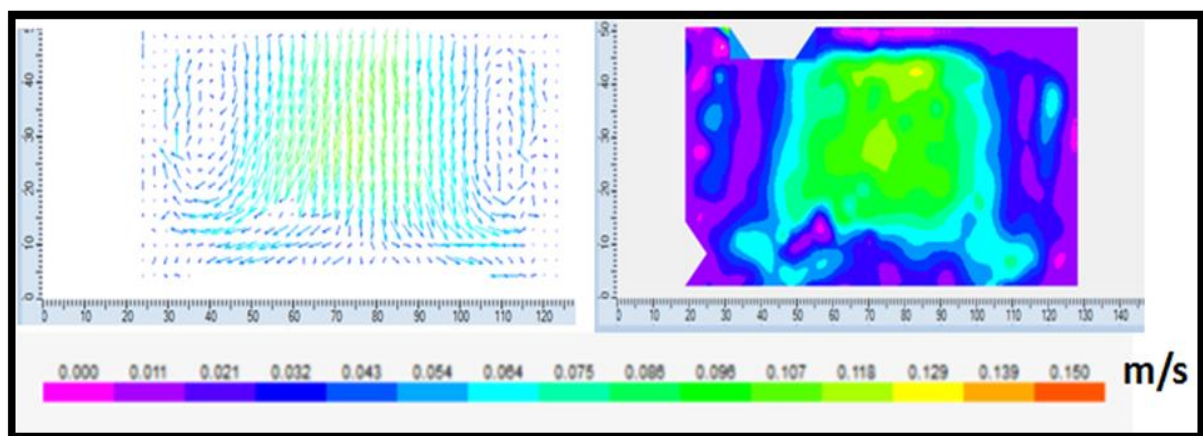
Figure 78. Vector and scalar maps for temperature gradient 51.0 ℃.

Vorticity contours for the instantaneous flow structure is a vector field that gives a microscopic measure of the rotation at any point in the fluid. Vector and scalar maps for temperature gradients corresponding to difference between human body and chilling atmosphere are shown in figures 75 to 78. Evaluation recorded is based on the relationship between speed, distance, and time, where distance represents the displacement of particles entrained in the surrounding fluid (air) flowing in a defined time interval between two laser pulses. The distance and air velocity diagram is shown in figure 79. These charts describe the behavior at different temperature gradients (between the textile sample and temperature of neighborhood). As it is expected, the fluid flow motion accelerates according to the increasing temperature gradient. This velocity profile is taken 25 mm above the free surface of the textile sample. The maximum velocity is reached with temperature gradient of 51.0 ℃. The construction of the testing chamber did not allow observing the situation just above the surface of textile sample due the reflections.
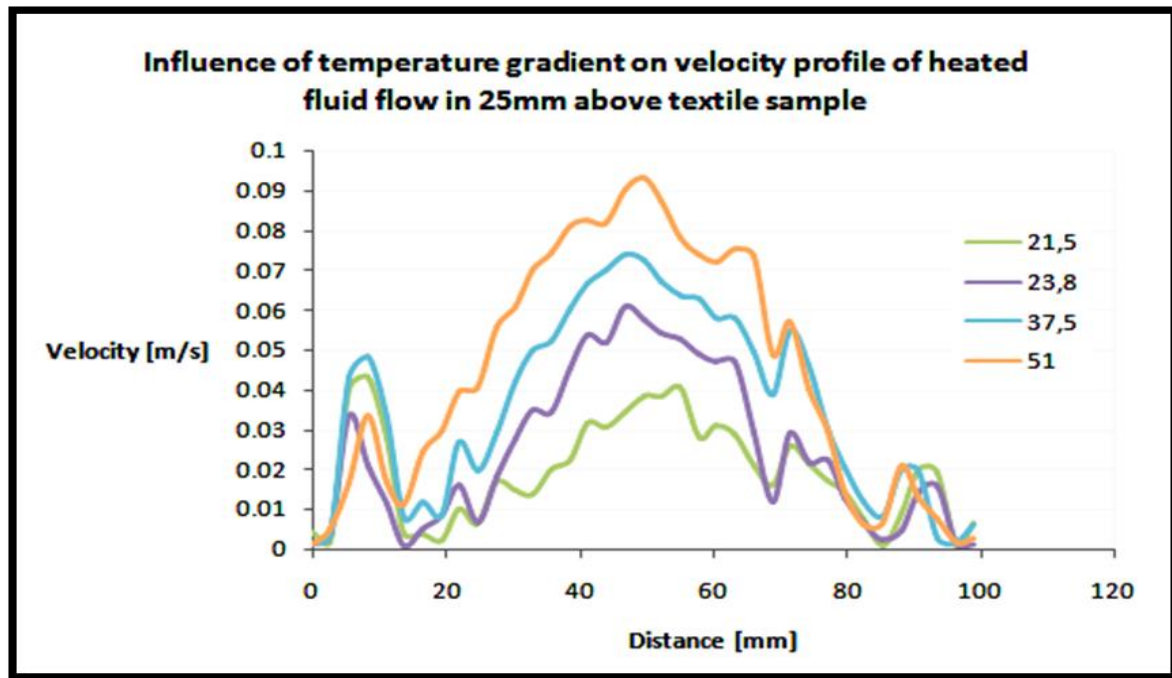
Figure 79. Distance and air velocity diagram.

These results are very important for setting the boundary condition of numerical simulation, describing the behavior of textile samples in the subzero temperature condition as well as for simulation of heat transfer through the porous media.

4.13 Thermal Properties of Electrospun Nanofibrous PUR and PVDF Layer embedded with SiO$_2$ Aerogel

Thermal conductivity as a function of areal density for PUR and PVDF electrospun nanofibrous layer embedded with silica aerogel is shown in figures 80 to 83. As shown in figure 80 to 83, thermal conductivity of the electrospun nanofibrous layer decreased with increase in density. This can be explained by the fact that as the density increases; it makes the fibrous structure more packed. This causes the mean free path (distance travelled by a photon before it collides with another fiber surface [152] for a photon movement to decrease thus causing a decrease in the heat transfer because of radiative conduction. When the density comes to a critical point, the increase in conduction through solid phase (fibers) and decrease in radiation conductivity results in an increase in total thermal conductivity [158, 159]. In fact, in fibrous structures the small size of the pores and the tortuous nature of the air channels present prevents any heat transfer by convection [160].

Equation y = a + b*x	Value	t-test Significance "Yes" or "No"	Adj. R- Square	F-test Significance "Yes" or "No"
Intercept	0.03103	Yes	-0.28677	Yes
Slope	2.82323E-5	Yes		
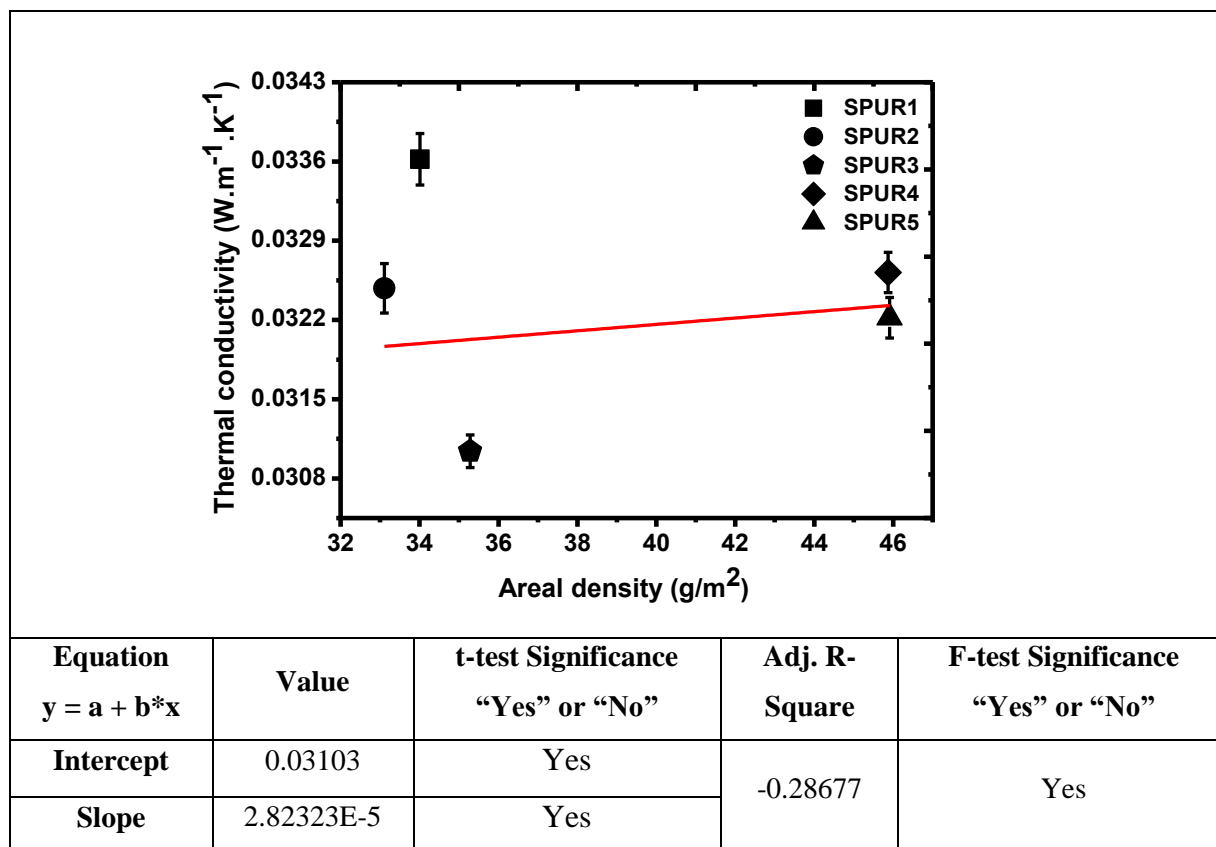
Figure 80. Thermal conductivity Vs GSM for PUR samples with spunbond PP.

Moreover, in fibrous insulation materials because of low fiber volume fraction, heat conduction through the solid phase (the fibers) is not significant and conduction through air is usually considered to be the conductivity of still air that is poor at room temperature. Thus, radiative conductivity is the prevalent mechanism of conductivity since it has a high porosity percentage of fibrous structures. By adding a nanofiber web, thermal conductivity was enhanced noticeably that is believed to be because of their extremely fine fiber and very high porosity of web. The superfine fibers in the web have better radiation absorption and extinction since their higher surface-area-to-volume ratio leads to decrease in the thermal conductivity. Moreover, smaller pore size between nanofibers decreases the mean free path for photon movement resulting in lower radiative energy transfer. This improvement becomes more significant when bulk density is increased. In high densities, increase in the thermal conductivity of the sample containing web was diminished which may be attributed to the presence of nanofiber and their natural compact structure that could compensate for increased thermal conductivity. According to thermal conductivity curves which is apparent in figures 80 to 83, decrease in the average nanofiber diameter leads to lower limit of conductivity.

Equation y = a + b*x	Value	t-test Significance "Yes" or "No"	Adj. R-Square	F-test Significance "Yes" or "No"
Intercept	0.03054	Yes	0.67506	Yes
Slope	-1.43757E-4	Yes		
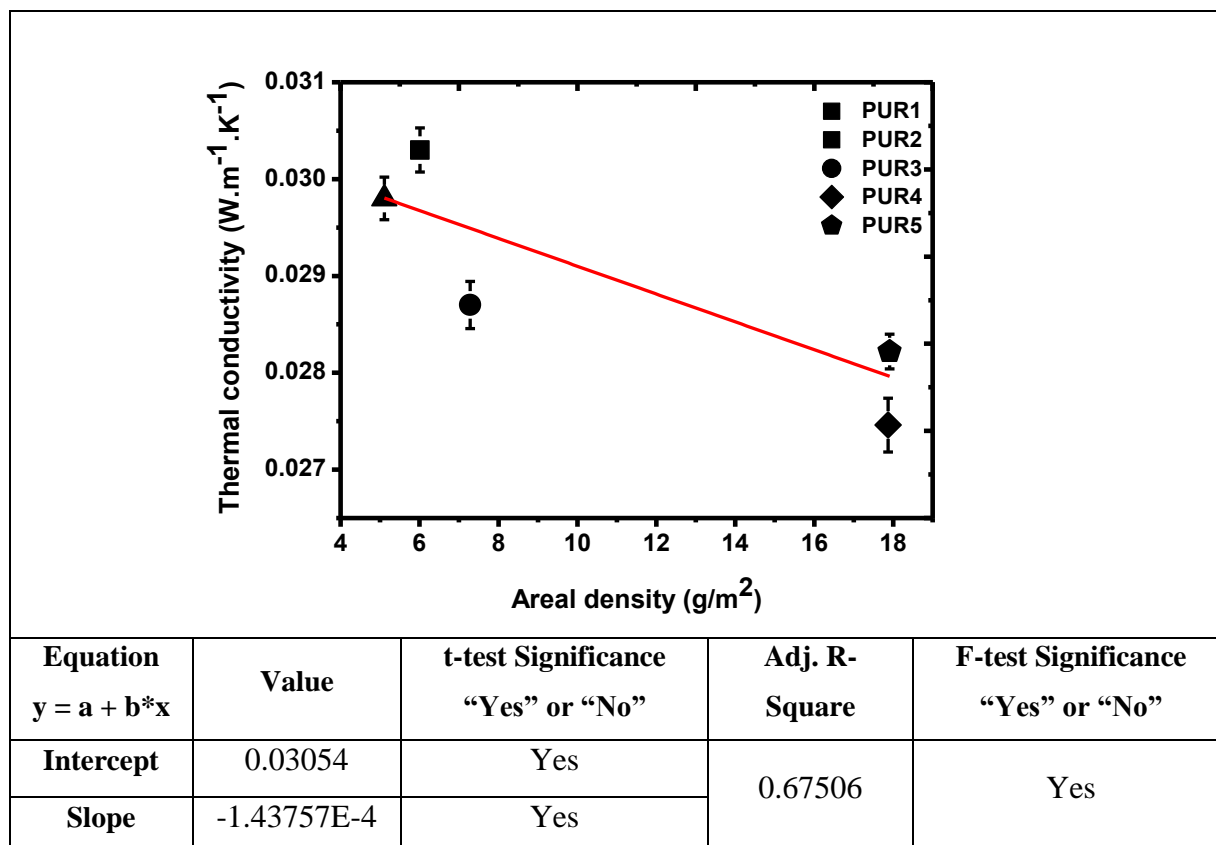
Figure 81. Thermal conductivity Vs GSM (Electrospun PUR nanofibrous layers embedded with silica aerogel).

Higher specific surface of thinner fibers [64] means more surface area for radiative absorption that results in lower thermal conductivity. Further, higher porosity of the web with a nanofiber diameter around 150 nm could be the other reason for their lowest thermal conductivity. Another explanation for reduction in conductivity can be smaller pore size in the web containing thinner nanofibers leading to lower radiative conductivity. For better understanding of how reduction in fiber diameter affected porosity of the nanofibers, it is clearly shown in SEM images in figure 40 & 41. In this context, it could be understood that using thinner nanofibers leads to noticeable performance and helps in achieving very low limit of thermal conductivity.

Equation y = a + b*x	Value	t-test Significance "Yes" or "No"	Adj. R- Square	F-test Significance "Yes" or "No"
Intercept	0.03296	Yes	-0.1736	Yes
Slope	-7.4276E-5	Yes		
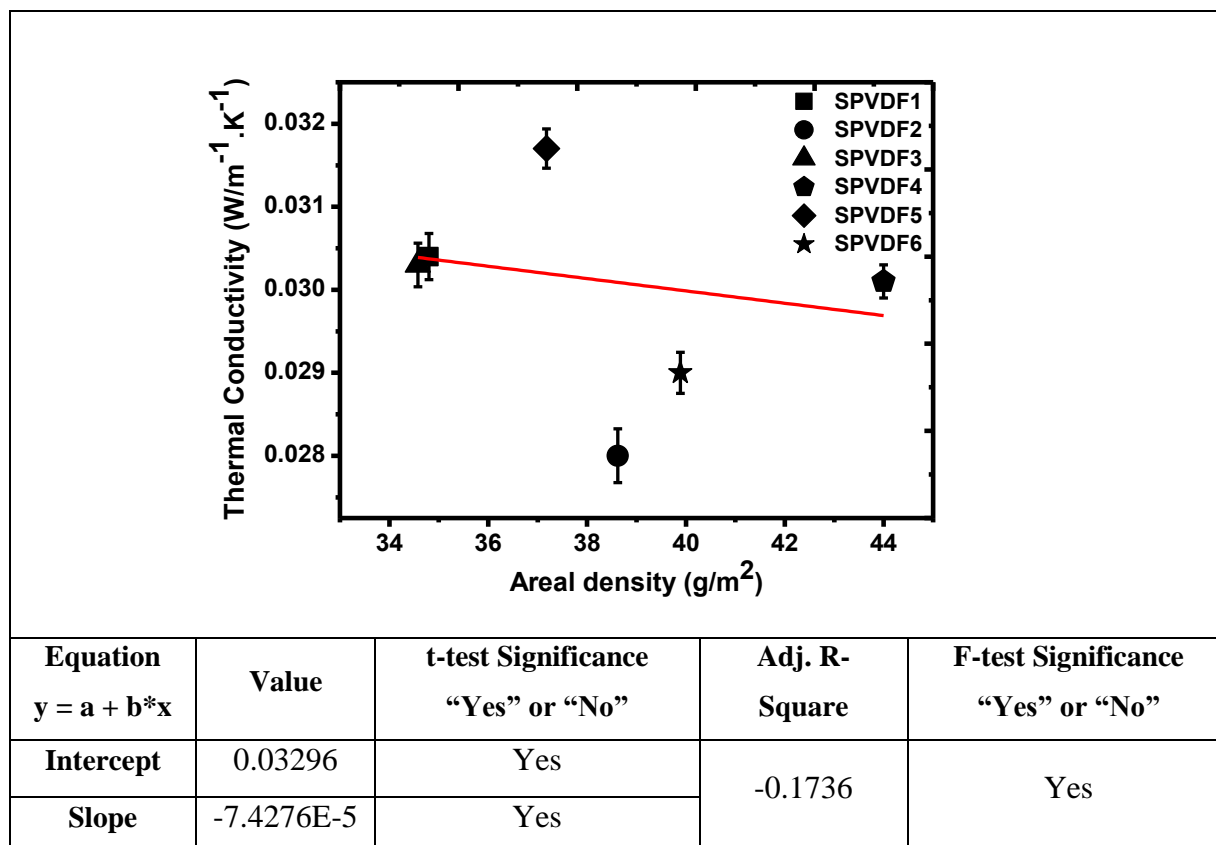
Figure 82. Thermal conductivity Vs GSM (Electrospun PVDF nanofibrous layers embedded with silica aerogel backed up with spun bond PP).

The results for the two nanofiber insulation materials (electrospun PUR and PVDF nanofibrous layer) showed excellent reduction in overall heat transfer compared to standard low-density fibrous insulating materials (at areal densities above 40 g/m^2). The PVDF nanofibrous layer, in particular, showed superior insulation at higher areal density values. Thermal conductivity testing confirmed that decreasing fiber diameter tends to increase the thermal resistance of fibrous insulation materials. However, the nanofiber/aerogel becomes an effective insulator since the aerogel structure suppresses conduction and convection, and the fibers reduce radiation heat transfer while increasing the strength of the brittle and weak aerogel structure. Although the aerogel/nanofiber combination has good thermal properties, the volume fraction of fiber must be fairly high to support and protect the aerogel matrix. Thus the aerogel materials can't achieve the same thermal conductivity at densities as fibrous insulation, but they do achieve better thermal resistance for an equivalent thickness of material.

Equation $y = a + b*x$	Value	t-test Significance "Yes" or "No"	Adj. R-Square	F-test Significance "Yes" or "No"
Intercept	0.02896	Yes	0.2315	Yes
Slope	-3.67182E-4	Yes		
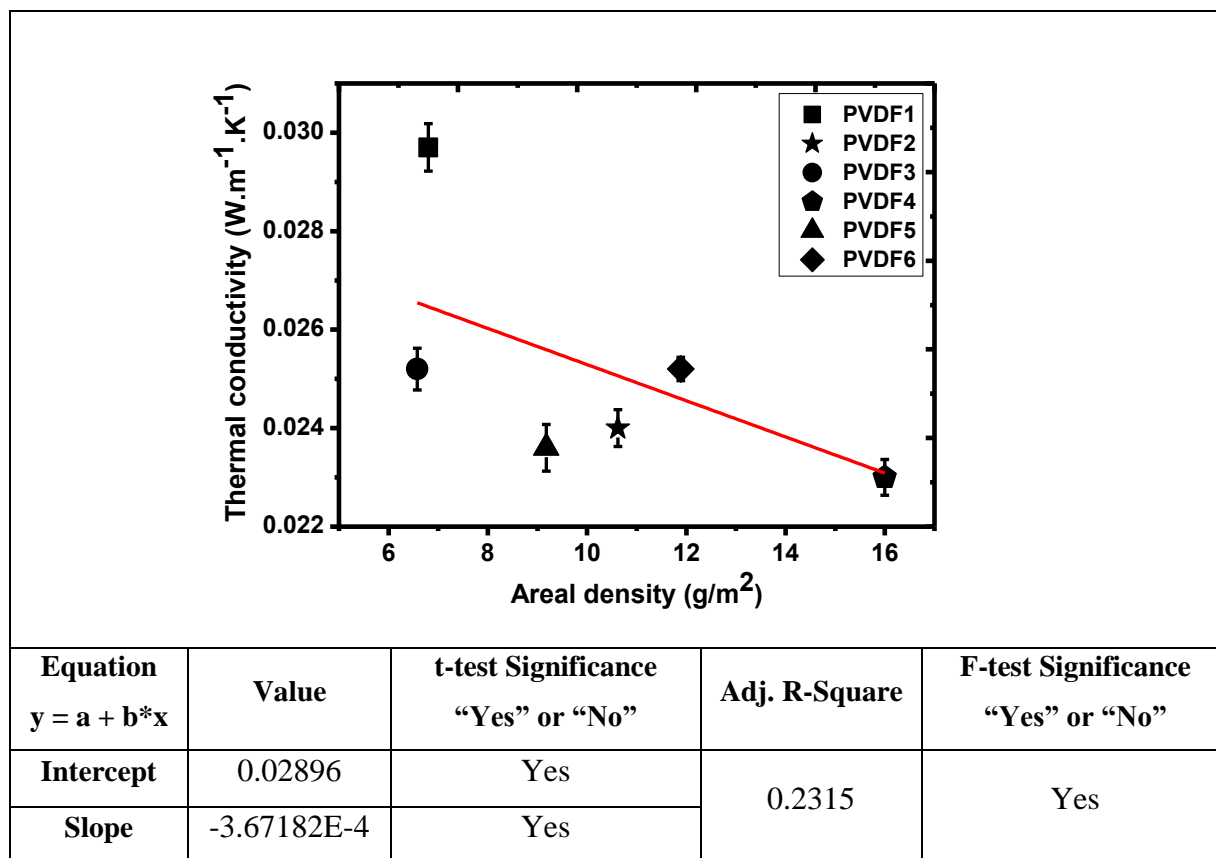
Figure 83. Thermal conductivity Vs GSM (Electrospun PVDF nanofibrous layers embedded with silica aerogel).

Equation $y = a + b*x$	Value	t-test Significance "Yes" or "No"	Adj. R-Square	F-test Significance "Yes" or "No"
Intercept	2.1591	Yes	0.8502	Yes
Slope	26.442	Yes		
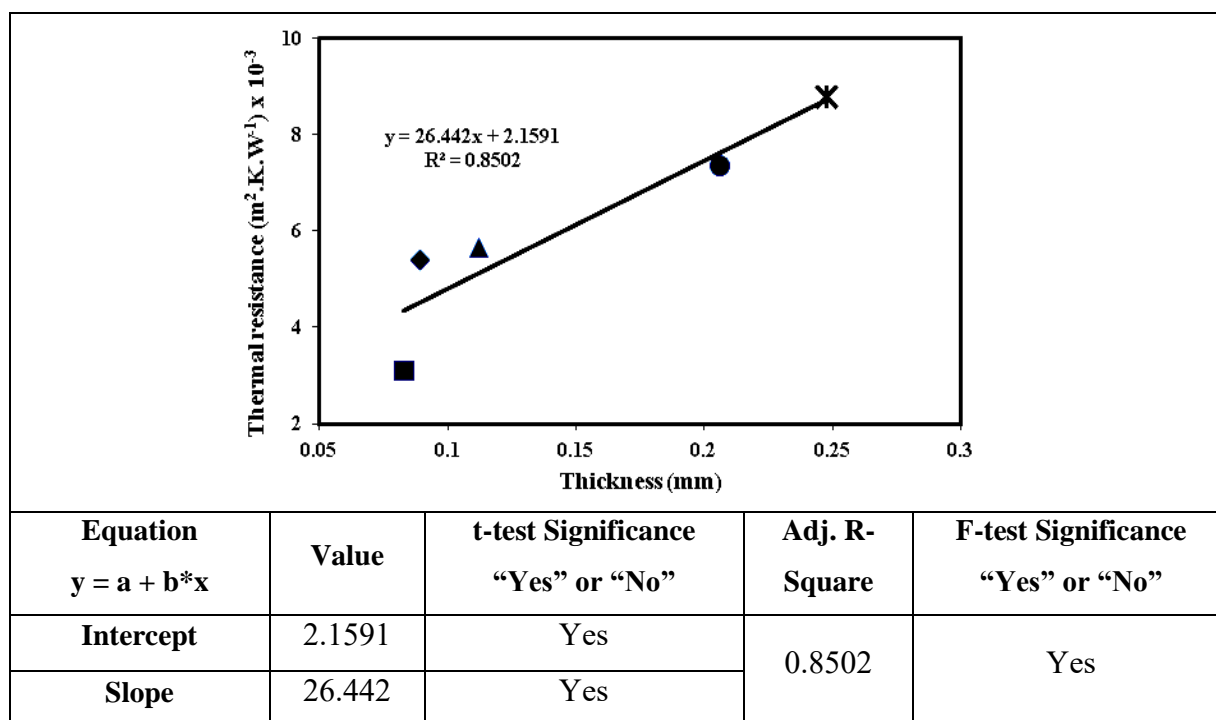
Figure 84. Thermal resistance Vs Thickness (Electrospun PUR nanofibrous layers embedded with silica aerogel) linear function.

Equation y = a + b*x	Value	t-test Significance "Yes" or "No"	Adj. R-Square	F-test Significance "Yes" or "No"
Intercept	0.1535	Yes	0.8935	Yes
Slope	30.154	Yes		

Figure 85. Thermal resistance Vs Thickness (Electrospun PUR nanofibrous layers embedded with silica aerogel backed up with spun bond PP) linear function.

Equation y = a + b*x	Value	t-test Significance "Yes" or "No"	Adj. R-Square	F-test Significance "Yes" or "No"
Intercept	2.04	Yes	0.9906	Yes
Slope	30.8	Yes		

Figure 86. Thermal resistance Vs Thickness (Electrospun PVDF nanofibrous layers embedded with silica aerogel).

High porosity of electrospun fibrous mesh is able to trap air which potentially gives it a good thermal insulation property. This is confirmed using thermal conductivity tests which show that decreasing fiber diameter leads to an increase in thermal resistance [4]. As mentioned previously, nanofiber/aerogel have shown superior insulation properties for applications where thickness is of concern.

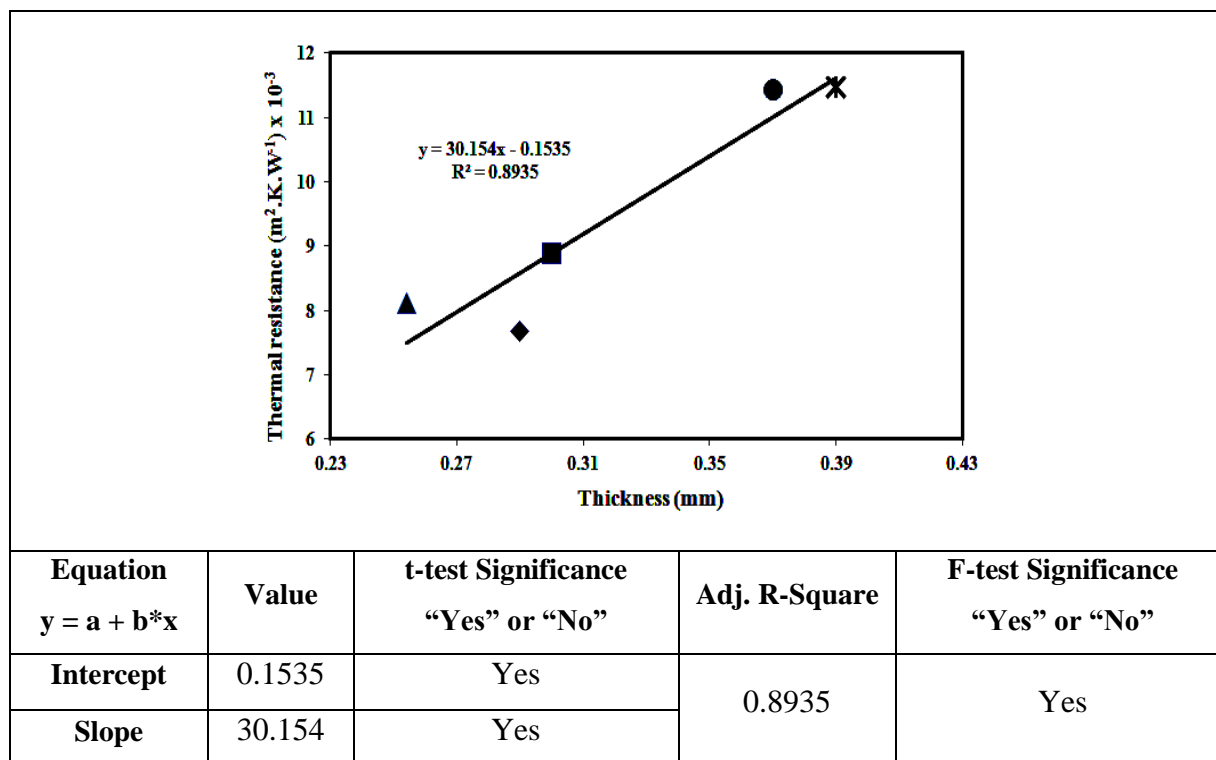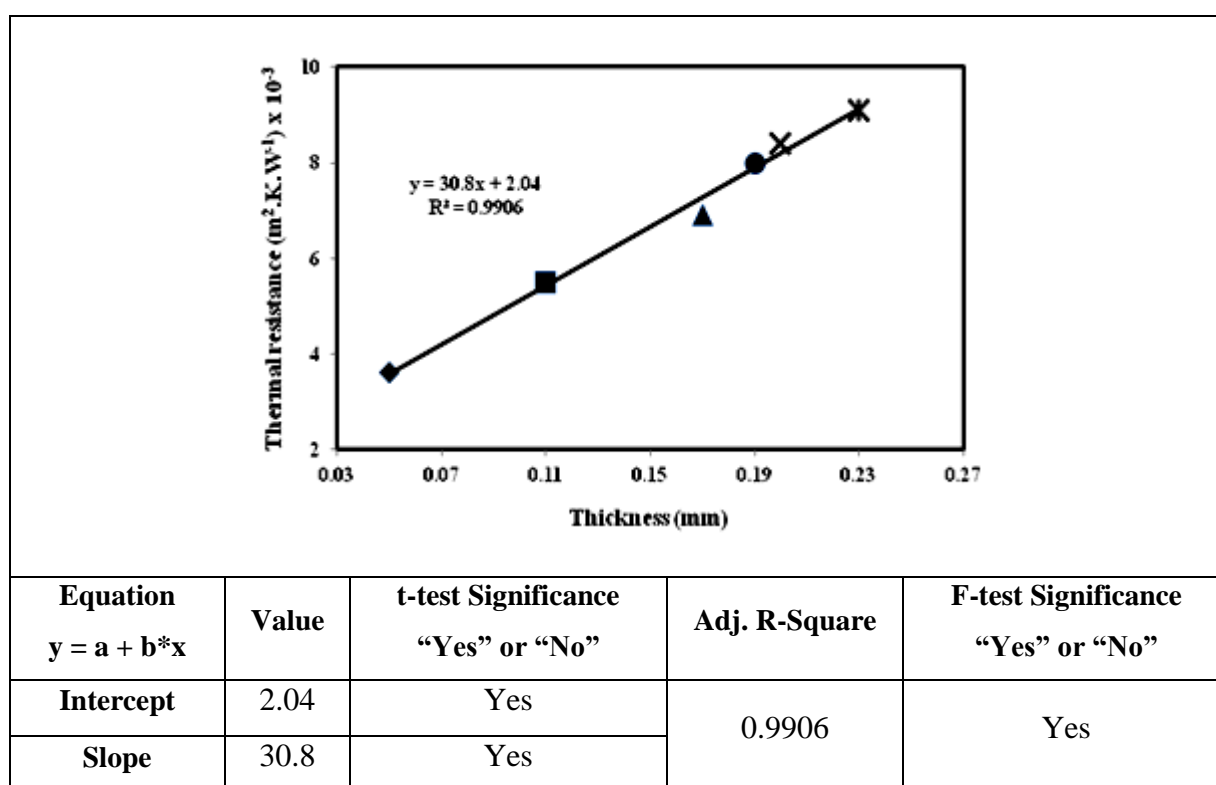| Equation y = a + b*x	Value	t-test Significance "Yes" or "No"	Adj. R-Square	F-test Significance "Yes" or "No"
Intercept	2.6879	Yes	0.9277	Yes
Slope	26.764	Yes		
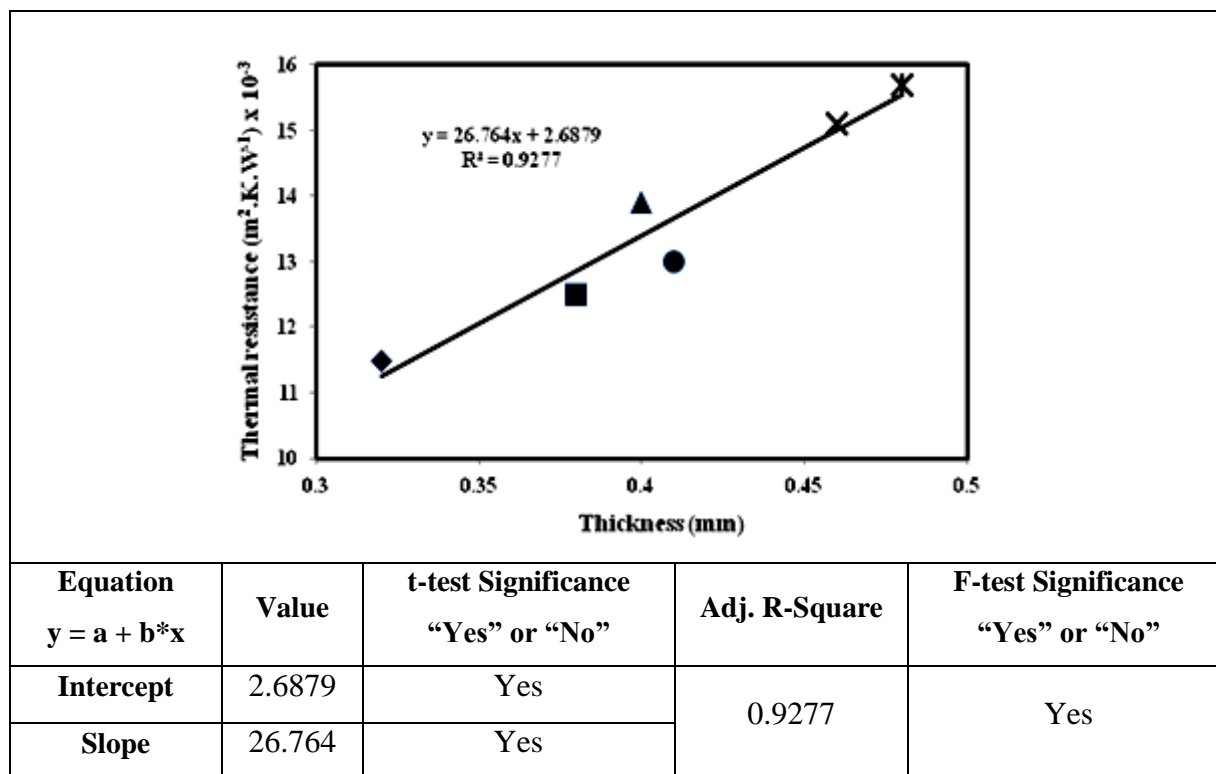
Figure 87. Thermal resistance Vs Thickness (Electrospun PVDF nanofibrous layers embedded with silica aerogel backed up with spun bond PP).

With respect to high porosity fibrous insulation materials, aerogel/nanofiber has excellent insulation per unit thickness properties, as shown in figure 84 to 87. From the figures, it can be seen that the thermal resistance increases with the increases in thickness. Also, the electrospun PVDF nanofibrous layer embedded with silica aerogel is higher than electrospun PUR nanofibrous layer embedded with silica aerogel.

4.13.1 Air Permeability of Nanofibrous Layer Embedded with SiO_2 Aerogel

Air permeability is a very important parameter for thermal insulation of electrospun nanofibrous layer. Lower air permeability causes lower air flow; consequently, more thermal insulation. The air permeability of electrospun nanofibrous layers are shown in figure 88 and 89. According to the figures; samples containing PUR nanofiber with double layer showed less air permeability. This behavior can be attributed to the finer diameter of PUR nanofiber compared to PVDF nanofiber diameter.

Pressure (Pa)	Equation y = a + b*x	Value	t-test Significance "Yes" or "No"	Adj. R-Square	F-test Significance "Yes" or "No"
100	Intercept	9.1614	Yes	0.7612	Yes
	Slope	-39.211	Yes		
200	Intercept	17.658	Yes	0.7158	Yes
	Slope	-72.383	Yes		
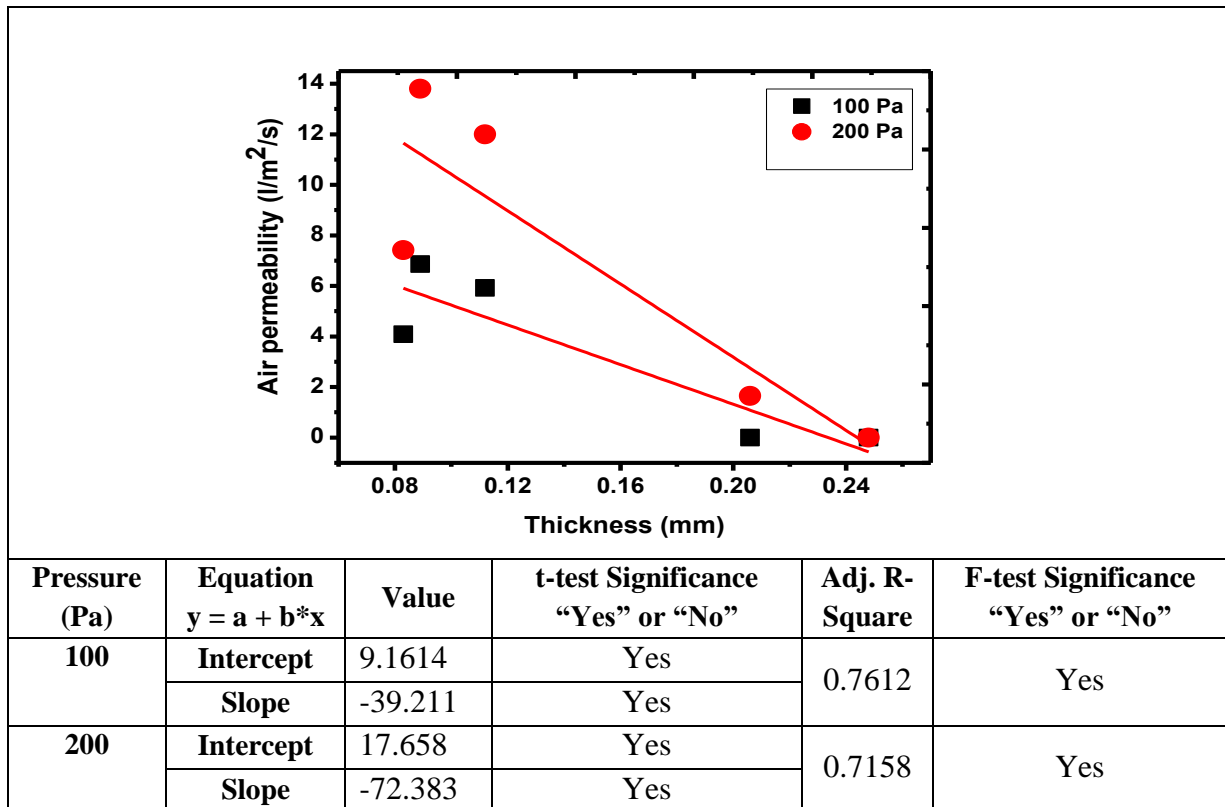
Figure 88. Air permeability (Electrospun PUR nanofibrous layer embedded with silica aerogel) 100 Pa.

Pressure (Pa)	Equation y = a + b*x	Value	t-test Significance "Yes" or "No"	Adj. R-Square	F-test Significance "Yes" or "No"
100	Intercept	4.58208	Yes	-0.2259	Yes
	Slope	4.31321	Yes		
200	Intercept	9.13117	Yes	-0.2261	Yes
	Slope	8.83472	Yes		
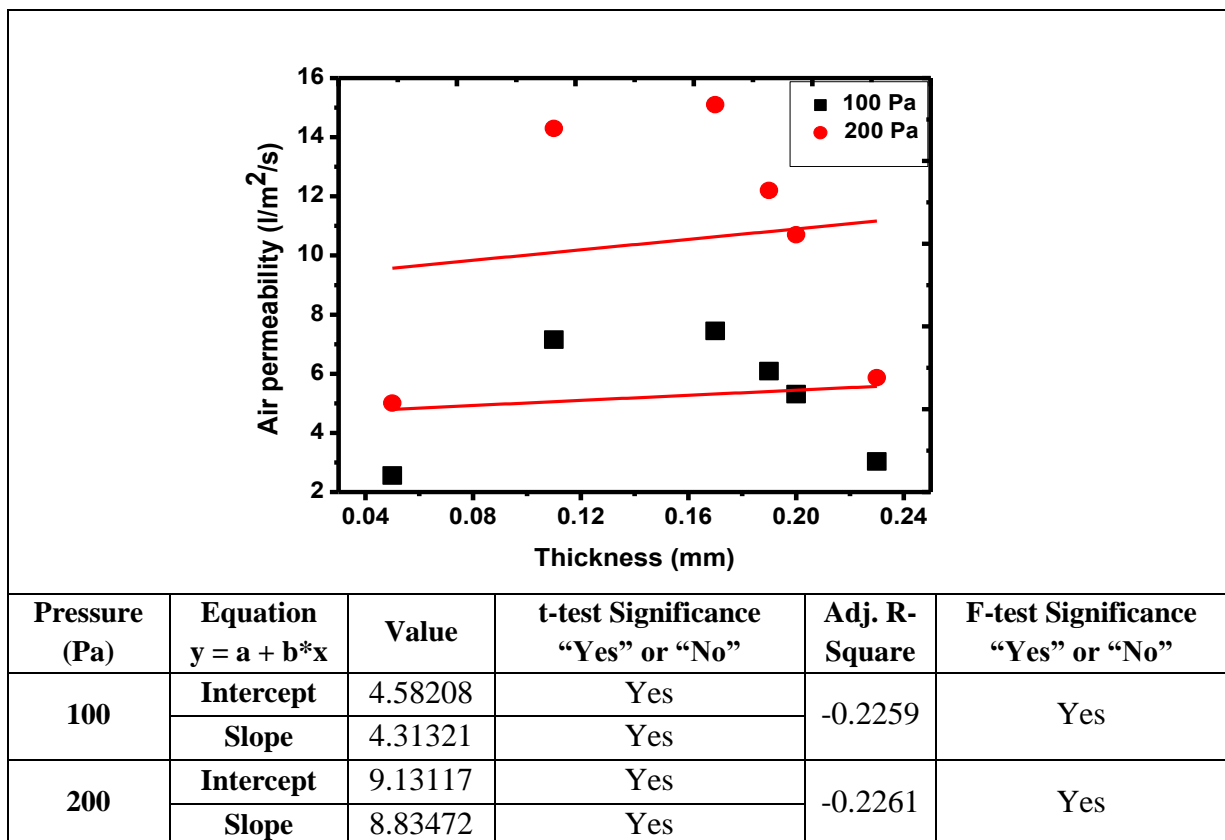
Figure 89. Air permeability (Electrospun PVDF nanofibrous layer embedded with silica aerogel)

As can be seen from the figures, by increasing the number of nanofibrous layers, lower air permeability was achieved, confirming the relation of this important parameter with thermal insulation ability. Figure 88 shows that sample PUR4, PUR5 and PVDF5 were impermeable at 100 and 200 Pa.

4.14 Modeling and Simulation of Heat Transfer by Convection Through Aerogel Treated Nonwoven Fabrics

4.14.1 Simulation from ANSYS

During simulation a constant ambient temperature of -10 ∘C was considered. Simulation was done so as to allow heat to flow along the thickness of the fabric (perpendicular to both the machine and the cross direction).

AIR as Insulator | Stagnant Air Conditions
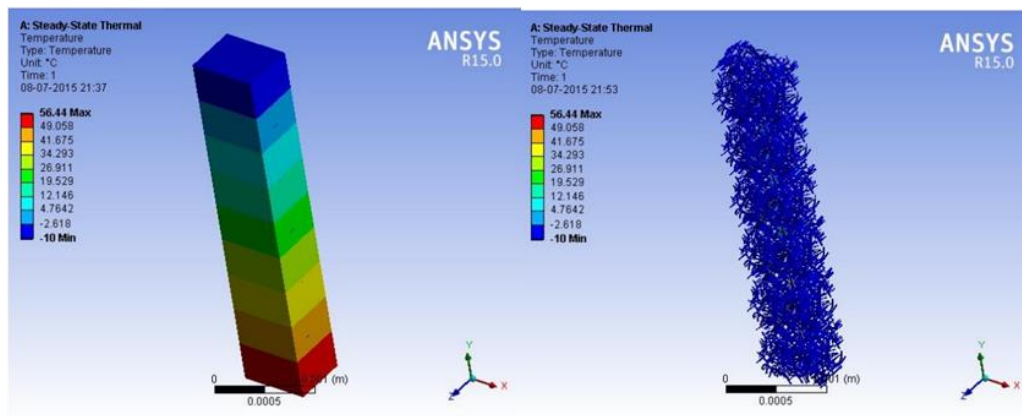
Figure 90. Temperature gradient for standard nonwoven without aerogel.

Aerogel as Insulator | Stagnant Air Conditions
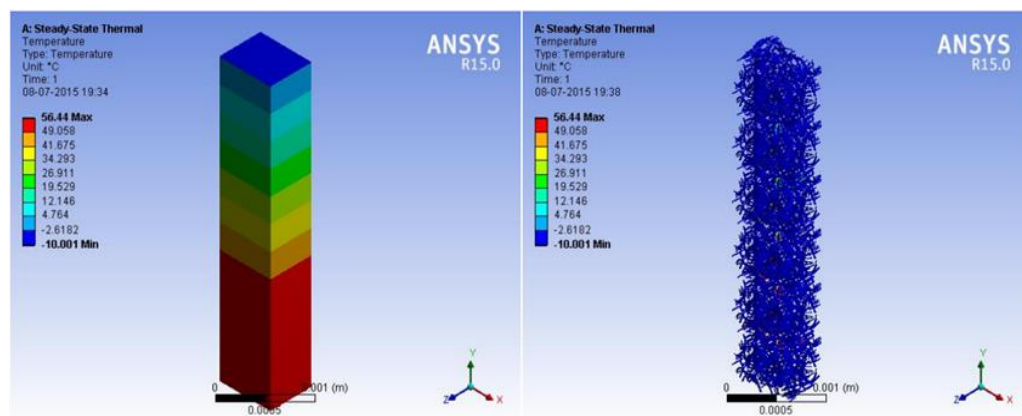
Figure 91. Temperature gradient for aerogel treated nonwoven.

As the heat flows under the temperature gradient provided, various levels of the fabric thickness settle down to different equilibrium temperatures which is depicted in the

131

'Temperature' diagram shown in figure 90 and 91. Apart from this, variations in the 'Total Heat Flux' and the 'Directional Heat Flux' (along the Y axis – because that is the major direction for heat transfer) have been shown. Clearly, the heat retention in the nonwoven structure with aerogel is 67% higher than in the nonwoven structure without aerogel implying that aerogel hinders heat transfer, thus keeping the body warmer.

4.14.2 Simulation from COMSOL

In the case of standard nonwoven without forced convection shown in figure 92, the temperature at the surface exposed to outside air was 329.18955 K and the heat rate through the fabric was 2.185 e^{-8} W.

Figure 92. Heat transfer through standard nonwoven without forced convection.
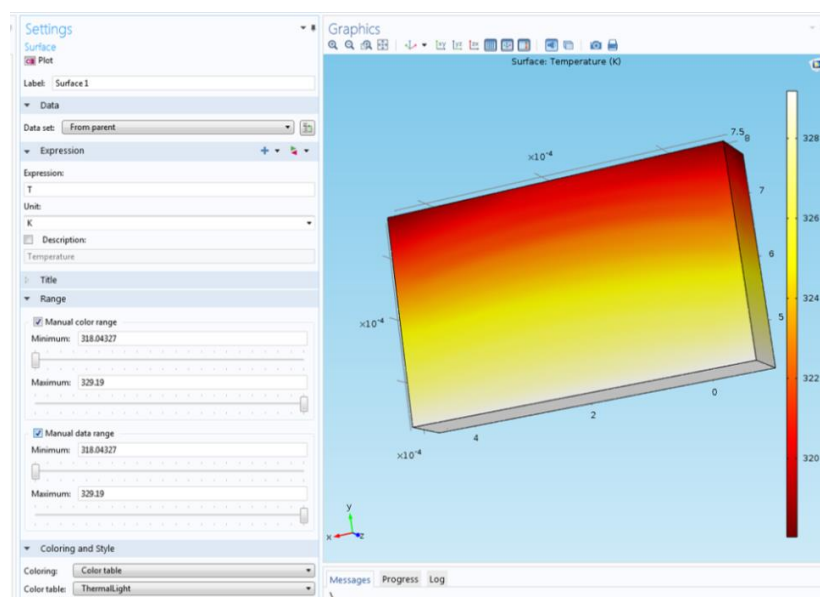
Figure 93. Heat transfer through standard nonwoven with forced convection.

In the case of standard nonwoven with forced convection showed in figure 93, the temperature at the surface exposed to outside air was 318.04327 K and the heat rate through the fabric was 1.024 e^{-8} W. In the case of nonwoven with aerogel and without forced convection shown in figure 94, the temperature at the surface exposed to outside air was 329.18949 K and the heat rate through the fabric was 1.267 e^{-8} W. In the case of nonwoven with aerogel and with forced convection shown in figure 95, the temperature at the surface exposed to outside air was 310.16686 K and the heat rate through the fabric was 9.801 e^{-9} W.
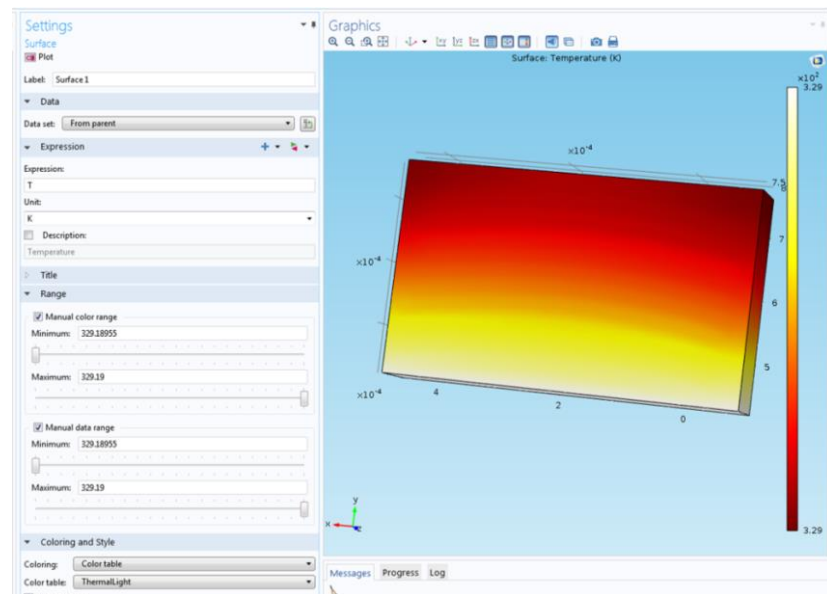

Figure 94. Heat transfer through aerogel treated nonwoven without forced convection.
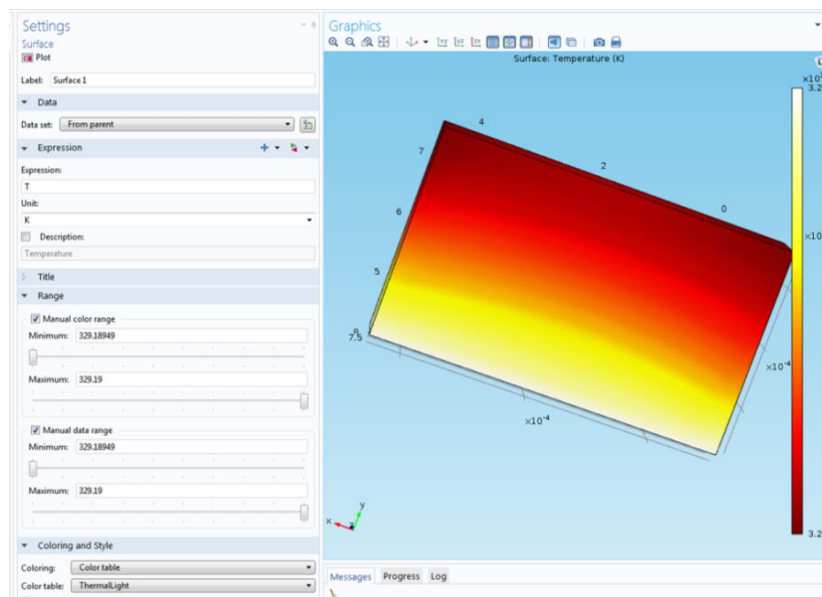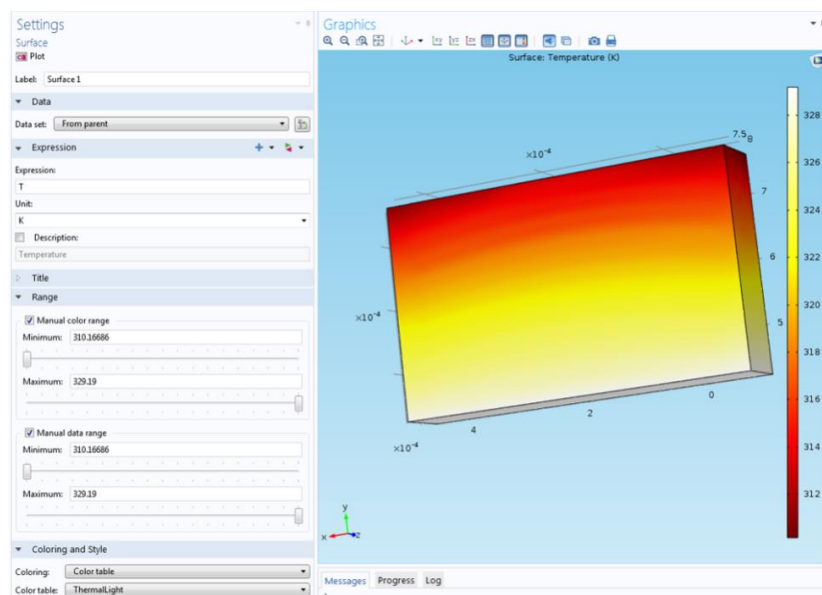

Figure 95. Heat transfer through aerogel treated nonwoven with forced convection.

In the case of forced convection, the difference between the surface temperatures in case of air and aerogel for is almost 8 K even for such a small unit cell. When forced convection was not taken into account, the temperature difference was very less (6 e^{-5} K). But in both cases, the heat flow through air is higher than in case of aerogel. In the case with forced convection, the heat rate was around 5% higher and in the case without forced convection, the heat rate was more than 72% higher. That is, the heat loss through the air is 1.7 times the heat loss through aerogel, in the case without any forced convection. The total net heat rate is defined as the net incoming and outgoing heat fluxes through all the surfaces of the body. This value for forced convection case is seen to be less in both aerogel and air because the outgoing flux is much more when there is a forced convection. The temperature versus length plot was also made. This was a smooth curve for the cases of forced convections but in the cases with no forced convections, the graph obtained had steps maybe because of very less variation of temperature in those regions.

4.14.3   Sources of Error

- Since the memory requirement for simulating bigger structures was high, the simulation was done for a very small unit cell. Due to this, the fluid motion may be different from what happens in bigger samples used in reality and therefore, heat flow in the bigger samples may be different.

- None of the fiber parts touch each other and therefore conduction between fibers is not considered in the heat flow simulation.

- Thermal conductivity for the fibers and the surrounding fluid is assumed to be a constant.

- The flow was assumed to be laminar instead of turbulent flow since simulation using turbulent model required more time.

- Mach number is taken to be less than 0.3, and therefore, density and viscosity changes due to the fluid motion are also considered to be negligible.

Chapter 5. Summary and Conclusion

5.1 Summary

This research was an endeavor to study the thermal insulation behavior of high performance fibrous materials. Based on the objectives set for this research, a detailed literature review was conducted on existing literature. The literature review provided necessary theoretical background, baseline data and insights into similar research conducted in the past. It assisted in understanding the gaps and limitations of the past research. The objectives were crystallized to add to this knowledgebase and also address a few of the identified gaps and limitations. The broad objectives of this research were to analyze the thermal measurement techniques used for insulation materials at different temperatures; to conduct a comparative analysis of thermal properties of different types of insulating materials; explore new techniques to conduct thermal measurements by fabricating new instruments; correlate results from conventional and unconventional experimental methods; study and analyze convective heat transfer through insulation material; study thermal behavior of electrospun PUR and PVDF nanofibrous layers embedded with silica aerogel; modeling and simulation of heat transfer by convection for aerogel treated nonwoven fabrics for the research conducted.

A range of samples made of different materials, composition and thicknesses were chosen. Polyester and polyethylene nonwoven composite fabrics of varying thicknesses embedded with amorphous aerogel, struto nonwoven fabrics and a few commercially available insulation materials were used as samples. The type of aerogel used was hydrophobic amorphous silica aerogel which was most suitable for application in textile material. Flexible electrospun nanofibrous layers embedded with silica aerogel was produced via electrospinning process. The aerogel particles were also added during thermal bonding of standard non-woven web. The struto nonwoven structure was produced in the laboratory. Thermal properties of the electrospun nanofibrous layers embedded with SiO_2 aerogel were analyzed. These studies were carried out under subzero temperature conditions and differ widely from commonly used conditions. Various conventional and unconventional techniques were used in additional to fabrication of new devices for thermal measurements.

The data generated from the experiments were validated against established theories and found to adhere to theoretical principles. The data was statistically analyzed and various conclusions were drawn based on the results.

5.2 Conclusions from the Research

Objective measurement methods are required for accurate results in evaluation of heat transmission properties. In this study, various thermal measurement techniques were used and different types of insulation materials were characterized with regard to thermodynamical properties at different temperature gradients. Alambeta and TCi experiments showed that the thermal conductivity of fibrous materials increase with increasing environmental temperature due to the contribution of radiation, convection, and conduction. It was observed that thermal conductivity of a fabric increases significantly with increases in the heating temperature. Thermal resistance (R_{ct}) of the fabric, which depends on the boundary layer of air, was directly proportionate to fabric thickness. The thermal resistance (R_{ct}) of the aerogel-treated nonwoven fabric was comparatively higher than other fabrics. Also, the air permeability was directly proportional to percentage of nanoporosity of the aerogel based composite structure. It was also noticed that, when the pressure level increases the flow rate also increases simultaneously. The relationship between the temperature gradient (between the textile sample and temperature of neighborhood) and velocity of fluid flow was described from the PIV measurements. As expected, the fluid flow motion accelerated according to the increasing temperature gradient.

The comparative analysis was done for the thermal properties for different subzero temperatures. It showed that the temperatures did not have much effect on the thermal conductivity. Compared to other fabrics, the aerogel-based fabric samples were found to have considerably lower thermal conductivity and higher thermal resistance even at extreme temperatures. This can be attributed to the low fabric density and the aerogel present in the fabric which has significant effect on thermal properties of aerogel-treated nonwoven fabrics. The differences in thermal behavior of aerogel treated samples are due to thickness variation. The vast difference can be seen in the thermal resistance compared to other fabrics. It can be concluded that aerogel treated nonwoven fabric is best suitable for thermal insulation under extreme temperature conditions. From the KES measurement, it has also been found that the thermal insulation is related to the weight and compressional properties of fabric. To make an insulating material effective it should have low compression set/high resiliency to make the still air entrapped into the material.

From the results, it can be concluded that the thickness, density and mainly the aerogel present in the fabrics are three important factors which determines the insulation property. The thickness of fabric strongly affects amount of heat insulation. In general, the greater the

fabric thickness, greater the thermal insulation. The custom built instrument and the laboratory set-up equipment were found to be effective in measuring the heat transport properties of fabrics as they measure the steady-state thermophysical properties (thermal insulation properties) even at sub-zero temperatures.

Study of the electrospun PUR and PVDF nanofibrous layer embedded with silica aerogel regarding their thermal behavior, show enhancement in thermal insulation by increasing the number and the weight per unit area of nanofibrous layers. Higher thermal resistance was observed in the case of samples containing PUR and PVDF nanofibrous layers, which can be attributed to the low air permeability and fiber diameter. Moreover, thermal measurements show that embedding silica aerogel in nanofibrous layers leads to increased thermal insulation. It is shown in this study that the experimental insulation material can enhance thermal resistance at extreme temperatures. Furthermore, weight and thickness can be reduced by means of nanofibrous layers. This study showed nanofibers to be useful as components in hybrid battings with high bulk densities. Fibers below 1 μm in diameter were not thermally efficient at low fiber volume fractions; this corresponds with previous research on fiberglass insulation. Performance gains in existing thermal insulation materials may be possible by incorporating a proportion of nanofibers into the structure, but large diameter fibers would still be necessary for durability and compression recovery.

From the heat transfer mechanisms, it can be concluded that high insulation is due to layered structure and higher thickness. In the case of cold weather clothing, higher thermal resistance is very important. The thermal resistance of the fabric is directly proportional to its thickness. The findings show that the aerogel based fabric samples show considerably low thermal conductivity and high thermal resistance even at extreme low temperatures. This may be attributed to decrease in heat losses due to insulation by nano airspaces inside aerogel present in the fabric. Thermal conductivity was found to be differing with respect to different temperatures and fabric density, which may be attributed to the fabric structure, fiber content, and mainly aerogel particles present in the nonwoven fabrics. Thermal resistance (R_{ct}) of the fabric, which depends on the boundary layer of air, showed an increase as the fabric thickness increases. The thermal resistance (R_{ct}) of the aerogel-treated nonwoven fabric shows a different trend when plotted with the fabric densities, which was due to the weight and thickness of the fabric. The comparative analysis was done for thermal properties at different subzero temperatures. It showed an insignificant difference, i.e. the temperatures did not have much effect on the thermal conductivity. Thus, the fabric density

and the aerogel present in the structures have a significant effect on thermal properties of aerogel-treated nonwoven fabrics. In general, the greater the fabric thickness, greater the thermal insulation. It has also been found that the thermal insulation is also related to the weight and compressional properties of fabric. To make an insulating material effective it should have low compression set/high resiliency to make the still air entrapped into the material.

The study explores the optimal usage of various thermal measurement techniques. It concludes that the selected aerogel treated fabrics have high thermal performance and thermal response as insulators as compared with other fabrics. The simulations were conducted created based on the potential demonstrated by aerogel treated samples. The newly fabricated and designed instruments were found to be suitable to measure conductivity and convection at sub-zero temperatures and convenient for the measurement and evaluation of various temperature variations at different positions of the fabric. This method of measurement still needs optimization and will be the subject of further research. Unconventional method like PIV was used gainfully to understand thermal measurements better. Thermal properties of electrospun nanofibrous layers from PUR and PVDF embedded with SiO_2 Aerogel was evaluated and found to have application as components in hybrid battings with high bulk densities.

5.3 Significant Outputs from the Research

This research has produced new ideas, large amount of data and conclusions that can have a significant impact on the research of thermal behavior of high performance textiles. A detailed analysis of various measurement techniques have helped in identifying the optimal one for different scenarios. A comparative analysis of thermal properties of insulating materials showed that aerogel has a significant potential to be used as insulation material for textile applications. New instruments were fabricated according to proven theoretical principles and were found to correlate with the results from other standard equipments. This provides an alternative mode to measure thermal properties. New insights into using unconventional techniques like PIV were gained. A detailed exercise to correlate results from conventional and unconventional techniques has generated a large amount of baseline data that could be useful for future research. By exploring electrospinning of PUR and PVDF nanofibrous layers embedded with silica aerogel, a new avenue to understand the potential of nanofibers and aerogel combined; in the area of high performance clothing has

arisen. The detailed study of the convective heat transfer through insulation material provided data and models to simulate the heat transfer mechanisms. This reduces the amount of effort required for lab and field experiments and empowers researchers to simulate test environments and generate relevant data. These results and findings have been published in various books, peer-reviewed journals and international conferences.

5.4 Future Direction

The ideas, experiments and data generated as part of this research, have added to the knowledgebase that could be useful to define the future direction and provide insightful references to researchers. The potential of this research can be realized by pursuing further studies into areas given below:

- Synthesis & Characterization of various types of aerogel suitable for textiles.
- Explore various conventional and unconventional thermal measurement techniques.
- Develop new methods to treat fabrics with aerogel particles.
- Fabrication of new devices for measurement of thermal properties in fibrous structures.
- Development of electrospun nanofibrous layers embedded with aerogel for low density and effective thermal insulation.
- Comparison of efficacy of different Insulation materials.
- Modeling of convective heat transfer phenomena in fabrics treated with aerogel.
- Develop or update standards for thermal measurement in insulation materials used for textile applications.

References

1. Varkiyani, S., Rahimzadeh, H., and Bafekrpoor, H., *Influence of punch density and fibre blends on thermal conductivity on nonwoven.* Open Textile Journal, 2011. **4**: p. 1-6.

2. Cohen, E., *Thermal properties of advanced aerogel insulation*, in *Department of Mechanical Engineering*. 2011, Massachusetts Institute of Technology: Massachusetts.

3. Gun, A.D., *Dimensional, Physical and Thermal Comfort Properties of Plain Knitted Fabrics Made from Modal Viscose Yarns Having Microfibers and Conventional Fibers* Fibers and Polymers, 2011. **12**(2): p. 258-267.

4. Frydrych, I., Dziworska, G., and Bilska, J., *Comparative analysis of the thermal insulation properties of fabrics made of natural and man-made cellulose fibres.* Fibre Textiles Eastern Europe, 2002. **39**: p. 40-44.

5. Farnworth, B., *Mechanism of heat flow through clothing insulation.* Textile Research Journal, 1983. **53**: p. 717–725.

6. Martin, J.R., and Lamb, G. E. R., *Measurement of thermal conductivity of nonwovens using a dynamic method.* Textile Research Journal, 1987 **57**: p. 721–727.

7. Mao, N., and Russell, S. J., *The thermal insulation properties of spacer fabrics with a mechanically integrated wool fiber surface.* Textile Research Journal, 2007. **77**: p. 914–922.

8. *Heat & Mass Transfer in Textiles*. World Scientific and Engineering Academy and Society, ed. A. HAGHI. 2011, Montreal, Canada: WSEAS Press.

9. Kistler, S.S., *Coherent expanded-aerogel.* Journal of Physical Chemistry, 1931. **36**: p. 52-64.

10. Xie, T., He, Y. L., and Hu, Z. J., *Theoretical study on thermal conductivities of silica aerogel composite insulating material.* International Journal of Heat and Mass Transfer, 2013. **58**: p. 540-552.

11. Bhattacharjee, D., and Kothari, V. K., *Measurement of Thermal Resistance of Woven Fabrics in Natural and Forced Convections.* Research Journal of Textile and Apparel, 2008. **12**(2).

12. *China National Standard Bureau, China National Standard (GB/T 18319-2001) – Textiles-Testing Method for Thermal Retention with Accumulated by Infrared Ray*. 2001, Beijing: China Standard Press.

13. *China Textile Industry Council FZ/T 64010-2000 Far Infrared Products*. 2000, China Standard Press: Beijing.

14. Sokolovskaya, T.S., *Measurement of the Thermal Conductivity Coefficient of Textile Materials by the regular cooling regime method.* Fibre Chemistry, 2005. **37**(1): p. 59-62.

15. Gustavsson, M., and Halldahl, L., *Thermal Conductivity Measurements of Thin Insulating Layers Deposited on High-Conducting Sheets.* International Journal of Thermophysics, 2006. **27**(1): p. 195-208.

16. Hu, J.Y., Li, Y., Yeung, K. W., and Wang, S. X., *Characterization of thermal radiation properties of polymeric materials.* Polymer Testing, 2006. **25**(3): p. 405-412.

17. Yuan, T., Huang, Y., Dong, S., Wang, T., and Xie, M., *Infrared reflection of conducting polyaniline polymer coating.* Polymer Testing, 2002. **21**(6): p. 641-646.

18. Kawabata, S., Niwa, M., and Sakaguchi, H., *Objective Measurement: Applications to Product Design and Process Control.* The Textile Machinery Society of Japan, 1985. **Osaka, Japan**: p. 343.

19. Hes, L., and Ivan, D., *New Method and Equipment for Measuring Thermal Properties of Textiles.* Sen'i Kikai Gakkaishi (Journal of the Textile Machinery Society of Japan) 1989. **42**(8): p. T124-T128.

20. Hes, L. *New achievements in the area of the objective evaluation of thermal insulation and thermal-contact properties of textiles*. in *The 3rd Asian Textile Conference, Vol. II*. 1995

21. *Determination of physiological properties - Measurement of thermal and water-vapourresistance under steady-state conditions (sweating guarded - hotplate test)*, in *UNI EN 31092*. 1996, Italian Standards Publications: Italy.

22. Romeli, G., Barigozzi, S., Esposito, G., Rosace., and Salesi, G., *High sensitivity measurements of thermal properties of textile fabrics.* Polymer Testing, 2013. **32**: p. 1029-1036.

23.   Ukponmwan, J.O., *The Thermal-Insulation Properties of Fabrics*. Textile Progress, 1993. **24**: p. 5.

24.   Sang., P., *Heat and Mass Transfer Analysis of Fabric in The Tenter Frame*. Textile Research Journal, 1997. **67**(5): p. 311-316.

25.   *Fabrics: Mathematical Model*. Mathematical and Computer Modelling, 1998. **12**(9): p. 1187.

26.   A.H. Nissan, D., Hansen & J.L., Walker, , *Heat Transfer in Porous Media Containing a Volatile Liquid*. Chem. Eng. Progr. Symp. Ser., 1963. **59**: p. 114.

27.   Kakac, S., and Yener, Y., *Heat conduction*. 1993: Taylor & Francis Pyblications.

28.   Gebhart, B., *Heat conduction and Mass Diffusion*. 1993: Mc Graw-Hill.

29.   Incropera, F.P., and DeWitt, D. P., *Fundamentals of heat and mass transfer*, in *Technology & Engineering*. 2002 John Wiley & Sons Australia. p. 981.

30.   CHALMERS, *Literature Review of High Performance Thermal Insulation* 2012, Chalmers University of Technology: Gothenburg, Sweden

31.   Simmler, H., Brunner, S., Heinemann, U., Schwab, H., Kumaran, K., Mukhopadhyaya, P., Quénard, D., Sallée, H., Noller, K., Kücükpinar-Niarchos, E., Stramm, C., Tenpierik, M. J., Cauberg, J. J. M., and Erb, M., *Vacuum Insulation Panels. Study on VIP-components and Panels for Service Life Prediction of VIP in Building Applications (Subtask A)*. IEA/ECBCS Annex 39 High Performance Thermal Insulation (HiPTI). 2005.

32.   Petersson, B.Å., *Tillämpad byggnadsfysik 3rd ed., Studentlitteratur. ISBN:978-91-44-04886-4*. 2007.

33.   AGA., *Gas Handbook*. Uppsala: Almquist & Wiksell, 1985: p. 1-4.

34.   Baetens, R., Jelle, B.P., and Gustavsen, A., *Aerogel insulation for building applications: A state-of-the-art review*. Energy and Buildings, 2010. **43**: p. 761-769.

35.   Engel, T., and Reid, P., *Physical Chemistry*. 2006, San Fransisco: Benjamin Cummings.

36.   Saville, B.P., *Physical testing of textiles*. 2002, Cambridge: The textile institute., Woodhead Publishing. 209–243.

37.   Weedall, P.J., and Goldie, L., *The objective measurement of the "Cool Feeling" in fabrics*. The Journal of Textile Institute, 2001. **92**: p. 379–386.

38.   Institution, B.S., *Method for determination of thermal resistance of textiles*, in *BS 4745*. 1971, British Standards Institution: London.

39.   ASTM, *Standard test method for thermal transmittance of textile materials*, in *ASTM D 1518-85*. 1990: West Conshohocken, PA.

40.   SENSORA, *Instruction manuals of alambeta, permetest instruments*, SENSORA, Editor. 1990, SENSORA, Liberec Registered Company: Liberec.

41.   Rowlands, R.J., *Comfort Properties of Blankets*. Textile Research Journal 1963. **33**: p. 343.

42.   Hollies, N., *A Study of Comfort Properties of Cold Weather Clothing*, in *Textile Engineering Laboratory Report, No. 164*. 1956, Headquarters Research and Development Command, Textile Clothing and Footwear Division.

43.   Fonseca, G.F., *Moisture Transfer Through Impermeable Foams*. Textile Research Journal, 1967. **37**: p. 1072.

44.   D.G. McMaster, *Thermal Conductivity of Compressible Porous Materials*. Tappi, 1964. **47**: p. 796.

45.   Herminge, L., *Heat Transfer in Porous Bodies at Various Temperatures and Moisture Contents*. Tappi, 1961. **44**: p. 570.

46.   Zeng, J.S.Q., Stevens, P. C., Hunt, A. J., Grief, R., and Lee, D., *Thin-film-heater thermal conductivity apparatus and measurement of thermal conductivity of silica aerogel*. International Journal of Heat and Mass Transfer, 1996. **39**: p. 2311–2317.

47.   Haranath, D., Pajon, G. M., Wagh, P. B., and Rao, A. V., *Effect of sol-gel processing parameters on thermal properties of silica aerogel*. Materials Chemistry and Physics, 1997. **49**: p. 129–134.

48.   Poco, J.F., Satcher, J. H., and Hrubesh, L. W., *Synthesis of high porosity monolithic alumina aerogel*. Journal of Non-crystalline Solids, 2001. **285**: p. 56–63.

49.   Kim, G.S., and Hyun, S. H., *Synthesis of window glazing coated with silica aerogel films via ambient drying*. Journal of Non-crystalline Solids, 2003. **320**: p. 125–132.

50. Bock, V., Nilsson, O., Blumm, J., and Fricke, J., *Thermal properties of carbon aerogel.* Journal of Non-crystalline Solids, 1995. **185**: p. 233–239.

51. Huang, J., *Sweating guarded hot plate test method.* Polymer Testing, 2006. **25** p. 709–716.

52. Mathis, N., and Chandler, C., *Orientation and position dependent thermal conductivity.* Journal of Cellular Plastics, 2000. **36**: p. 327–336.

53. Schneider AM., H.B., *Heat transfer through moist fabrics.* Textile Research Journal, 1992. **62**: p. 61-66.

54. Jirsak, O., Gok, T., and Ozipek, B., *Comparing dynamic and static methods for measuring thermal conductive properties of textiles.* Textile Research Journal, 1998. **68**: p. 47–56.

55. Morris, G.J., *Thermal Properties of Textile Materials.* Journal of Textile Institute, 1953. **44**: p. T449.

56. Baxter, S., and Cassie, A. B. D., *Thermal Insulating Properties of Clothing.* Journal of Textile Institute, 1943. **34**: p. T41.

57. Latham, B.J., *The Structure of Shirting Fabrics in Relation to Comfort in Wear.* Clothing Research Journal, 1973. **1**: p. 3.

58. Gagge, A.P., Burton, A.C., and Bazett, H.C., *A Practical System of Units for the Description of the Heat Exchange of Man with his Environment.* Science, 1941. **94**: p. 428.

59. Militky, J., Mangat, M., and Hes, L., *Selected properties of functional materials*. Thermal Comfort of Cotton Denim Fabric in Wet State, ed. D. Křemenáková, Mishra, R., Militký, J., Mareš, J., and Šesták, J.,. 2013.

60. Venkataraman, M., Mishra, R., Křemenáková, D., Militký, J., Kotresh, TM., Misra, S., and Arumugam, V., *Progress in Fibrous Material Science*. Advanced Fibrous Materials for Thermal Insulation-II, ed. D. Kremenakova, Militky, J., and Mishra, R.,. 2014, Liberec, Czech Republic.

61. Clulow, E.E., and Rees, W.H., *The Transmission of Heat Through Textile Fabrics.* Journal of Textile Institute, 1968. **59**: p. 285.

62. Hes, L., and Promerova, M., *The Effect of Thermal Resistance and Absorptivity of Various Fabrics on their Thermal Contact Characteristics*, in *21st Textile Research Symposium.* 1992: Mt. Fuji, Japan.

63. Das, B.R., Bhattacharjee, D., Kumar, K., and Srivastava, A., *Thermo-physiological Comfort Characteristics of Fine-denier Polypropylene Fabrics.* Research Journal of Textile and Apparel, 2013. **17**(1).

64. Venkataraman, M., Mishra, R., Jasikova, D., Kotresh, T. M., and Militky, J. , *Thermodynamics of aerogel treated nonwoven fabrics at subzero temperatures.* Journal of Industrial Textiles, 2014.

65. *http://www.ctherm.com/products/tci_thermal_conductivity/*. [cited 2015 12 SEPTEMBER].

66. Cha, J., Seo, J., and Kim S., *Building materials thermal conductivity measurement and correlation with heat flow meter, laser flash analysis and TCi.* Journal of Thermal Analysis & Calorimetry, 2012. **109**: p. 295–300.

67. Kuvandykova, D., *A new transient method to measure thermal conductivity of asphalt.* C-Therm Technology, 2010. **7**: p. 1-10.

68. *http://www.tx.ncsu.edu/tpacc/comfort-performance/kawabata-evaluation-system.cfm*. [cited 2015 12 SEPTEMBER].

69. Yoneda, M., and Kawabata, S., *Analysis of Transient Heat Conduction in Textiles and its Applications.* Journal of Textile Machinery Society of Japan 1983. **Part II**(31): p. 73-81.

70. Kawabata, S., Niwa, S., and Sakaguchi, H., *Application of the new thermal tester `thermolabo' to the evaluation of the clothing comfort.* Journal of Textile Machinery Society of Japan, 1985: p. 343-353.

71. *http://www.thermoanalytics.com/services/human-simulation/thermal-manikin*. [cited 2015 12 SEPTEMBER].

72. Kelnberger, M., and Schwitzgebel, G., *Application of single oscillator double pulse laser systems for Particle Image Velocimetry.* Erschienen in Laurin Photonics Handbook, Innolas GmbH, Krailling, Germany, 2005.

73. Melling, A., *Tracer particles and seeding for particle image velocimetry.* Measurement Science and Technology, 1997. **8**: p. 1406–1416.

74. Frydrych I., D.G., & Bilska J., *Comparative analysis of the thermal insulation properties of fabrics made of natural and man-made cellulose fibres.* Fibre Textiles Eastern Europe, 2002. **39**: p. 40-44.

75. Anna, S., Silvija, K., Janis, G., Rimvydas, M., and Jolanta, M., *Nanofibre Electrospinning Poly(vinyl alcohol) and Cellulose Composite Mats Obtained by Use of a Cylindrical Electrode.* Advances in Materials Science and Engineering, 2013. **2013** p. 6.

76. Morton, W.E., and Hearle, J.W.S., *Physical Properties of Textile Fibres.* The Textile Institute, 1962.

77. Speakman, J.B., and Chamberlain, N.H., *The Thermal Conductivity of Textile Materials and Fabrics.* Journal of Textile Institute, 1930. **21**: p. T29.

78. Bogaty, H., Hollies, N.R.S., and Harris, M., *Some Thermal Properties of Fabrics.* Textile Research Journal, 1957. **27**: p. 445.

79. Fonseca, G.F., and Hoge, H.J., *The Thermal Conductivity of a Multilayer Sample of Underwear Material Under a Variety of Experimental Conditions*, in *Technical Report PR-8.* 1962, Quartermaster Research and Development Center, Pioneering Research Division.

80. Monego, C.J., and Golub, S. J., *Insulating Values of Fabrics, Foams and Laminates.* American Dyestuff Reporter, 1963. **52**: p. 21.

81. Peirce, F.T., and Rees, W.H., *The Transmission of Heat Through Textile Fabrics.* Journal of Textile Institute, 1946. **37**: p. T181.

82. Rees, W.H., *The Transmission of Heat Through Textile Fabrics.* Journal of Textile Institute, 1941. **32**: p. T149.

83. Morris, M.A., *Thermal Insulation of Single and Multiple Layers of Fabrics.* Textile Research Journal, 1955. **25**: p. 766.

84. C.A. Levell, J.R., Breckenbridge & R.F., Goldman,, *Effect of Laundering and Starching on Insulation and Vapor Permeability of Standard Fatigues.* Textile Research Journal, 1970. **40**: p. 281.

85. Aelion, D.L., and Brown, H.C., *The Effect of Certain Physical Characteristics of Fabrics Upon Heat Transmission.* Bulletin Lowell Technological Institute 1956. **3**: p. 3.

86. Fourt, L., Lyerly, G.A., Edwards, G.C., and Poland, E.D.W., *Dry Thermal Insulation of Thick Clothing*, in *Textile Engineering Laboratory Report No. 263.* 1960, Quartermaster Research and Engineering Center, U.S. Army: Natick, Massachusetts.

87. C.P. Black & J.A. Matthew, *The Physical Properties of Fabrics in Relation to Clothing.* J. Text. Inst., 1934. **25**: p. T249.

88. Finck, J.L., *Mechanism of Heat Flow in Fibrous Materials.* Bureau of Standards Journal of Research, 1930. **5**: p. 973-984.

89. Gillings, D.R., Cooper, D.S., and Dickins, T.L., *The Transfer of Heat and Moisture Through Clothing Fabrics*, in *Report No. 44/72.* 1972, Army Personnel Research Establishment.

90. Fonseca, G.F., *Heat Transfer Properties of Ten Underwear-Outerwear Ensembles.* Textile Research Journal, 1970. **40**: p. 553.

91. Hardy, H.B., Ballou, J.W., and Wetmore, O.C., *The Prediction of Equilibrium Thermal Comfort from Physical Data on Fabrics.* Textile Research Journal, 1953. **23**: p. 1.

92. C.D. Niven., *A Simplified Hot Plate Apparatus.* Textile Research Journal, 1962. **32**: p. 890.

93. Hammel, T., *Thermal Properties of Fur, II.* American Journal of Physiology, 1955. **182**: p. 369.

94. Staff, H., *The Effect of Humidity on the Thermal Conductivity of Wool and Cotton.* Physical Review, 1925. **25**: p. 252.

95. Baxter, S., *The Thermal Conductivity of Textiles.* Proceedings of the Physical Society, 1946. **58**: p. 105.

96. Hollies, N.R.S., and Bogaty, H., *Some Thermal Properties of Fabrics.* Textile Research Journal, 1965. **35**: p. 187.

97. C.D. Niven., *The Measurement of the Thermal Insulation of Textiles in Wind.* Can. J. Technol., 1956. **34**: p. 254.

98. Schneider, A.M., and Holcombe, B V. *The role of radiation in fabric warmth'.* in *Advanced workshop on the application of mathematics and physics in the wool industry.* 1988. Lincoln, New Zealand.

99.   Holcombe, B., *The thermal insulation performance of textile fabrics.* Wool Science Review, 1984. **60**(April): p. 12-22.

100.   Holcombe, B.V., Brooks, J. H., Schneider, A. M., and Watt, I. C., *The objective measurement of clothing comfort*, in *Annual World Conference*. 1988, The Textile Institute: Sydney. p. 436-445.

101.   Bogaty, H., Hollies, N. R. S., Hintermaier, J. C., and Harris, M., *The nature of a fabric surface: thickness-pressure relationships.* Textile Research Journal, 1953. **23**(2): p. 108-114.

102.   Epps, H.H., and Song, M. K., *Thermal transmittance and air permeability of plain weave fabrics.* Clothing and Textiles Research Journal, 1992. **11**(1): p. 10-17.

103.   Morris, M.A., *Thermal insulation of single and multiple layers of fabrics.* Textile Research Journal, 1955. **25**(9): p. 766-773.

104.   Goldman, R.F., *Standards for human exposure to heat*, in *Environmental ergonomics*, I.B. Mekjavic, Banister, E. W. and Morrison, J. B, Editor. 1988, Taylor and Francis Ltd.: London. p. 99–136.

105.   Bo, Q., and Nakajima, T., *A numerical study on the heat loss from clothed humans—effects of air space and clothing properties.* Journal of the Human-Environment System, 2001. **5**(1): p. 33-40.

106.   Fonseca, G.F., and Breckenridge, J. R., *Wind penetration through fabric systems. Part I.* Textile Research Journal, 1965. **35**(2): p. 95-103.

107.   Lotens, W.A., *The actual insulation of multilayer clothing.* Scandinavian Journal of Work Environment & Health, 1989. **15**(Suppl. 1): p. 66-75.

108.   Nielsen, R., Olesen, B. W., and Fanger, P. O., *Effect of physical activity and air velocity on the thermal insulation of clothing.* Ergonomics, 1985. **28**(12): p. 1617-1631.

109.   Wilson, C.A., Laing, R. M., and Niven, B. E., *Multiplelayerbedding materials and the effect of air spaces on 'wet' thermal resistance of dry materials.* Journal of the Human-Environment System, 2000. **4**(1): p. 23–32.

110.   Wilson, C.A., Laing, R. M., and Niven, B. E., *Estimating thermal resistance of multiple-layer bedding materials - re-examining the problem.* Journal of the Human-Environment System, 1999. **2**(1): p. 69-85.

111.   Lotens, W.A., and Havenith, G., *Ventilation of rainwear determined by a trace gas method*, in *Environmental ergonomics: sustaining human performance in harsh environments*, I.B. Mekjavic, Banister, E. W., and Morrison, J. B.,, Editor. 1988, Taylor and Francis Ltd: London.

112.   Holcombe, B.V., and Hoschke, B. N., *Dry heat transfer characteristics of underwear fabrics.* Textile Research Journal, 1983. **53**(6): p. 368-375.

113.   Obendorf, S.K., and Smith, J. P., *Heat transfer characteristics of nonwoven insulating materials.* Textile Research Journal, 1986. **56**(11): p. 691-696.

114.   Fan, J., and Keighley, J. H., *Theoretical and experimentalstudy of thermal insulation of clothing in windy conditions.* International Journal of Clothing Science and Technology, 1989. **1**(1): p. 21-29.

115.   McCullough, E.A., Jones, B. W., and Zbikowski, P. J., *The effect of garment design on the thermal insulation values of clothing.* American Society of Heating, Refrigerating and Air-Conditioning Engineers, 1983. **89**(2A): p. 327-352.

116.   Spencer-Smith, J.L., *The physical basis of clothing comfort. Part 2: heat transfer through dry clothing assemblies.* Clothing Research Journal, 1977. **5**(1): p. 3-17.

117.   Peirce, F.T., and Rees, W. H., *The transmission of heatthrough textile fabrics—Part II.* Journal of The Textile Institute, 1946. **37**(9): p. T181-T204.

118.   Ukponmwan, J.O., *The Thermal-Insulation Properties of Fabrics.* Textile Progress, 1993. **24**(4): p. 1-57.

119.   Havenith, G., Heus, R., and Lotens, W. A., *Resultant clothinginsulation: a function of body movement, posture, wind, clothing fit and ensemble thickness.* Ergonomics, 1990. **33**(1): p. 67-84.

120.   Havenith, G., *Heat balance when wearing protective clothing.* Annals of Occupational Hygiene, 1999. **43**(5): p. 289-296.

121. Parker, S.P., *McGraw-Hill dictionary of scientificand technical terms (5th ed.)*. Vol. 5. 1994, New York: Mc-Graw-Hill Inc.

122. Ruckman, J.E., Murray, R., and Choi, H. S., *Engineering of clothing systems for improved thermophysiological comfort. The effect of openings.* International Journal of Clothing Science and Technology, 1999. **11**(1): p. 37-52.

123. Weder, M.S., Zimmerli, T., and Rossi, R. M., *A sweating and moving arm for the measurement of thermal insulation and water vapour resistance of clothing*, in *Performance of protective clothing. ASTM STP 1237*, J.S. Johnson, and Mansdorf, S. Z.,, Editor. 1996, American Society for Testing and Materials: West Conshohocken. p. 257–268.

124. Bomberg, M., *Application of three ASTM test methods to measure thermal resistance of clothing*, in *Performance of protective clothing: ASTM STP 1133*, J.P. McBriarty, and Henry, N. W.,, Editor. 1992, American Society for Testing and Materials: Philadelphia.

125. Gretton, J.C., Brook, D. B., Dyson, H. M., and Harlock, S.C., *Moisture vapor transport through waterproof breathable fabrics and clothing systems under a temperature gradient.* Textile Research Journal, 1998. **68**(12): p. 936-941.

126. Cain, B., and Farnworth, B., *Two new techniques for determining the thermal radiative properties of thin fabrics.* Journal of Thermal Insulation, 1986. **9**(April): p. 301-322.

127. Fowle, F.E., *Smithsonian physical tables*. 1933, Washington: Smithsonian Institute.

128. *ISO 11092: Textiles—Physiological effects—Measurement of thermal and water-vapour resistance under steady-state conditions (sweating guarded-hotplate test)*. 1993, International Organization for Standardization: Geneve.

129. Belding., H.S., Russell., H. D, Darling., R. C, and Folk., G.E,, *Analysis of factors concerned in maintaining energy balance for dressed men in extreme cold: effects of activityon the protective value and comfort of an Arctic uniform.* The American Journal of Physiology, 1947. **149**: p. 223- 239.

130. Kerslake, D.M., *The insulation provided by infants bed clothes.* Ergonomics, 1991. **34**(7): p. 893-907.

131. Hollands, K.G.T., Unny, T. E., Raithby, G. D., and Konicek, L., *Free convective heat transfer across inclined air layers.* Journal of Heat Transfer, 1976. **98**(2): p. 189-193.

132. Arlon J. Hunt, C.A.J., Wanqing Cao, *Aerogel – a high performance insulating material at 0.1 bar*. Insulation materials: testing and applications, ed. W.D. Graves RS. Vol. 2. 1991, Philadelphia: American Society for Testing and Materials.

133. Fricke, J. *Thermal transport in porous superinsulations*. in *Aerogels* 1986: Springer Proceedings in Physics.

134. Novak, Z., and Knez., Z., *Diffusion of methanol-liquid CO_2 and methanol-supercritical CO_2 in silica aerogels.* Journal of NonCrystalline Solids, 1997. **221**(2-3): p. 163-169.

135. Tamon, H., Kitamura, T., and Okazaki, M., *Preparation of silica aerogel from TEOS.* Journal of Colloid and Interface Science, 1998. **197**(2): p. 353-359.

136. Li, Y., Plante, M., and Holcombe, B. V., *Fibre hygroscopicity and perceptions of dampness part-II: Physical mechanisms.* Textile Research Journal, 1995. **65**: p. Textile Research Journal.

137. Dorcheh, A.S., and Abbasi, M. H., *Silica aerogel; synthesis, properties and characterization.* Journal of Materials Processing Technology, 2008. **199**(1): p. 10-26.

138. Patel, R.P., Purohit, N. S., and Suthar, A. M., *An overview of silica aerogels.* International Journal of ChemTech Research, 2009. **1**(4): p. 1052-1057.

139. Hosticka, B., Norris, P. M., Brenizer, J. S., and Daitch, C. E., *Gas flow through aerogels.* Journal of Non-Crystalline Solids, 1998. **225**(1-3): p. 293-297.

140. http://energy.lbl.gov/ecs/aerogels/sa-pore.html. [cited 2015 03 June].

141. Milan, M., and Militky, J., *Statistical Data Analysis*. 2011, New Delhi: Woodhead Publishing 763.

142. Raffel, M., Willert, C. I., Wereley, S. T., and Kompenhans, J., *Particle Image Velocity. Second Edition.* 1998.

143. Dubinin, M.M., *Theory of physical adsorption of gases and vapors and the adsorption properties of some adsorbents differing in nature and having a porous structure.* Izvestiya Akademii Nauk SSSR.Seriya Khimicheskaya, 1960. **7**: p. 1153-1161.

144. Dubinin, M.M., *The potential theory of adsorption of gases and vapors for adsorbents with energetically nonuniform surfaces.* Chemical Reviews, 1960. **60**: p. 235-241.

145. *IUPAC Manual of Symbols and Terminology, Appendix 2, Pt.1,Colloid and Surface Chemistry.* Pure Applied Chemistry, 1972. **31**: p. 578.

146. Lizak, P., *Structure of yarn and its influence on properties of fabrics.* Vlakna a Textil, 1998. **4**: p. 213-221.

147. Abdel-Rehim, Z.S., Saad, M. M., El-Shakankery, M., and Hanafy, I., *Textile fabrics as thermal insulators.* Autex Research Journal, 2006. **6**(148-161).

148. Mohammadi, M., and Banks, L. P. , *Determining effective thermal conductivity of multilayered nonwovens fabrics.* Textile Research Journal, 2003. **73**: p. 802-808.

149. Houston, P.L., *Chemical kinetics and reaction dynamics.* 2007, New York, NY: Dover.

150. Hrubesh, L.W., *Aerogel applications.* Journal of Noncrystalline Solids, 1998(225): p. 335–342.

151. Slater, K., *Comfort properties of textiles.* The Textile Institute 1977: p. 1-11.

152. Li Y., a.H., B. V., *Mathematical Simulation of Heat and Moisture Transfer in a Human-Clothing-Environment System.* Textile Research Journal, 1998. **68**(6): p. 389-397.

153. Necati Ozisik, M., *Heat transfer – A basic approach.* 1985, New York: McGraw Hill.

154. ASHRAE, *Handbook of Fundamentals.* 1977, American Society of Heating, Refrigerating and Air-Conditioning Engineers Inc.

155. Kind, R.J., Jenkins., and Broughton, C.A., *Measurements and prediction of wind-induced heat transfer through permeable cold-weather clothing.* Cold Regions Science and Technology, 1995. **23**(4): p. 305–316.

156. Stoecker, W.F., and Jones, J.W., *Refrigeration and air conditioning* Vol. 2. 1982, Singapore: McGraw-Hill Book Company.

157. Konarska, M., Sołtynski, K., Sudoł-Szopińska, I., and Chojnacka, A., *Comparative Evaluation of Clothing Thermal Insulation Measured on a Thermal Manikin and on Volunteers.* Fibres & Textiles in Eastern Europe, 2007. **15**(2): p. 61.

158. Fohr, J.P., Couton, D., and Treguier, G., *Dynamic Heat and Water Transfer Through Layered Fabrics.* Textile Research Journal, 2002. **72**(1): p. 1-12.

159. Sukigara, S., Yokura, H., and Fujimoto, T., *Compression and Thermal Properties of Recycled Fiber Assemblies Made from Industrial Waste of Seawater Products.* Textile Research Journal, 2003. **73**(4): p. 310-315.

160. Reim, M., Korner, W., Manara, J., Korder, S., Arduini-Schuster, M., Ebert, H. P., and Fricke, J., *Silica aerogel granulate material for thermal insulation and daylighting.* Solar Energy, 2005. **79**: p. 131-139.

Research Outputs

Journal Publications

[1] Mohanapriya Venkataraman, Rajesh Mishra, T. M. Kotresh, Tomonori Sakoi, Jiri Militky, *Effect of compressibility on heat transport phenomena in aerogel treated nonwoven fabrics*, Journal of Textile Institute - accepted, 2015 (***Impact factor: 0.722***).

[2] Mohanapriya Venkataraman, Rajesh Mishra, Darina Jasikova, T M Kotresh, Jiri Militky, *Thermodynamics of aerogel treated nonwoven fabrics at subzero temperatures*, Journal of Industrial Textiles, doi:10.1177/1528083714534711, 2014 (***Impact factor: 1.349***).

[3] Mohanapriya Venkataraman, Rajesh Mishra, Jakub Wiener, T M Kotresh, Jiri Militky, Miroslav Vaclavik, *Novel techniques to analyze thermal performance of aerogel treated blankets under extreme temperatures*, Journal of the Textile Institute, Accepted, June, http://dx.doi.org/10.1080/00405000.2014.939808, 2014 (***Impact factor: 0.722***).

[4] Mohanapriya Venkataraman, Rajesh Mishra, Jiri Militky, *Aerogel based nanoporous fibrous materials for thermal insulation*, Fibers and Polymers, Vol 15, No. 7, pp. 1444-1449, 2014 (***Impact factor: 0.881***).

[5] Mohanapriya Venkataraman, Rajesh Mishra, *Application of silver nanoparticles to industrial sewing threads: effects on physico-functional properties & seam efficiency*, Fibers and Polymers, Vol.15, No.3, 510-518, 2014 (***Impact factor: 0.881***).

[6] Mohanapriya Venkataraman, Rajesh Mishra, Jakub Weiner, Adnan Mazari, Jiri Militky, Veera Kumar Arumugam., *Innovative Techniques for Characterization of Nonwoven Insulation Materials Embedded with Aerogel*, International Journal of Chemical, Nuclear, Metallurgical and Materials Engineering, Vol.8 No.9, 2014.

[7] Mohanapriya Venkataraman, Rajesh Mishra, Jiri Militky, Veerakumar Arumugam & Srabani Misra, *Thermal properties of high performance nonwoven padding fabrics at sub zero temperatures*, Vlakna a textil, ISSN 1335-0617, Vol:3, 2014, ***Scopus***.

[8] Mohanapriya Venkataraman, Rajesh Mishra, Jaromir Marek, Jiri Militky, *Electrospun nanofibers from PUR and PVDF embedded with SiO_2 Aerogel for Advanced Thermal Properties*, Nanoletters (under review).

[9] Mohanapriya Venkataraman, Rajesh Mishra, Guocheng Zhu, Jiri Militky, *Dynamic heat flux measurement for advanced insulation materials*, Journal of Industrial Textiles (under review).

[10] Mohanapriya Venkataraman, Rajesh Mishra, Jakub Wiener, Jiri Militky, *Comparative Analysis of High Performance Thermal Insulation Materials*, Autex Research Journal (under review).

[11] M. Venkataraman, R. Mishra, T. M. Kotresh, J. Militky and H. Jamshaid, *Aerogels for thermal insulation in high-performance textiles*, Textile Progress, Taylor& Francis (under review).

Book Chapters

[1] Mohanapriya Venkataraman, Rajesh Mishra, Jiri Militky, "*Advanced fibrous materials for thermal insulation-I*". in: Progress in fibrous material science. 2014. ISBN:978-80-87269-40-4

[2] Mohanapriya Venkataraman, Rajesh Mishra, Jiri Militky, "*Advanced fibrous materials for thermal insulation-II*". in: Progress in fibrous material science. 2014. ISBN:978-80-87269-40-4

[3] Mohanapriya Venkataraman, Rajesh Mishra, Jiri Militky, "*Performance of aerogel treated blankets under extreme temperatures*". in: Progress in fibrous material science. 2014. ISBN:978-80-87269-40-4

[4] Mohanapriya Venkataraman, Rajesh Mishra, Hafsa Jamshaid and Jiri Militky, "*Aerogels: Novel Materials for Insulative Textiles*". in: Selected Properties of Functional Materials. OPS, 2013. ISBN: 978-80-87269-29-9

[5] Mohanapriya Venkataraman, Rajesh Mishra, Hafsa Jamshaid and Jiri Militky, "*Aerogel Based Insulation Materials: Characterization of Thermal, Electrical and Electromagnetic Behavior.*" in: Selected Properties of Functional Materials. OPS, 2013. ISBN: 978-80-87269-29-9

Conference Publications

[1] Mohanapriya Venkataraman, Rajesh Mishra and Jiri Militky, *Heat Transport Phenomena in Aerogel Treated Nonwoven Fabrics*, 11th Joint International Conference CLOTECH'2015, June 17th-19th, 2015 Lodz, Poland.

[2] Mohanapriya Venkataraman, Rajesh Mishra and Jiri Militky, *Heat Transport Phenomena in Advanced Insulation Materials*, 6th International Technical Textiles Congress, 14-16 October, 2015 İzmir-TÜRKİYE.

[3] Mohanapriya Venkataraman, Rajesh Mishra, Jakub Weiner, Marie Stepankova, Veerakumar Arumugam, Jiri Miltky, *Effect of Laser Irradiation on Kevlar Fabric Treated with Nanoporous Aerogel,* 7th International Conference on Nanomaterials - Research & Application (NANOCON 2015), October 14th - 16th 2015 / Hotel Voronez I, Brno, Czech Republic, EU, ***Thomson Reuter, Indexed in ISI Web of Knowledge***.

[4] Mohanapriya Venkataraman*, Dynamic Thermal Measurement for Advanced Insulation Materials and Their Biological Implications*, 8th Textile Bioengineering and Informatics Symposium (TBIS), Zadar, Croatia , 2015, ***CPCI/ISTP, ISI web of knowledge, Scopus & Ei compendex***.

[5] Mohanapriya Venkataraman, Rajesh Mishra, Jakub Weiner, Adnan Mazari, Jiri Militky, Veera Kumar Arumugam, *Innovative Techniques for Characterization of Nonwoven Insulation Materials Embedded with Aerogel*, ICTCME 2014, Switzerland

[6] Mohanapriya Venkataraman, Rajesh Mishra, Jiri Militky and Veerakumar Arumugam, *Acoustic properties of aerogel embedded nonwoven fabrics*, NANOCON, November 5-7, Brno, 2014, ***Thomson Reuter, Indexed in ISI Web of Knowledge***.

[7] Mohanapriya Venkataraman, Rajesh Mishra, Veerakumar Arumugam and Jiri Militky, *Thermal analysis of aerogel treated non woven fabrics*, Fibre society spring conference, May 21-23, 2014, ***Scopus***.

[8] Mohanapriya Venkataraman, Rajesh Mishra, Jiri Militky, Veerakumar Arumugam & Srabani Misra, *Thermal Properties of High Performance Nonwoven Padding Fabrics at Sub Zero Temperatures*, Ruzomberok, Slovakia, 27-28, August 2014, ISBN 978-80-8075-660-42, 7-28 August 2014.

[9] Mohanapriya Venkataraman, Rajesh Mishra, Jakub Weiner, Adnan Mazari, Jiri Militky, Veera Kumar Arumugam, *Novel Techniques to Analyze Thermal Performance of Aerogel Blankets under Extreme Temperatures*, TBIS 2014, ***CPCI/ISTP, ISI web of knowledge, Scopus & Ei compendex, ISSN 19423438***.

[10] Mohanapriya Venkataraman, Rajesh Mishra, Jiri Miltky, *Unconventional Methods to Study Thermodynamics of Aerogel Treated Fabrics*, XIIIth International İzmir Textile & Apparel Symposium (IITAS), Antalya, Turkey, 02-05, April 2014.

[11] Mohanapriya Venkataraman, Rajesh Mishra, Veerakumar Arumugam and Jiri Militky *Thermodynamical Characterization of Aerogel Treated Nonwoven Fabrics*, 7th International Textile, Clothing & Design Conference (ITC&DC), Dubrovnik, Croatia, 05-08, October, 2014, ISBN 978-953-7105-549, ***CPCI/ISTP ISI web of knowledge***.

[12] Mohanapriya Venkataraman, Rajesh Mishra, Veerakumar Arumugam and Jiri Militky, *Thermodynamics of aerogel treated non woven fabrics*, ICIC 2014, Coimbatore , 29-30 April 2014, ISBN: 9788192375243.

[13] Mohanapriya Venkataraman, Rajesh Mishra and Jiri Militky, *Thermodynamic analysis of insulating materials at subzero temperatures*, Workshop Svetlanka, Svetlanka, Czech Republic. September 2014.

[14] Mohanapriya Venkataraman, Rajesh Mishra and Jiri Militky, *Analysis of thermal properties of aerogel treated non-woven fabrics*. 42nd Textile Research Symposium. Mount Fuji, Japan, 28th to 30th August 2013.

[15] Mohanapriya Venkataraman, Rajesh Mishra and Jiri Militky, *Analysis of thermal properties of aerogel treated non-woven fabrics*. 8th International Conference-Textile Science. Liberec, Czech Republic. 23rd to 25th September 2013. ISBN:978-80-7372-989-9

[16] Mohanapriya Venkataraman, Rajesh Mishra, Jakub Wiener and Jiri Militky, *A study on penetration of polymers in aerogel granular particles*. 8th International Conference-Textile Science. Liberec, Czech Republic. 23rd to 25th September 2013. ISBN:978-80-7372-989-9

[17] Mohanapriya Venkataraman, Rajesh Mishra and Jiri Militky*, Evaluation of thermal properties of high performance nonwoven padding fabric*. 8th International Conference-Textile Science. Liberec, Czech Republic. 23rd to 25th September 2013. ISBN:978-80-7372-989-9

[18] Mohanapriya Venkataraman, Rajesh Mishra, Jakub Wiener and Jiri Militky, *A study on penetration of polymers in aerogel granular particles*. 5th International conference (NANOCON 2013). Brno, Czech Republic. 16th to 18th October 2013. ISBN: 978-80-87294-44-4, ***Thomson Reuter, Indexed in ISI Web of Knowledge***.

[19] Mohanapriya Venkataraman, Rajesh Mishra and Jiri Militky, *Unconventional Methods for Measuring Thermal Properties*. Workshop Svetlanka, Svetlanka, Czech Republic. September 2013.

[20] Mohanapriya Venkataraman, Rajesh Mishra and Jiri Militky, *Unconventional Methods to Study Thermodynamics of Aerogel Treated Fabrics*. 3rd International Science Congress. Karunya University, Coimbatore, India. December 2013

[21] Mohanapriya Venkataraman, Rajesh Mishra and Jiri Militky, *Aerogels: A Novel Material for Thermal Insulation*. 19th International Conference STRUTEX. Liberec, Czech Republic. December 2012. ISBN: 978-80-73729-13-4

[22] Mohanapriya Venkataraman, Rajesh Mishra and Jiri Militky, *Comparative Analysis of Thermal Insulation Measurement Techniques in Textiles*. 19th International Conference STRUTEX. Liberec, Czech Republic. December 2012. ISBN: 978-80-73729-13-4